Whole Number 252, ISSN 0429-8284

FUJI ELECTRIC REVIEW

2016 Vol.62 No. 1

Simulation Technologies for Product Development

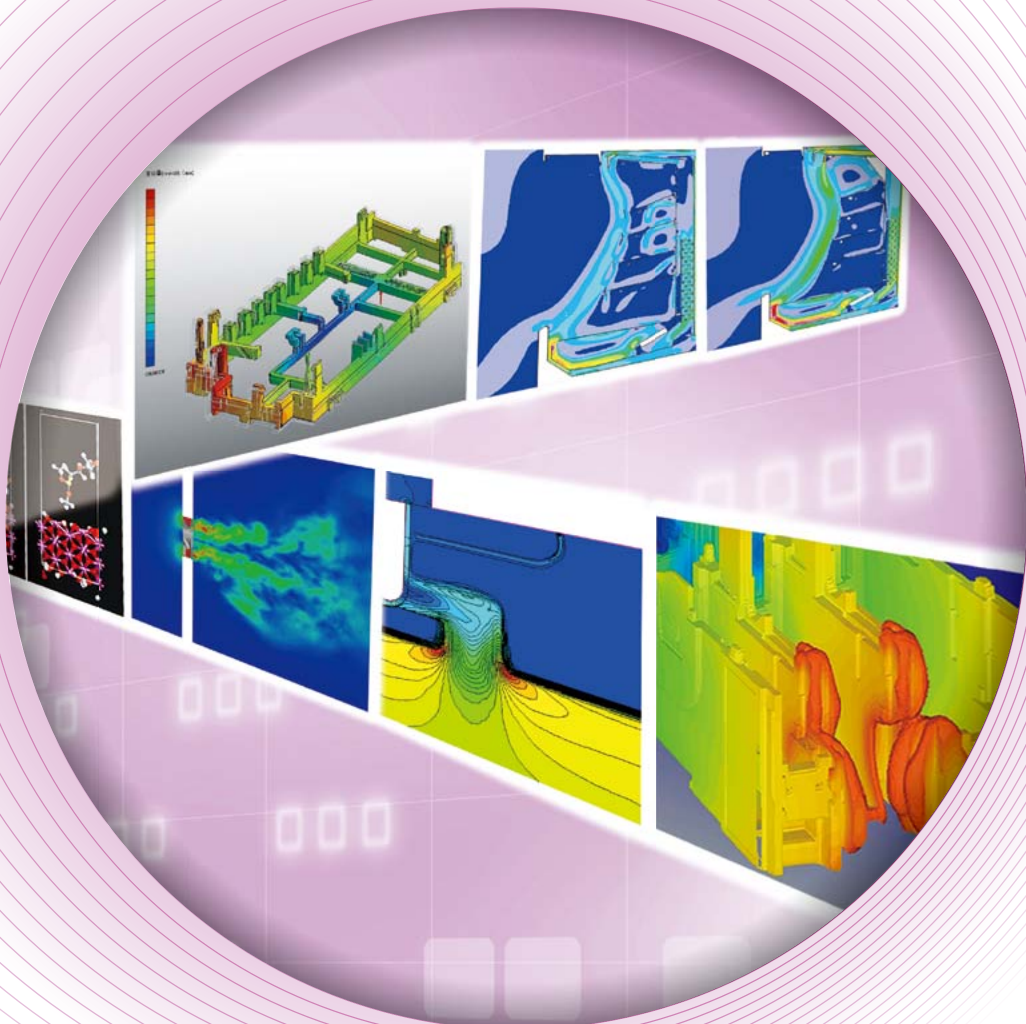

Fuji Electric

Innovating Energy Technology

FUJI ELECTRIC
REVIEW

2016
Vol.62 No. 1

Simulation Technologies for Product Development

Aiming to help bring about a responsible and sustainable society, Fuji Electric provides environmentally friendly products that can most efficiently use energy for social and industrial infrastructure and other various fields. In order to develop products that meet the needs of the market in a timely manner, it is essential to quantify physical phenomena, which form the basis of the functions and performance of products. As a powerful means to that end, we develop and exploit various simulation technologies.

This special issue presents the simulation technologies that support the product development of Fuji Electric.

Cover Photo (clockwise from the upper left):

Example of warpage analysis of power electronics equipment part, Results of simulation of wind velocity distribution (new air curtain system, conventional system), Example of filling analysis for housing of low-voltage circuit breaker (after optimization), Electric field intensity distribution inside the device when retaining the withstand voltage, Fan flow speed distribution, Dissociation structure between epoxysilane and aluminum

FUJI ELECTRIC REVIEW vol.62 no.1 2016
date of issue: June 30, 2016

editor-in-chief and publisher **EGUCHI Naoya**
Corporate R & D Headquarters
Fuji Electric Co., Ltd.
Gate City Ohsaki, East Tower,
11-2, Osaki 1-chome, Shinagawa-ku,
Tokyo 141-0032, Japan
http://www.fujielectric.co.jp

editorial office Fuji Electric Journal Editorial Office
c/o Fuji Office & Life Service Co., Ltd.
1, Fujimachi, Hino-shi, Tokyo 191-8502,
Japan

Contents

Simulation Technologies for Product Development

Supplemental Explanation

New Products

Mismatch Between Simulation and Experiment? Let's Consider Model Systems for Better Interplay!

KOYAMA, Michihisa*

Do we agree that, as results of the promulgation of computers and progress in computer science and computational theory made in the last couple of decades, there are ample examples of successful application and utilization of simulation technology today? If we consider product-oriented simulation technology such as computer-aided design (CAD), we may have the impression that such technology is well past the evaluation phase and has already become ubiquitous. If we think of material-oriented simulation technology, however, successful cases may seem to be few in number.

Simulation technology is used in two phases: analysis and design. The former starts with a validation of the methods and models employed. The simulation results are validated against the phenomena or properties measured to ascertain that the target attributes and features are simulated precisely. This is a vital process for any system. Unfavorable results obtained in this process will not allow the researcher to move to the subsequent process of identifying dominant factors, let alone the design phase that follows. In this case, the reputation of simulation technology may be considerably harmed.

What is important for the validation of a simulation? Naturally, there may be a variety of factors that are case-dependent, but for the purpose of simplification, let's take instrumental analysis as an analogy. The measurement results can only originate from the sample used. Therefore, after determining the measuring instrument, it is the sample preparation that determines the spectra that will be obtained. Ideally, the samples of practical structure should be measured in operando, i.e., in an actual operating environment. We have to, however, use model measurement method due to constraints such as a sample holder in many cases. High-precision measurement is also desired, for example, using SPring-8 (large synchrotron radiation facility). However, we are often obliged to perform measurement with devices readily accessible from a laboratory on a daily basis even if less accurate. Similar issues arise in terms of selecting simulation methods and a computational environment. Simulation results are fully determined by the parameters and structural models as an input once the methods are chosen. If there is a discrepancy between the simulation results and actual measurements, it must be attributed to the accuracy of the parameters of physical properties or structural models that are employed, supposing that the methods and computational conditions are appropriate. It is not difficult to assume that, in molecular simulation, presupposition of an ideal composition or surface/interface structure causes the discrepancy. In finite element analysis, a discrepancy may be attributed to the simplified representations of complex structures, such as a porous structure, and the use of encompassing values as physical properties. When researchers and engineers come across such a discrepancy, how would they respond?

For instance, some may opt for an alternative approach assuming that the simulation technology is not likely to help. Others may make effort to tune the simulation so that the results agree with the actual measurements. Is it too much to say that these actions are a 20th century approach? One may consider that the measured object must be different from what they have assumed and try to measure again after a careful consideration of conditions. It is too idealistic, conversely, if I call it a 21st century approach. What is the reality in laboratories of today? Rather than considering the current status, we should foresee the situation in 15 years' time, around the year 2030, to see the ideal conditions for addressing the issue. It is envisaged that the population of Japan will decrease by 10 million, with a higher proportion of elderly citizens. While China has gone into a population decline, that of India is still growing, and it will have surpassed China. Given this trend, to maintain a global competitiveness, Japan must consider deploying intelligence in manufacturing, although it has hitherto largely relied on spirit, intuition and guts. Simulation technology is a tool to facilitate virtual experiments using models that represent the reality, leveraging the human "knowledge" implemented as software on a computer. Even if a computer works over 8,000 hours per year, it won't raise the issue of unethical labor conditions, nor will the supervisory authority intervene in the issue. Looking at society in 15 years' time, what can we do to ensure the younger generation, who will be the driving force of their companies, can be at ease with using

* Ph.D. (Engineering), Professor, INAMORI Frontier Research Center, Kyushu University

simulation technology?

The young researchers and engineers who are already adept at using simulation technology today will be assuming positions as leaders or assessors in 2030. They will have appropriate evaluation standards in place, as well as the competence to practice them. Then they will need to focus more on the training of those who follow. Imagine a future where we have more young talents who can support better 'interplay' between experiments and simulations. When they come across discrepancies between them, they may intend to propose that they should experimentally measure the sample characteristics to validate the simulation based on an ideal model experimental system, in addition to conducting the simulation based on a realistic system model rather than an ideal system model. Such promising researchers or engineers will start to play an active part one after another. If this is the picture of our future, there must be a variety of options that we can look into.

Simulation Technologies for Product Development: Current Status and Future Outlook

WATANABE, Masahide* NAGAYASU, Yoshihiko* YASUKAWA, Yukio*

1. Introduction

Along with the recent progress of computational science brought about by improved computer performance and software versatility, simulation technologies are now widely applied in various phases from R&D to product design.

At Fuji Electric, simulation technologies are applied in a wide variety of fields. For semiconductor devices, we are working to make use of molecular simulation and analysis technologies to clarify phenomena at the atomic level as well as analysis and estimation of electrical characteristics. In addition, we are taking an approach to use simulation technologies for clarifying material properties, which was something that mostly depended on rules of thumb in the past, to make efficient use of materials. Furthermore, approaches to achieving the optimum design of electrical equipment by taking advantage of simulation technologies such as electromagnetic noise analysis, acoustic noise analysis and fluid analysis are also becoming widespread.

In any case, we aim to provide customers with high-performance, high-reliability products with short delivery times. We will do this by making use of computational science to accurately identify physical phenomena, which form the basis of functions and performance of products, and grasping the mechanisms scientifically and quantitatively to apply them to the design of products.

* Corporate R&D Headquarters, Fuji Electric Co., Ltd.

2. Simulation Technologies to Support Development of Devices and Materials

2.1 SiC power semiconductor devices

Simulation technologies, which are already being used to develop silicon (Si) devices, are also important in the development of silicon carbide (SiC)[*1] devices. They are used to reduce the number of prototypes required, grasp physical phenomena and optimize the device structures to improve the development efficiency and offer higher-performance products.

SiC as a substrate material may have varying mobility, interface charges and the impact ionization rate depending on the crystal surface[*2]. Hence, it was difficult to have highly accurate prediction of device characteristics that are affected by them, including the on-state voltage, threshold and withstand voltage. To deal with this issue, Fuji Electric has collaborated in research with the National Institute of Advanced Industrial Science and Technology to build a simulation model based on the actual measured values to predict characteristics of a trench metal-oxide-semiconductor field-effect transistor (MOSFET)[*3]. We have also met the demands for energy saving and miniaturization of power electronics equipment and developed a low-loss 1.2 kV-class trench MOSFET (see Fig. 1). Trench MOSFETs have the gate formed on the sides of the trench and this allows cell pitch to be reduced more easily than planar MOSFETs and the on-resistance $R_{on}{\cdot}A$ is lower.

With trench MOSFETs, the a-face and m-face

***1: SiC**

A compound of silicon (Si) and carbon (C). With many structural polymorphisms of crystals existing such as 3C, 4H and 6H, SiC is known as a wide gap semiconductor with a band gap ranging from 2.2 to 3.3 eV depending on the structure. Because of its properties that are advantageous as power devices such as the high breakdown voltage and thermal conductivity, it is applied to practical applications for its capability to realize devices with high withstand voltage, low loss and high-temperature operation.

***2: Crystal surface**

Refer to Supplemental explanation 1: "SiC Crystal Types and Crystal Surface" on page 62.

***3: Trench MOSFET**

Trench metal-oxide-semiconductor field-effect transistor (MOSFET) is a type of power MOSFET. While planar MOSFETs have the gate formed on the semiconductor surface, trench MOSFETs are characterized by formation of the gate in a trench made in the direction of depth of the semiconductor. Because the channel is formed in the direction of depth, the trench gate structure allows easy planar miniaturization and hence improvement of the channel density, which makes it possible to reduce the on-resistance per area.

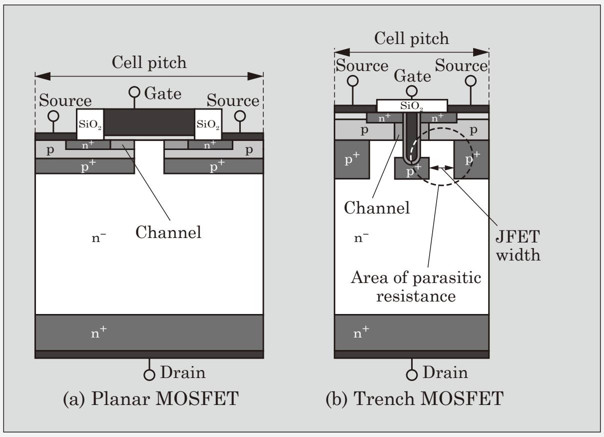

Fig.1 MOSFET cross-sectional view

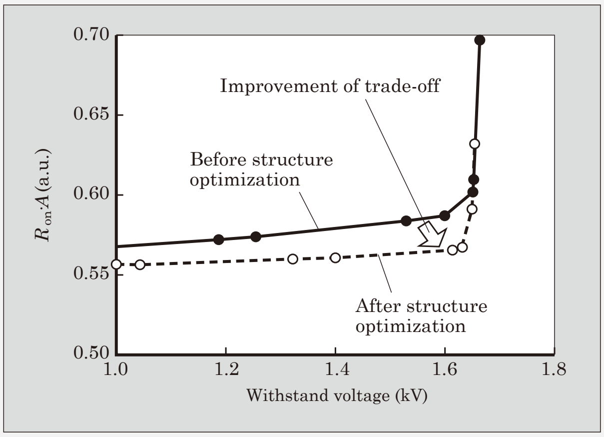

Fig.2 Trade-off between $R_{on}{\cdot}A$ and withstand voltage before and after structure optimization

are used for the trench sides and a model of mobility that accommodates these faces is required. Accordingly, we have focused on the fact that the device operates in the region that the mobility depends on the gate voltage and Coulomb scattering[*4]. We thus incorporated into simulation a Coulomb scattering model, allowing the mobility in low electric field to match the measured mobility. For withstand voltage, because the avalanche breakdown[*5] of SiC is affected by the lateral electric field in addition to the crystal surface, we used a Hatakeyama model, which takes the lateral electric field into consideration. And we have made corrections by the a-face and m-face to restructure the parameters. As a result, the simulated $R_{on}{\cdot}A$ and withstand voltage showed good agreement with the measured values. In addition, we confirmed that potential distribution analysis of $R_{on}{\cdot}A$ could be used to optimize the structure and the impurity concentration of the n-type layer in the junction field-effect transistor (JFET) portion. This made it possible to further improve the trade-off between $R_{on}{\cdot}A$ and withstand voltage (see Fig. 2) (Refer to “Simulation Based Prediction of SiC Trench MOSFET Characteristics” on page 12).

In addition to unipolar devices such as Schottky barrier diodes (SBDs)[*6] and MOSFETs, Fuji Electric has developed bipolar devices such as PiN diodes and insulated gate bipolar transistors (IGBTs)[*7]. Bipolar devices make it possible to easily increase the current and withstand voltage and we are currently conducting research on 13 kV PiN diodes and IGBTs. With bipolar devices, the mobility of electrons and holes, lifetime and the injection efficiency of carriers of the p-type collector greatly affect the device characteristics. However, these parameters, which may also be caused by crystal defects and activation rate of the p-type region, are difficult to apply to a simulation model. Accordingly, Fuji Electric has identified problems with real elements by using simulation to estimate ideal characteristics and comparing them with measured values. We have also attempted to improve the accuracy by fitting measured values to a simulation so as to improve the characteristics.

We combined a device simulator and a circuit simulator to conduct switching simulation in view of inductive load and predicted losses at a bus voltage of 6.6 kV. Figure 3 shows a comparison of the generated losses between the current and improved structures. The current structure has high injec-

***4: Coulomb scattering**

Refer to Supplemental explanation 2: “MOSFET Carrier Scattering” on page 62.

***5: Avalanche breakdown**

If reverse voltage is applied to a semiconductor device, free electrons and holes are accelerated in the electric field and collide with lattice atoms of silicon, etc. When the electric field intensity is sufficiently large, it causes collisional ionization. This results in repetition of the process of free electrons and holes being released and accelerated again and the number of free electrons and holes are increased like an avalanche to cause a large current to flow. This phenomenon is referred to as avalanche withstand and constitutes a factor that determines the breakdown voltage of a semiconductor device.

***6: SBD**

Stands for Schottky barrier diode. It is a diode providing rectifying action by using a Schottky barrier created by junction between a metal and a semiconductor. It is being applied to the FWDs of SiC-SBDs because of its excellent electrical characteristics. As compared with a P-intrinsic-N (PiN) diode, which also uses minority carriers, an SBD, which operates only on majority carriers, offers a higher reverse recovery speed and smaller reverse recovery loss.

***7: IGBT**

Stands for insulated-gate bipolar transistor. An IGBT is a voltage-controlled device that has a gate insulated with an oxide insulating film, the same gate structure as that of a MOSFET. It combines the strengths of a MOSFET and a bipolar transistor. Its bipolar operation, which allows use of conductivity modulation, makes it possible to realize both a switching speed sufficient for application to inverters and high withstand voltage combined with low on-resistance.

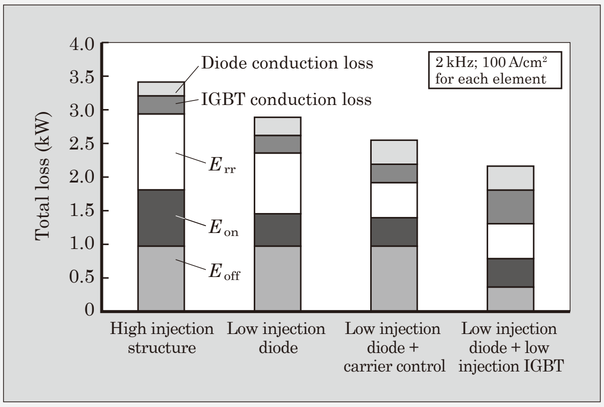

Fig.3 Results of estimation of losses with improved structure

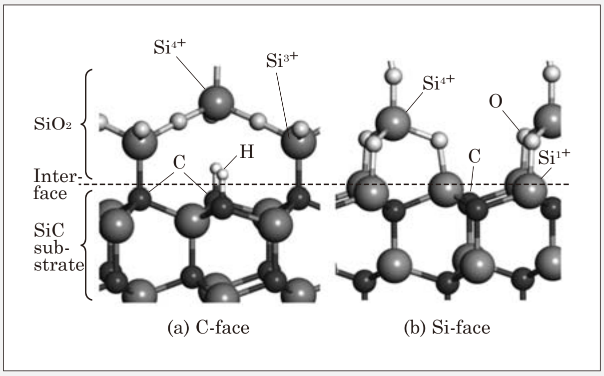

Fig.4 Estimated structural model of dry oxide film interface with ideal interface assumed

tion of carriers in the p-type collector and the p-type anode of the diode, which causes a large switching loss. Accordingly, we attempted to reduce the switching loss by incorporating a low-injection structure and other measures. As compared with the high-injection structure, a reduction to 44% has been confirmed in the switching loss and a 37% improvement in the total loss including the conduction loss at an operating frequency of 2 kHz (Refer to "Development of SiC Bipolar Devices Using Simulation" on page 17).

2.2 Clarification of MOSFET interface phenomena by first-principles calculation

The interface phenomena of SiC devices are still mostly unclear and the C (carbon) face, Si (silicon) face, a-face and m-face have different interface phenomena respectively. Accordingly, there are needs to clarify the interface phenomena for the respective face orientations. Currently, Fuji Electric is working on clarifying phenomena on interfaces and inside crystals at the atomic level by utilizing computational scientific techniques including the first-principles calculation in addition to using electrical characteristics and making analytical observations. The first-principles calculation is a technique of solving the electronic state in a substance based on quantum mechanics by using numerical calculations. It makes it possible to estimate properties of unknown substances and physical and chemical phenomena at the atomic level that cannot be measured by way of experiment.

Figure 4 shows an example of modeling by using first-principles calculation assuming the ideal interface structure of the SiC/SiO_2 interface after the dry oxidation process respectively for the C-face and Si-face. This leads to an estimation that Si existing on the interface is in the chemical state Si^{3+} on the C-face and Si^{1+} on the Si-face. X-ray photoelectron spectroscopy (XPS) analysis of the interface has actually shown Si^{3+} on the C-face and Si^{1+} on the Si-face, which supports the validity of this model. In this way, assuming the ideal interface structure makes it possible to estimate the origin of the suboxide (incomplete SiO_2) obtained by XPS analysis, and the choice of measures for realizing an ideal interface can be narrowed down.

The results of study of the interface structure with the ideal interface structure of the Si-face provided with a dangling bond (DB) of Si are shown in Fig. 5. The calculation shows that the interface state of the DB is formed in the band gap of SiC. An interface state like this traps a charge and causes a reduction in mobility due to Coulomb scattering, leading to a variation of V_{th}. A similar calculation of the bonding state of atoms other than the DB makes it possible to calculate various interface states. They can then be compared with the ac-

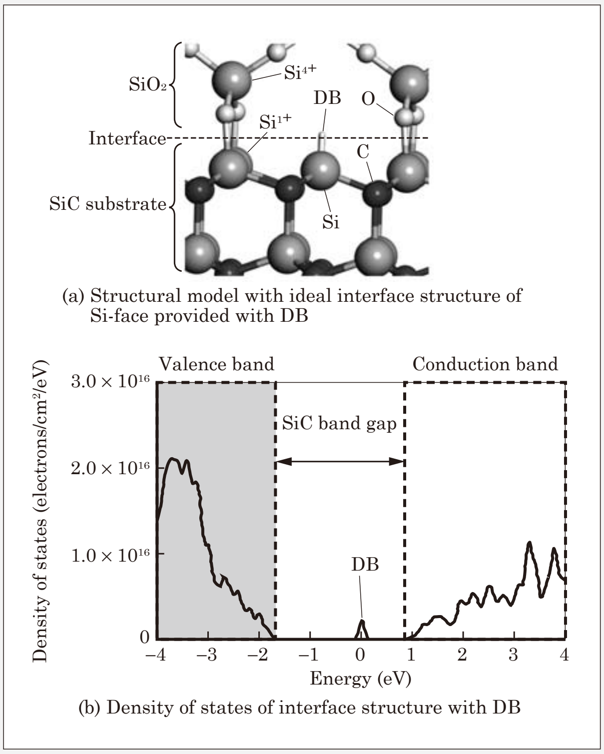

Fig.5 Results of study of interface structure with ideal interface structure of Si-face provided with DB

tual electrical characteristics and analysis results to clarify interface phenomena that are not actually visible.

In the future, we intend to make use of clarifying phenomena at the atomic level using a simulation including first-principles calculation in addition to measured values and analysis results. We will incorporate it in a device simulator, and thereby help to improve the performance of SiC-MOSFET (Refer to "Atomic Level Analysis of SiC Devices Using Numerical Simulation" on page 23).

2.3 Resin material characteristics

With products that use power semiconductor devices, it is important to improve the performance of semiconductor devices as well as the encapsulation resin. In particular, encapsulation resin has a significant influence on the long-term reliability. Therefore, resin materials must be selected in view of the impact of residual stress due to actual molding and the like. In order to meet this need, we are conducting simulation with resins modeled at the atomic level by first-principles calculation and molecular dynamics calculation. The aim is to grasp the mechanical characteristics and adhesion of resins so that a resin framework and adhesion aid can be selected. We are also working to gain an understanding of resin behavior. This is done with the resin flow and curing rate distribution during the actual molding process taken into consideration, by using 3D fluid analysis coupled with thermal stress analysis.

The adhesion between resin and metal may involve complicated factors. And the study of encapsulation resin conducted up to now has adopted a method of actually testing candidate materials so as to narrow down the choice. In order to improve the efficiency of this material selection, we are working on the development of technology to predict characteristics. It utilizes simulation technologies such as first-principles calculation and molecular dynamics calculation.

Adhesion of resin is assumed to depend mainly on the chemical bond between the component and resin, the anchor effect or presence of dirt on the surface and mechanical characteristics such as the coefficient of elasticity and coefficient of linear expansion of the resin. Of these, the anchor effect is a factor that depends on the component and the first thing to consider in design of the resin is the chemical bond between the component and resin and mechanical characteristics of the resin.

Mechanical characteristics of a resin and the chemical bonding force with the component to be adhered to can now be calculated from the molecular structure of the resin framework and adhesion aid. As shown in Fig. 6, energy in the state of adhesion between the base material and resin and that in the state of separation can be determined and the energy difference between them indicates the chemical bonding force in the ideal state. The actual adhesion can be estimated by using the chemical bonding force in this ideal state as the basis and considering external factors such as the anchor effect and dirt and the interfacial stress due to mechanical characteristics.

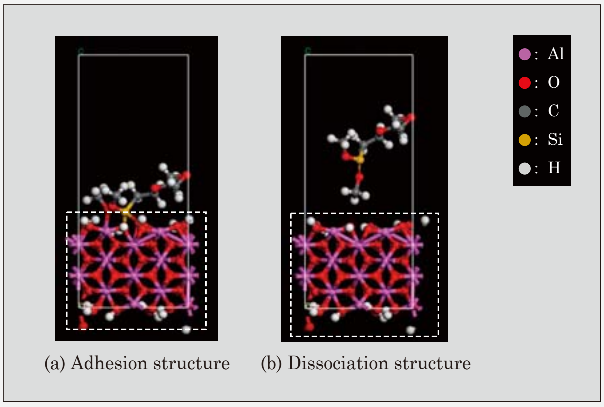

Fig.6 Molecular structures of epoxysilane and aluminum after structure optimization calculation

At this point, we are not ready to completely account for the measured values of adhesion from the results of simulation. But in the future, we aim to further improve the reliability of semiconductor modules encapsulated with resin by predicting characteristics including resin framework, adhesion aid and reliability (Refer to "Study of Adhesion of Resin Materials by Molecular Simulation" on page 28).

Computer-aided engineering (CAE) analysis, which has been used for structurally designing semiconductor modules up to now, handles resin cured after molding as a single elastic body without distribution. And it sometimes caused a deviation from the results of reliability evaluation. One possible factor in this is that, with actual resin moldings, a distribution is generated in the curing rate because of temperature unevenness during molding arising from the differences in the thermal conductivity, structure and heating method of the component. This causes residual stress due to a variation of the volume shrinkage factor depending on the location. Accordingly, for the purpose of improving the analytical precision of resin moldings, Fuji Electric has developed a simulation technology that takes into consideration the viscosity change due to heating and volume shrinkage behavior at the time of solidification from liquid.

By using 3D thermo-fluid analysis software, the irreversible change of resin from liquid to solid can be represented and, even for a product with a complicated shape, residual stress distribution can be visualized by performing a calculation from its heat distribution. This method takes into consideration the resin material properties including the density,

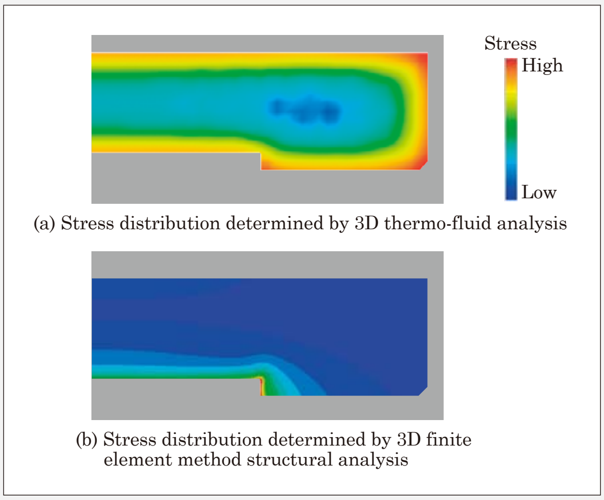

Fig.7 Results of stress distribution analysis in resin curing

coefficient of elasticity and temperature dependence and shear velocity dependence of viscosity together with the curing reaction rate and heat of reaction of the resin. Figure 7 shows the stress distribution inside resin where a copper block is encapsulated with the resin, as an example of calculation results. The calculation result using the conventional 3D finite element method structural analysis software Fig. 7(b) shows a high stress region only on the boundary of the component. Meanwhile, Fig. 7(a) for 3D thermo-fluid analysis reflects the temperature distribution at the time of molding. It shows the presence of a high-stress region on the circumference of the resin rather than inside it, which is a result closer to the reality of the system. In this way, we are making it possible to conduct product development with even higher reliability by applying high-precision structural design (Refer to "Residual Stress Distribution and Adhesive Interface Strength Analysis of Thermosetting Resin Molding" on page 32).

3. Simulation Technologies to Support Development of Machinery and Equipment

3.1 Electromagnetic noise

Power electronics equipment is used at the core of equipment and facilities for energy conservation to ensure efficient use of electric energy and energy creation such as photovoltaic power generation and wind power generation. Power semiconductors used in power electronics equipment feature high-speed switching that allows electricity to be freely converted into easy-to-use forms. At the same time, however, they may emit large amounts of electromagnetic noise during operation.

One traditional measure to reduce electromagnetic noise was to repeat cycles of trial and error after prototyping equipment. In contrast, at Fuji Electric, we have been developing electromagnetic noise simulation technologies for power electronics equipment. Our aim is to explore measures starting in the design phase, and such measures are being widely used for clarifying electromagnetic noise phenomena and reducing noise during product development.

Electromagnetic noise is generated as conduction noise if it is radiated outside through I/O cables and as emission noise if emitted as radio waves from various locations.

For simulation of conduction noise, rough analysis by a simplified model is performed in the initial stage of development. In later stages of development, detailed analysis by a more precise model and simulations with different levels of analytical precision according to the process are appropriately applied to product development.

For simulation of emission noise, simulation with part of the equipment extracted, rather than analysis of the entire equipment, is conducted and the results are applied to structural design (see Fig. 8). Such simulation with part of the equipment extracted features simple modeling and short analysis time, and it makes it possible to search for a better equipment configuration while analysis is repeated.

We are also working on simulation technology intended for preventing electromagnetic noise failure on sites where power electronics equipment is installed. The electromagnetic noise that is radiated through the grounding electrode when power electronics equipment is operated affects external equipment. Clarification of this mechanism and proposal of methods to reduce the noise is included in the fields that mainly depended on know-how without theoretical approaches taken up to now. We are expanding the scope of application of electromagnetic noise simulation in this area (Refer to "Electromagnetic Noise Simulation Technology for Power Electronics Equipment" on page 37).

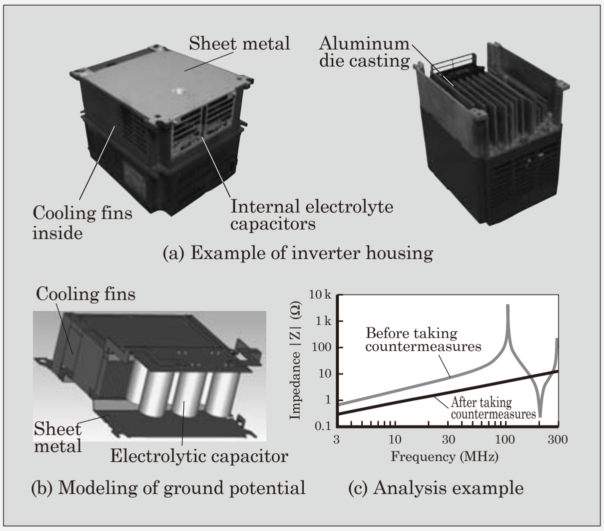

Fig.8 Housing analysis example

3.2 Aerodynamic noise

The demands for miniaturization of various types of electrical equipment have caused a tendency toward a yearly increase in the heat generation density of products. With air-cooled products that use fans, an increase in heat generation density causes the required air volume to increase as well, and aerodynamic noise generated from cooling air may become an issue.

At Fuji Electric, we are working on technology for simulating aerodynamic noise to gain an understanding of the mechanism of noise generation. This can be done by visualizing flow and pressure change, which becomes a source of aerodynamic noise, and studying the structure for noise reduction.

For simulation of aerodynamic noise, we have realized estimation of variation in the flow that provides a source of noise and the sound level by calculation of the flow of a fan (see Fig. 9) with massively parallel computing by using large eddy simulation (LES), which is capable of high-precision reproduction of turbulence phenomena.

Use of this simulation has made it possible to estimate the peak frequency and sound pressure level for noise arising from rotation of the vanes of a cooling fan and flow around the casing. In addition, we have confirmed that the tendency of noise being caused by the positional relationship between a cooling fan and the surrounding structure can be reproduced through comparison with a model simulating an air cooling structure of power electronics equipment. At present, we are working to apply this simulation to a study on a design for reducing the noise of products (Refer to "Aerodynamic Noise Simulation Technology for Developing Low Noise Products" on page 42).

3.3 Switchgear internal arcs

In the development of switching devices used for power transmission, reception and distribution systems, arc analysis for predicting performance at the time of current cutoff has been used mainly to quantify phenomena in the vicinity of contacts up to now. For example, such analysis has been used to predict arc elongation and movement in the breaking chamber of low-voltage equipment. The results are then used to determine the structure and arrangement of arc extinguishing grids in order to reduce wear of contactors and improve breaking performance. For high-voltage circuit breakers, the analysis has been used for insulation design by predicting the reduction in dielectric strength due to a decrease in gas density of the high-temperature gas that is generated by arc heat generation and that diffuses inside.

For improving the analytical precision, modeling relating to the atmospheric gas generated by temperature increase to a few thousand Kelvin of the arc generated between contacts in view of complicated physical phenomena including dissociation and ionization is essential. Fuji Electric has applied this technology to develop design technology for ensuring safety in the event of arc fault inside switchgears. To switchgear for overseas markets, an IEC standard (IEC 62271-200) is applied. This standard contains strengthened approaches to safe structures such as classification of structures relating to operation continuity during failure and maintenance and classification relating to protection of people in the surrounding areas, which has made development of new technology necessary in order to meet these requirements. One major issue is to avoid increase in analysis time due to expansion of the analysis domain and increase of computational load in relation to prediction of pressure rises in the event of internal arc faults, which required reconsideration of the analysis method. To that end, we aimed to realize both reduced computation time and ensured analytical precision and measured the behavior during pressure relief operation, which involves high computational load, and reflected the results to analysis, thereby developing an analysis method specialized in prediction of pressure rises in the event of in-

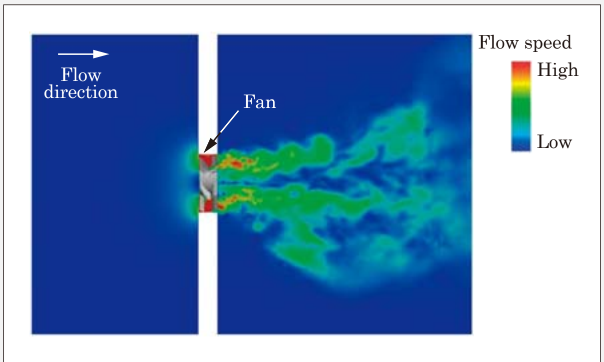

Fig.9 Fan flow speed distribution (instantaneous value)

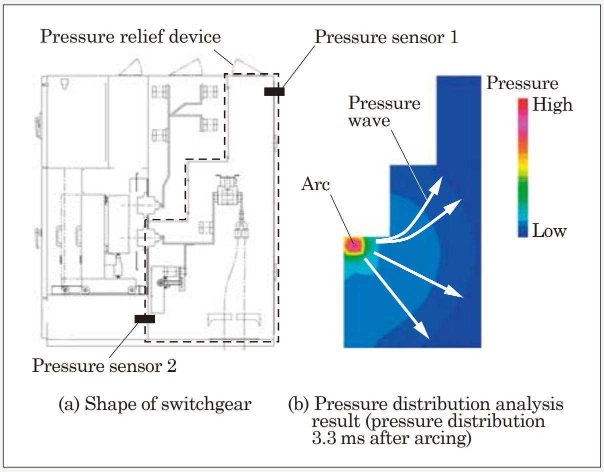

Fig.10 Example of switchgear shape and pressure analysis result

issue: Simulation Technologies for Product Development ternal arc faults (see Fig. 10). By using this method, we have developed a product that ensures safety in the event of internal arc faults in switchgears (Refer to “Analysis of Pressure Rise During Internal Arc Faults in Switchgear” on page 47).

3.4 Thermo-fluid simulation

Fuji Electric offers “smart stores” that make efficient use of energy at stores such as supermarkets and convenience stores. In these stores, freezing-refrigerating equipment including open showcases consume the most energy. For energy saving of open showcases, performance improvement of air curtains by reduction of heat entering through them is required. Frosting of the evaporator that generates cold air causes deterioration of the circulating air volume and characteristics of an air curtain. To address this issue, we have developed a thermo-fluid simulation technology that allows prediction of chronological variations of air curtain performance caused by frost formation and used this technology to develop a new air curtain system.

For simulation with frost formation taken into consideration, we have built a calculation model that allows estimation of the wind speed decrease of the evaporator due to growth of frost and temperature and humidity variations, which has made it possible to predict the average temperature rise over time in a showcase. In addition, we have built a showcase design tool (see Fig. 11) capable of automatic creation of simulation models and developed an optimization design technology for balancing between the many design factors for open showcases.

The new air curtain system developed by the optimization design technology has achieved a reduction in the supply air flow speed of an air curtain by gradually mixing the cold air from the back with the air curtain. It has been confirmed to offer an energy saving effect of over 30% from the conventional system through evaluation with a demonstration model (Refer to “Thermo-Fluid Simulation Technique for Achieving Energy Saving in Open Showcases” on page 53).

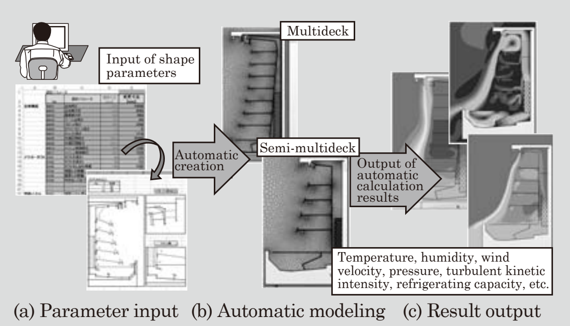

Fig.11 Showcase design tool

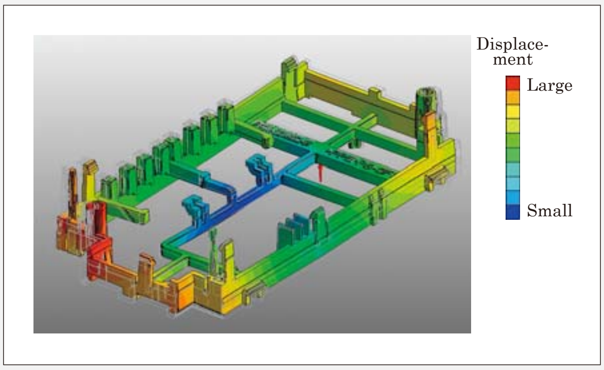

Fig.12 Example of warpage analysis

3.5 Resin flow in molding

Plastic, which has excellent electrical insulating properties and is often provided with kinetic properties and functions that can be used for industrial parts, is used in many products. In molding of plastic parts, it is important to build quality in the initial phase of development, when the degrees of freedom of the product shapes and mold structures are high and modification costs are low.

Fuji Electric is also working to raise the quality of injection molded parts by utilizing resin flow simulation and other simulation technologies with the focus given to resin, which is the principal ingredient of plastic materials.

For warping of moldings, which affects the functions of parts, fit with other parts and feasibility of automatic assembly, we use a 3D printer to output the shape after deformation obtained by resin flow simulation for verifying assemblability (see Fig. 12). In addition, to avoid the formation of welds in high-stress areas and achieve a structure that discharges the corrosive gas generated as resin decomposition gas, we have applied a filling simulation to study product shapes and gate locations.

To improve productivity by decreasing the cool time for injection molded parts, we have established high-speed molding technology that significantly reduces the molding cycle time while ensuring high quality by actively controlling the mold temperature in the molding cycle. We have combined this technology with a prediction of resin temperature distribution by resin flow simulation and used a 3D printer to produce parts with a 3D cooling channel formed inside. In this way, we have realized uniform mold temperature (Refer to “Simulation Technologies Supporting Quality Improvement in Injection Molding” on page 57).

4. Postscript

This paper has described the current status and future outlook of simulation technologies for product development. In the future, we intend to improve the efficiency of research and development and product design by adopting ever-advancing simulation technologies before others and applying them to a wider range of fields and applications for providing products that meet customer needs in a timely manner.

Simulation Based Prediction of SiC Trench MOSFET Characteristics

KOBAYASHI, Yusuke* KINOSHITA, Akimasa* ONISHI, Yasuhiko*

ABSTRACT

The development of semiconductor devices that use SiC (silicon carbide) based materials has been increasing as a means of achieving further energy savings in power electronic products. SiC trench MOSFET are capable of reducing loss even more than conventional planar types. Fuji Electric is implementing simulation based characteristic prediction in order to improve the efficiency of new SiC device development. It is necessary to consider the newly utilized crystal surface characteristics for the simulation of the trench-type because the characteristics of SiC differ by its crystal surfaces. We have established a convenient method for incorporating the parameters into the simulation model, which enabled reproduction of actual observations and prediction of performance improvements.

1. Introduction

There has been an increasing need for energy conserving products that can contribute to achieving a low carbon society. In addition, semiconductor devices for use in power electronics equipment are also being required to deliver energy savings. In recent years, there has been frequent development and commercialization of semiconductor devices that adopt silicon carbide (SiC) as a material capable of dissipating less power.

Fuji Electric has also commercialized energy-conserving power electronics equipment that utilizes SiC metal-oxide-semiconductor field-effect transistor (SiC-MOSFET) and SiC Schottky barrier diode (SiC-SBD) such as its power conditioning sub-systems for large-capacity mega solar facilities[1].

In order to reduce loss in SiC devices, it is useful to understand the internal state of devices at the time of applying a voltage, and then improve on the device structure. The use of device simulations can make it easier to understand the internal state of devices, while also making it possible to know with high efficiency the improvement effect of changing multiple design parameters.

2. SiC Trench MOSFET

Currently, the mainstream type of SiC-MOSFET is the planar MOSFET. It forms a gate on the substrate surface. In order to respond to the market demand for further energy savings and cost reductions, it has been effective to decrease on-resistance $R_{on} \cdot A$ during MOSFET conduction. As such, trench MOSFET have been attracting attention as a next-generation structure (see Fig. 1). Since the trench MOSFET embeds the gate in the trench, it is expected to reduce on-resistance via cell pitch reduction as compared with the planar MOSFET[2]. However, when attempting to make use of high breakdown electric field intensity, which is a characteristic of SiC, there is concern that breakdown could occur as a result of a high electric field being applied to the oxide film on the bottom of the trench[3]. Therefore, in order to ease the electric field intensity of the oxide film, we have been developing a trench MOSFET that equips the bottom of the trench with a p^+ type layer.

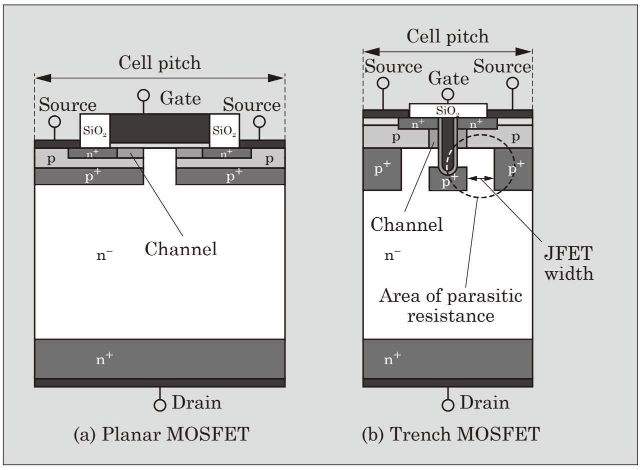

Fig.1 MOSFET cross-sectional view

In order to reduce on-resistance, a structure design that minimizes parasitic resistance after accurately estimating channel resistance is very important. Parasitic resistance can be reduced by expanding the width of the n-type layer that is enclosed by the p^+ type layer and by intensifying the impurity concentration, but withstand voltage will drop due to the simultaneous concentration of electric field in the corner of the deep p^+ type layer. As a result, design must be imple-

* Corporate R&D Headquarters, Fuji Electric Co., Ltd.

mented so as to minimize parasitic resistance in consideration of the trade-off between on-resistance and withstand voltage.

3. SiC Trench MOSFET Simulation

3.1 Simulation tasks

The use of simulations makes it possible to clarify the optimum structure and dimensions for on-resistance and withstand voltage, while increasing the potential for shortening development time by decreasing the number of trial productions. Furthermore, making use of high-precision simulations can lead to the analysis of unexpected phenomena. However, since current device simulations are configured based on data acquired from silicon, they may not always yield the accuracy required for SiC. For example, attention needs to be paid to how the electrical behavior of SiC differs based on the crystal surface*1. The crystal surface orientation and atomic arrangement of SiC is shown in Fig. 2. Either a carbon face (C-face) or silicon face (Si-face) is used for the channel component of the planar MOSFET (see Fig. 1), whereas either an a-face or m-face of the side wall of the created trench is used as a channel for the trench MOSFET. Since the channel characteristics differ from the planar MOSFET, new simulation parameters need to be created. In addition, the impact ionization coefficient(4) is also different for SiC as a result of the crystal surface, thus making the withstand voltage of the a-face and m-face lower than that of the Si-face and C-face. Since the depletion layer extends from the p^+ type layer, the place enclosed by the p^+ type layer of the bottom of the trench and the p^+ type layer below the source functions as a junction field-effect transistor (JFET) parasitic element. The place of concentration of electric field when retaining the withstand voltage depends on the width of JFET, and since the cell pitch and the width of JFET are more narrow for the trench MOSFET than the planar MOSFET, there will be a subtle change in withstand voltage with respect to the dimensions, enabling high-precision calculation of withstand voltage for both the a-face and the m-face.

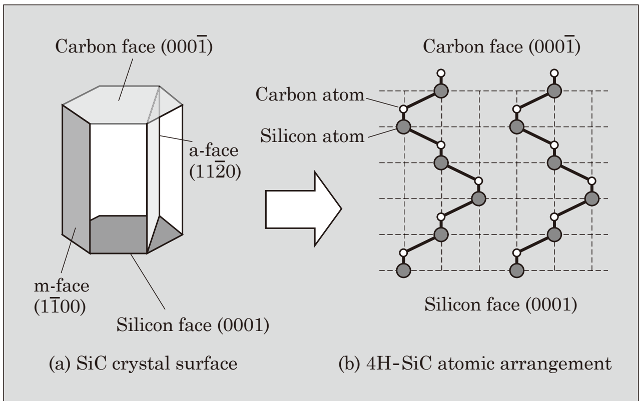

Fig.2 SiC crystal surface and atomic arrangement

In this regard, it can be thought that simulation models and parameter adjustments are not currently being sufficiently implemented for SiC with respect to actual experimental data. In order to accomplish these tasks, we utilized SenTaurus*2 by Synopsys to improve the accuracy of simulations(5).

3.2 Adoption of Coulomb scattering model

We studied mobility in order to consider the crystal surface dependence of the channel characteristic via simulation. As shown in Fig. 3, it can be seen that dominant factors differ for channel mobility, namely, Coulomb scattering, phonon scattering and surface roughness scattering*3 as a result of electric field intensity of the gate oxide film(6). Furthermore, since SiC is characterized by a large number of defects for the oxide film and interface, low electric field mobility decreases(7)(8). By introducing defects into the simulation, the poor convergence of calculation creates the problem of there being a need to adjust many parameters. Therefore, we matched up maximum mobility with the actual values by adjusting the high electric field mobility parameters. However, channel resistance is determined by integrating mobility as shown in Fig. 4, and in addition, it is necessary to make adjustment for the low electric field mobility curve in order to improve calculation precision. Therefore, we used a Coulomb scattering model that was capable of adjusting the low electric field mobility to implement a means of reproduction. As shown in Fig. 4, the new model has decreased the error between the simulation results and the actual mobility integration. In this manner, we have constructed a high-precision simulation capable of calculating channel resistance. The simulation

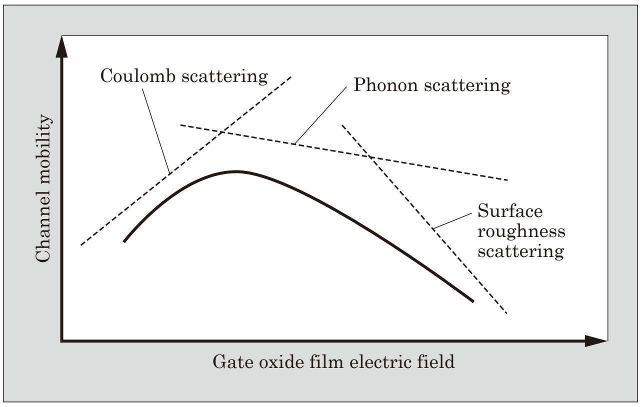

Fig.3 Universal curve of channel mobility

*1: Crystal surface: Refer to “Supplemental explanation 1” on page 62.

*2: SenTaurus is a trademark of Synopsys, Inc. in the U.S. and/or other countries.

*3: Coulomb scattering, phonon scattering and surface roughness scattering: Refer to “Supplemental explanation 2” on page 62.

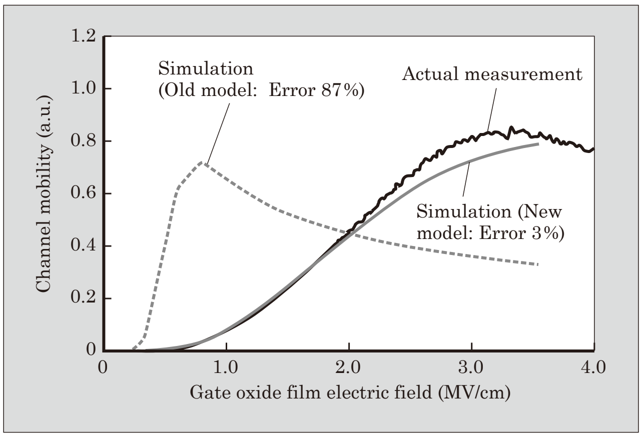

Fig.4 Comparison between channel mobility actual measurement values and simulation

makes it easy to implement adjustments and exhibits good calculation convergence.

3.3 Optimization of the impact ionization coefficient

We have studied the parameters related to the crystal surface of the impact ionization coefficient and have improved the accuracy of the withstand voltage calculation. The electric field distribution inside the device when retaining the withstand voltage is shown in Fig. 5. This suggests that an electric field concentrates in the corner of the p-type layer and that the various characteristics of the crystal surface compound to determine the withstand voltage. By adopting a Hatakeyama model[4] in the simulation, it is possible to reproduce the differences in the impact ionization coefficient by means of the SiC crystal surface. Since current parameters are set to the values obtained based on the actual values of low withstand voltage devices, it is necessary to improve calculation precision for high withstand voltage. The actual high withstand voltage parameter values for the Si-face and C-face are as reported[9], and by adopting these into the simulator, it is possible to improve precision[10].

We estimated the parameter error for the a-face

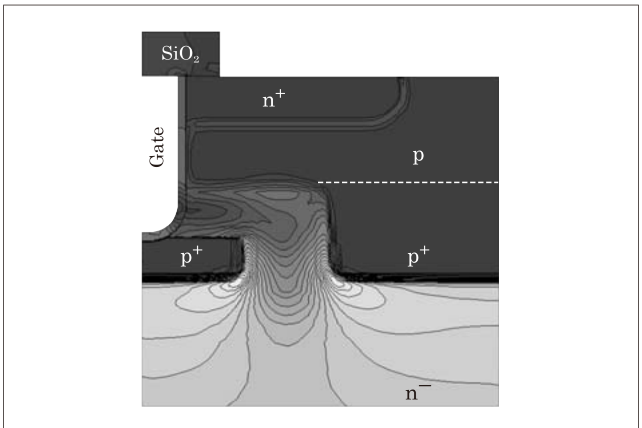

Fig.5 Electric field intensity distribution inside device when retaining withstand voltage

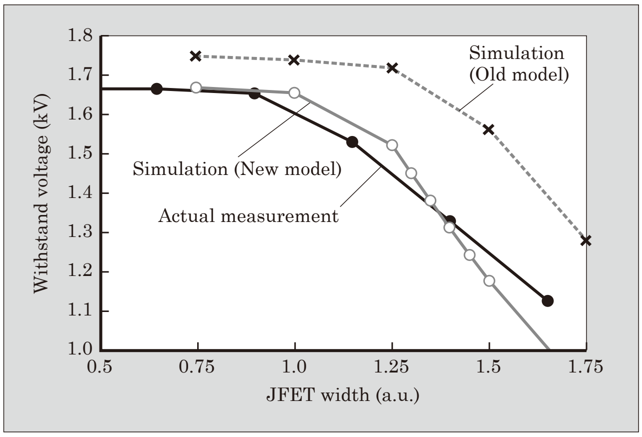

Fig.6 Withstand voltage JFET width dependence

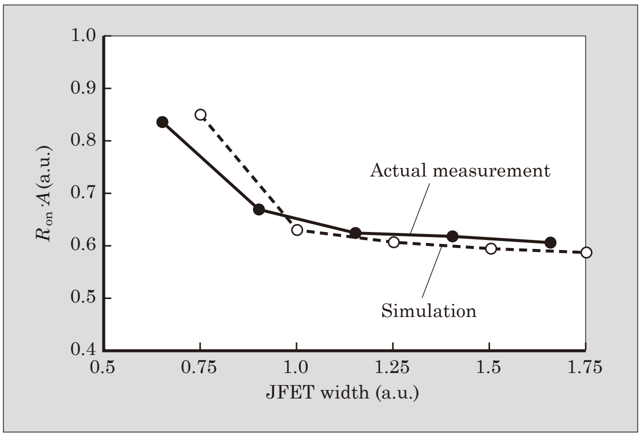

Fig.7 $R_{on}{\cdot}A$ JFET width dependence

and m-face and reconstructed the setting values. It was learned that the simulation results of the JFET width dependence of the withstand voltage after reconstructing the parameters closely matched the actual measurement values (see Fig. 6). In addition, Fig. 7 shows the JFET width dependence for $R_{on}{\cdot}A$. When the withstand voltage is high, there is a tendency for the on-resistance to rise due to the parasitic resistance of the JFET, and it can be seen that there is a trade-off relationship between $R_{on}{\cdot}A$ and withstand voltage. By using the high-precision simulation that we constructed during this study, it has become easy to optimize device structure in consideration of trade-off.

4. Improvement of Device Characteristics via Simulation

By taking into account the new model introduced in Chapter 3, we studied how to improve device characteristics by using a precision enhanced simulation.

4.1 Improvement of trade-off between on-resistance and withstand voltage

In order to improve the trade-off between $R_{on}{\cdot}A$ and withstand voltage, we investigated particularly large areas of JFET parasitic resistance. The elec-

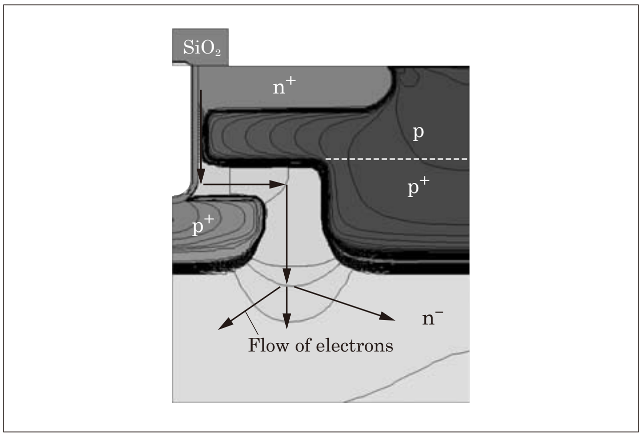

Fig.8 Electric potential distribution inside device when “ON”

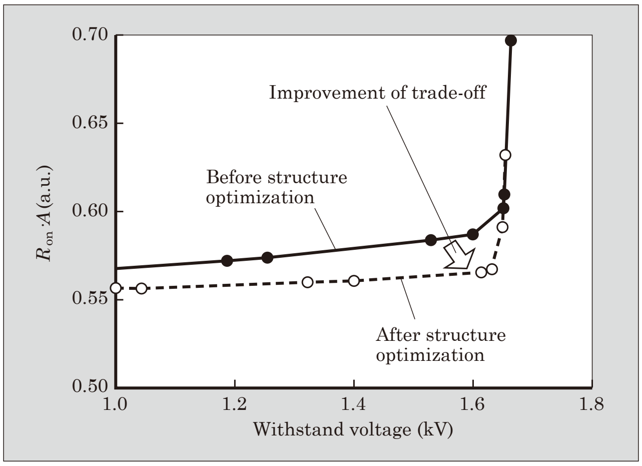

Fig.9 Trade-off between R_{on}·A and withstand voltage before and after device structure optimization

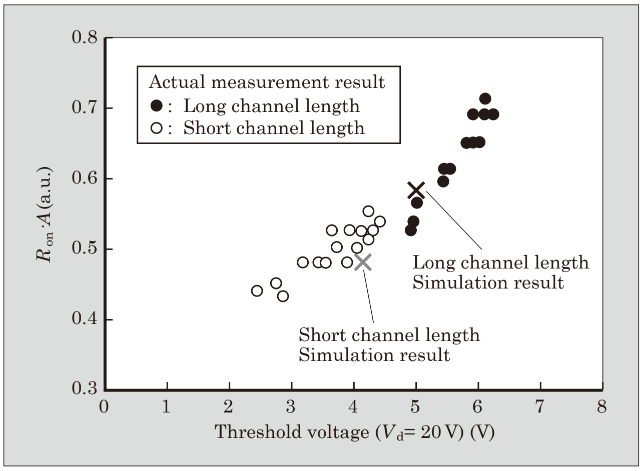

Fig.10 Relationship between R_{on}·A and threshold voltage

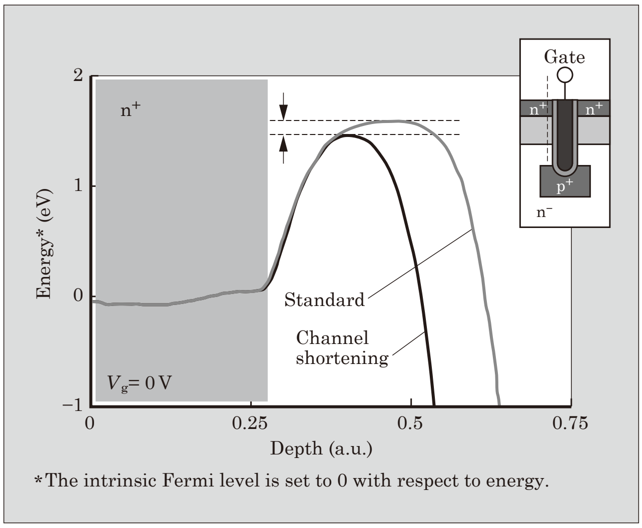

Fig.11 Conduction band figure of channel

tric potential distribution inside the device when on is shown in Fig. 8. Since parasitic resistance is large for areas with thick potential lines, optimizing device structure with priority given to these areas increases expectation that the trade-off between R_{on}·A and withstand voltage can be improved. Figure 9 shows the trade-off between R_{on}·A and withstand voltage before and after device structure optimization. We learn that the trade-off can be improved by optimizing the impurity concentration of the n-type layer and the device structure.

4.2 Channel shortening

The relationship between the R_{on}·A of a channel-length shortened trial production and threshold voltage V_{th} is shown in Fig. 10. R_{on}·A can be reduced as a result of shortening the channel length to reduce channel resistance. However, since the threshold value decreases at the same time, the relationship between R_{on}·A and V_{th} becomes nearly a straight line. The cause was analyzed by simulation.

Figure 11 shows the conduction band of the channel. The height of the peak of the convex part of the conduction band determines the V_{th}, but we learned that the height of the convex part decreases as a result of channel shortening. We also learned that this is due to one of the effects of channel shortening, namely, drain induced barrier lowering (DIBL), for which V_{th} is affected by the depletion layer that extends from the drain side.

5. Future Tasks

The construction of high-precision simulations plays a role in shortening the development time of high-quality, high-performance devices. Since SiC is a new material compared with conventional silicon, it is necessary to improve precision even for calculations other than on-resistance and withstand voltage. For example, a few items requiring improvement would include the reproduction of temperature dependence, reproduction of impurity concentration dependence, reproduction of the impact of the number of defects caused by the creation of simplified types, reproduction of leakage current characteristics and reproduction of device reliability.

6. Postscript

In order to predict the characteristics of SiC trench MOSFET, we studied simulation models and parameters related to SiC crystal surface dependence, thus enabling us to reproduce actual measurement values, verify performance improvement methods and analyze physical phenomena. Since the construction of high-precision simulations plays a role in shortening the development time of high-quality, high-performance power devices, we will continue our efforts to improve the precision of SiC simulations, while striving to contribute to the realization of an energy-conserving society.

This research was carried out as part of a project of the joint research body "Tsukuba Power Electronics Constellations (TPEC)." We would like to conclude by expressing our appreciation to all those involved in this project.

References

(1) Matsumoto, Y. et al. Power Electronics Equipment Applying SiC Devices. FUJI ELECTRIC REVIEW. 2012, vol.58, no.4, p.212-216.
(2) B. J. Baliga, Microelectronic Engineering, 1995, vol.28, p.177-184.
(3) Harada, S. et al. Power Semiconductor Devices and ICs (ISPSD), 2012, p.253-256.
(4) Hatakeyama, T. et al. Materials Science Forum, 2003, vol.457-460, p.673-676.
(5) SenTaurus on http://www.synopsys.com/, (accessed 2015-12-10).
(6) Takagi, S. et al. Electron Devices IEEE Transactions, 1994, vol.41, p.2357-2362.
(7) Ono, S. et al. Materials Science Forum, 2014, vol. 778-780, p.571-574.
(8) Kutsuki, K. et al. Materials Science Forum, 2015, vol. 821-823, p.757-760.
(9) Niwa, H. et al. Materials Science Forum, 2014, vols. 778-780, p.461-466.
(10) Shiomi, H. et al. International Conference on Silicon Carbide and Related Materials (ICSCRM), Th-P-34, 2015.

Development of SiC Bipolar Devices Using Simulation

MATSUNAGA, Shinichiro* **TAKEI, Manabu***

ABSTRACT

In SiC (silicon carbide) devices, which are wide band-gap semiconductors, bipolar devices are considered beneficial for achieving a high withstand voltage in excess of 13 kV. Fuji Electric has improved prediction accuracy by repeatedly adjusting parameters based on the analysis of differences between simulation predictions and actual results. We implemented withstand voltage characteristic simulations, forward characteristic simulations, and switching characteristic simulations, and then reflected the measured physical property values into the parameters, while also taking into account interface charges and parasitic resistance. As a result, we were able to reproduce with a high level of accuracy the characteristics of actual devices.

1. Introduction

In recent years, wide band-gap semiconductors have started to be put to practical use as semiconductors for power devices, replacing conventional silicon (Si) ones. Wide band-gap semiconductors can offer device characteristics of a high withstand voltage and low resistance because they have a low intrinsic carrier concentration and do not produce a leakage current easily unless a higher temperature/electric field than that which causes Si to do so is applied. Table 1 shows the physical property values of major wide band-gap semiconductors[(1)]. For silicon carbide (SiC) devices, in particular, materials and constituents have been improved through research and development for many years. Some unipolar devices have already been commercialized, including Schottky barrier diodes and transistors (metal-oxide-semiconductor field-effect transistor [MOSFET], junction field-effect transistor [JFET]). On the other hand, bipolar devices, which have excellent properties as large-current high-withstand-voltage devices, are still in the stage of research and development. This is because some issues remain regarding the characteristics and processes of p-type semiconductors used as a supply source of hole carriers, and the problem of degradation promoted by the recombination of holes and electrons has not been solved yet.

Table 1 Physical property values of wide band-gap semiconductors

Item	Wide band-gap semiconductor				Si
	3C-SiC	4H-SiC	6H-SiC	GaN	
Band-gap (eV)	2.36	3.26	3.02	3.42	1.12
Electron mobility (cm^2/Vs)	1,000	1,000	450	1,500	1,350
Hole mobility (cm^2/Vs)	100	120	100	150	600
Dielectric breakdown strength (MV/cm)	1.4	2.8	3.0	3.0	0.3
Saturated drift velocity (cm/s)	2.0×10^7	2.2×10^7	1.9×10^7	2.4×10^7	1.0×10^7
Thermal conductivity [W/(cm·K)]	4.9	4.9	4.9	2.0	1.5
Baliga's figure of merit*	62	495	274	1,128	1

* Baliga's figure of merit is a figure of merit for unipolar devices proposed by Baliga. It is an indicator of the limitation characteristics determined by materials.

By using simulations to predict ideal characteristics and comparing them with the result of actual measurement, we can identify problems in the devices and make use of them for improvement. The accuracy with which various physical property parameters and process dependence can be identified has also been improved by fitting data between the simulation and the result of measuring electrical characteristics using prototypes.

2. SiC Bipolar Devices

The research and development of bipolar devices which allow large-current operations, such as SiC-PiN diode or SiC insulated-gate bipolar transistor (SiC-IGBT), has continued since 2009 at the National Institute of Advanced Industrial Science and Technology. This R&D is part of the Tsunenobu KIMOTO project of the Funding Program for World-Leading Innovative R&D on Science and Technology (FIRST). Fuji Electric has also been participating in

* Corporate R&D Headquarters, Fuji Electric Co., Ltd.

this project since the beginning. Bipolar devices require a bias voltage higher than the built-in voltage related to the band gap for forward operation, and SiC requires 2.5 V or higher. Although unipolar devices have high resistance, they have no built-in voltage. Consequently, bipolar devices are expected to have advantages in terms of conduction loss probably in a high-voltage region where the withstand voltage exceeds 5 kV. Figure 1 shows examples of structural cross-sectional views of a PiN diode and an n-type IGBT. Figure 2 shows photos of the prototypes of an n-type IGBT chip and wafer.

From the beginning, FIRST set 13-kV-class devices as a target, developed an n-type IGBT with target specifications of a 13-kV withstand voltage, 11 mΩcm^2 characteristic differential on-resistance, 8 × 8 mm^2 chip size and 60 A per chip, and confirmed the switching operation at 6 kV.

In order to obtain a withstand voltage exceeding 10 kV, even SiC devices which can provide a high-withstand voltage require a low impurity concentration layer of 150 µm or more. Unlike Si, there is no SiC substrate with a low impurity concentration. One of the methods of creating a substrate is the sublimation method that sublimates SiC powder material at the extremely high temperature of 2,000 °C or more to grow a layer on a seed crystal. Unfortunately, the substrates created by this method cannot avoid being contaminated with the surrounding materials. Hence, it is impossible to keep impurities to 1 × 10^{16}/cm^3 or less, which is required of high-withstand voltage devices. PiN diodes use wafers on which a low-impurity-concentration layer is epitaxially grown on an n-type substrate with a CVD device. On the other hand, there is no p-type substrate for n-type IGBTs that has a low defect density applicable to creating devices. As a countermeasure, they create a substrate by epitaxially growing a low-concentration n layer of 150 µm or more on an n-type substrate and then a high-concentration p layer of approximately 200 µm on it, and scraping off the n-type substrate completely. Due to the use of thick epitaxial layers having different types of impurities and concentration levels, the presence of a certain amount of defects that cause degradation is inevitable. There are problems of not only the person-hours required for substrate manufacturing, but also the frequent breakage of substrates due to large warpage and high stress, resulting in an insufficient number of prototypes.

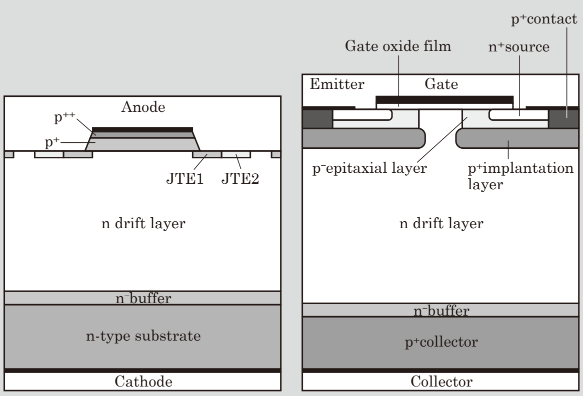

Fig.1 Examples of structural cross-sectional views of PiN diode and n-type IGBT

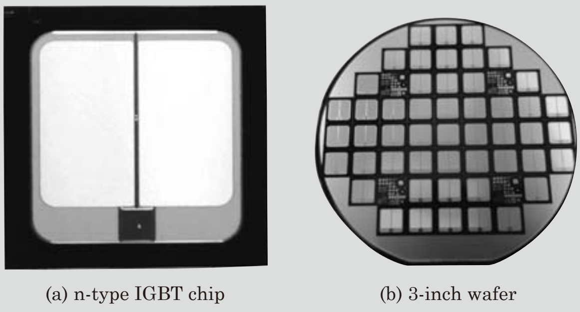

Fig.2 Prototypes of n-type IGBT chip and wafer

3. Simulation Using Ultra-High-Withstand Voltage Bipolar Devices

3.1 Challenges in simulation

Since the number of prototypes for development is limited, it is effective to use device simulation to consider a preliminary design. Unfortunately, the accuracy of the parameters for conducting a simulation is imperfect compared with the case of Si. The characteristics concerning p-type semiconductors, in particular, often show lower performance than the ideal values, and greatly depend on the processes specific to manufacturing lines. Table 2 shows major causes for simulation errors of ultra-high-withstand voltage bipolar devices. We improved the prediction accuracy by analyzing the differences between the results of the simulation prediction and actual measurement and repeatedly correcting the parameters.

The simulation of wide band-gap semiconductors uses more bits than usual for a floating point calculation because it is necessary to improve the calculation accuracy so that low leak current characteristics can be

Table 2 Major causes of simulation errors

Item		Cause
Related to p-type semiconductor	Low ionization rate	Deep Al impurity level
	Low activation rate	Damage or low recovery from ion implantation
	High contact resistance	Immature silicide electrode process
Related to thick epitaxial film	Low mobility	Existence of defect/downfall
	Low lifetime	The process centers on recombination resulting in the existence of defects of density in the order of 10^{12} to 10^{13}/cm^3.

handled. Consequently, the calculation tends to take longer. In order to improve convergence, carrier concentration is enhanced artificially with heat and light excitation and calculations are performed within the range where the actual withstand voltage is not affected.

3.2 Simulation of withstand voltage characteristics

Several institutions have reported the electric field dependence of an impact ionization coefficient that greatly affects withstand voltage calculations, including doping density dependence and temperature dependence[1]. The currently used SiC has a configuration of a hexagonal crystal system called 4H, and is anisotropic in terms of mobility and an impact ionization coefficient. There have been reports on the use of an anisotropic impact ionization model that defines a value in the direction of the <0001> axis and a value in the direction perpendicular to the axis individually. It is suggested this would improve the accuracy of the withstand voltage simulation at the device termination section where the electric field in the direction perpendicular to the <0001> axis is important[2].

Figure 3 shows a diagram of the termination structure of a 13-kV n-type IGBT. In order to mitigate the horizontal electric field intensity at the termination section, the junction termination extension (JTE) forms a p-type impurity layer. To achieve an ultra-high-withstand voltage, we provided JTE sections with 2 different levels of concentration. The JTE has a length of 500 μm, providing an extremely short termination structure compared with high-withstand-voltage Si devices. In order to achieve a structure with a high withstand voltage, it is necessary to adjust the JTE concentration so that the electric field intensity from the inside to the outside of the JTE is uniform.

As stated above, you cannot use n-type SiC substrates directly to create n-type IGBTs, and so experimental prototyping of many number of substrates is difficult. On the other hand, PiN diodes can be created with n-type substrates and it is relatively easy to prepare substrates for experimental prototyping. Consequently, we started experimentally prototyping high-withstand-voltage devices from PiN diodes. Figure 4 shows the JTE dose dependence of the withstand voltage in a PiN diode. It shows the predicted values of the simulated withstand voltage and the results of measuring a prototype of PiN diodes in which impurity concentration levels in the drift layer are $5 \times 10^{14}/cm^3$ and $6 \times 10^{14}/cm^3$. The JTE dose on the X axis represents the total amount of impurities per unit area which is ion-planted to the JTE section; and the Y axis represents the withstand voltage.

The withstand voltage values tend to become higher as the JTE dose increases; however, the values of the simulation prediction and actual measurement do not coincide. This PiN diode has anode electrodes formed on the SiC carbon face (C-face) as in the case of IGBTs, so that the p-type JTE region of the termination section is also formed on the C-face. MOS capacity measurement has suggested the existence of a large quantity of interface charges on the interface between the p-type SiC and oxide film. These interface charges may have some influence on the withstand voltage. Figure 4 is the result of the withstand voltage simulation in which positive charges are placed on the interface. We found that the measured value and simulation prediction value coincide when approximately $2 \times 10^{12}/cm^2$ of positive charges exist.

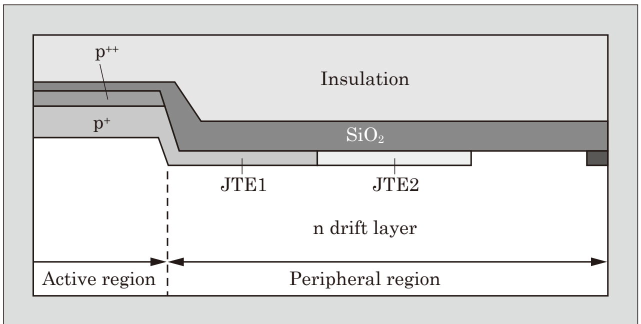

Fig.3 Diagram of termination structure of 13-kV n-type IGBT

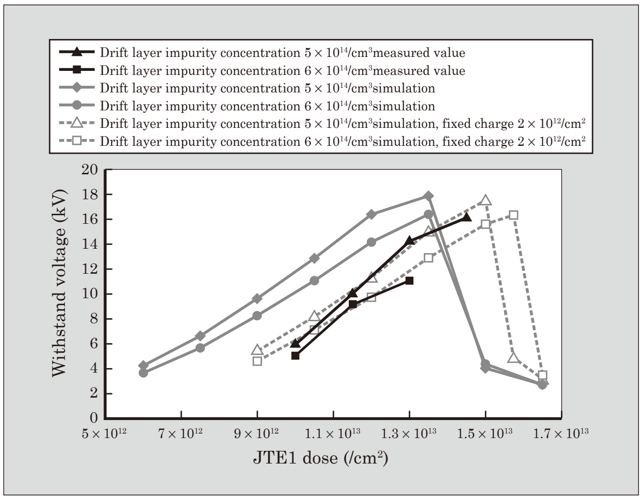

Fig. 4 JTE dose dependence of withstand voltage in PiN diode

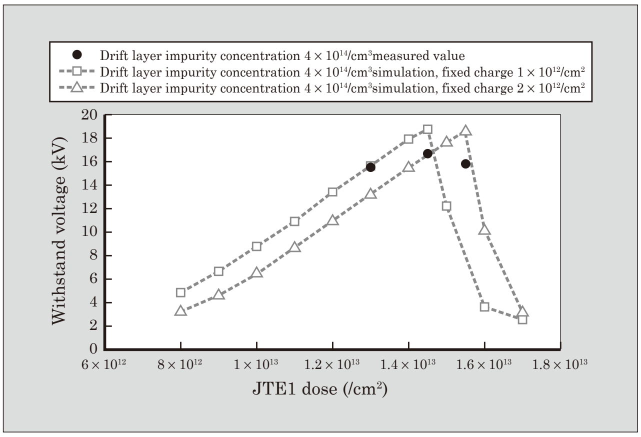

Fig.5 JTE dose dependence of withstand voltage in n-type IGBT

Figure 5 shows the JTE dose dependence of the withstand voltage in an n-type IGBT. It compares the predicted withstand voltage value and the withstand voltage of actual measurement of an n-type IGBT. In an IGBT, holes flow in through the p-type collector on the back side. Consequently, a drop of several kV in the withstand voltage is expected compared with the case of PiN diodes. By applying the prototyping result of the device for a PiN diode withstand voltage evaluation and adjusting the JTE dose in advance considering the amount of fixed charges, we obtained a target withstand voltage that exceeds 13 kV.

3.3 Forward characteristics simulation

Simulating the forward characteristics of bipolar devices requires actual mobility and lifetime of electrons and holes. For a thick n-type drift layer exceeding 150 µm, the ideal lifetime is 10 µs or more; however, the current lifetime remains at several µs or less. The $Z_{1/2}$ center, which is the typical point defect of SiC, is said to be the killer level making the lifetime shorter. A report suggests that p-type semiconductors have a specific killer level resulting from the point defects related to Al acceptors. It is considered that this level may also have an influence on bipolar devices. Predicting the hole implantation amount requires the activation rate and ionization rate of the p-type layer. The activation rate of the impurities in an epitaxially grown p-type layer is almost 100%, whereas in the case of ion implantation, the activation rate greatly depends on the process. Moreover, Al acceptors, which are the source of hole carriers, exist in a deep level so that their ionization rate at room temperature is low. Due to imperfect accuracy of the temperature, concentration and process dependence in the parameters including lifetime, ionization rate and activation rate, the accuracy of predicting the forward characteristics is insufficient.

Figure 6 shows the forward characteristics of a 13-kV PiN diode. It compares the I-V waveforms of the simulation and actual measurement result of the PiN diode using a p-type epitaxially grown layer as an anode at room temperature and 200 °C. The characteristics in the minute current range near the built-in voltage that is dependent on the band gap are close to and coincide well with the ideal values. In the large-current region, however, the measured forward voltage V_{on} is higher and indicates higher resistance than that in the ideal state. It is expected that the inclusion of large-resistance components is caused by the fact that the current increased linearly instead of exponentially with the bias voltage.

A p-type SiC tends to have higher contact resistance with the electrode than that of an n-type SiC. And it can be thought that this diode has a high contact resistance in the order of $10^{-2}\,\Omega\mathrm{cm}^2$ at room temperature. Although measurement using the transfer length method (TLM) showed a contact resistance in the order of $10^{-3}\,\Omega\mathrm{cm}^2$, an actual device seems to have several times higher resistance. Another institution has also reported an example of improved forward characteristics when the electrode formation process was improved to reduce contact resistance. We can expect characteristics to be improved when processes are improved.

The forward voltage of a SiC PiN diode drops at a high temperature. This is because the lifetime becomes longer by several times at a high temperature and the higher ionization rate of Al impurities promotes a better contact resistance and hole carrier injection. The longer lifetime seems to be caused by the fact that the influence of the $Z_{1/2}$ center forming the major killer level decreases at a higher temperature. By considering these factors and applying them to the temperature dependence of the lifetime and contact resistance, we could reproduce the forward characteristics at 200 °C. Figure 7 shows the forward characteristics of a 13-kV n-type IGBT. It compares the results of measurement and simulation of the 13-kV n-type IGBT prototype. This IGBT has the same gate structure as the implantation and epitaxial MOSFET (IEMOS) of the National Institute of Advanced Industrial Science and Technology. Consequently, we estimated its forward characteristics by applying the channel mobility of the IEMOS and the parameters of the PiN diode. It can be thought that a higher operat-

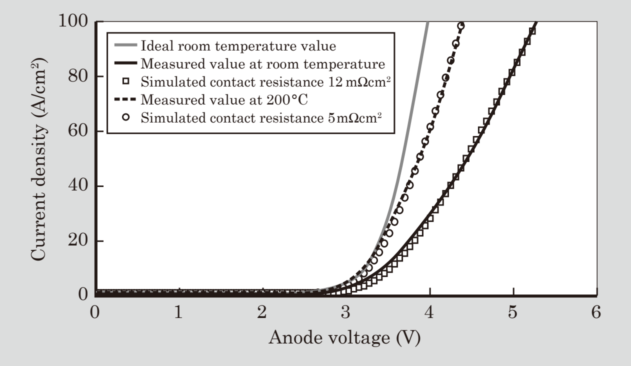

Fig.6 Forward characteristics of 13-kV PiN diode

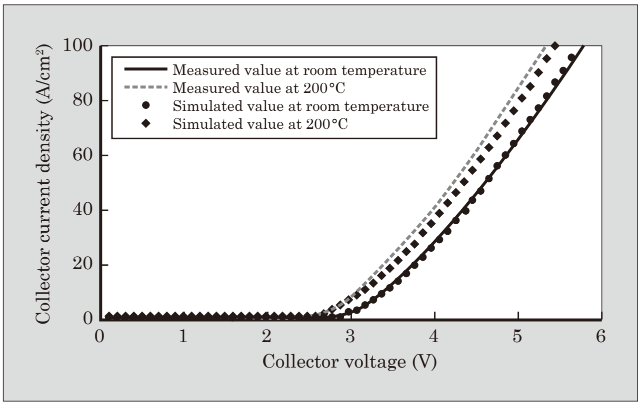

Fig.7 Forward characteristics of 13-kV n-type IGBT

ing voltage than that of the PiN diode is caused by the carrier density on the surface which is still low. We are planning to improve the operating voltage by enhancing the device's surface structure in the future.

3.4 Switching characteristics simulation

Bipolar devices require a longer switching time to draw out carriers injected in high concentration during switching, resulting in a large switching loss. For SiC devices, the thickness of the drift region for keeping the withstand voltage can be reduced to about one-tenth of that of Si devices. Hence, it may be possible to reduce the total amount of the accumulated carriers and cut switching loss. We used a device simulator and a circuit simulator to conduct a switching simulation by taking the inductive load (L load) into account, and predicted the loss in a bipolar device at a bus voltage of 6.6 kV.

The expected switching waveforms of the current structure and the improved structure using the low carrier injection IGBT are shown in Fig. 8. In the current structure, the switching is slow and the transition time is 4 µs or longer. This means that even operation at a carrier frequency of about 1 kHz is difficult. The estimated switching loss is 2 J/pulse or more per active area of 1 cm², which can only be used at low carrier frequencies. The cause of the slow switching is the high injection in the IGBT and diode. The following improvements can reduce the switching loss while minimizing the increase of the conduction loss.

(a) Controlling the amount of carrier injection on the back side.
(b) Using a structure to allow the necessary amount of surface carriers to be accumulated.
(c) Dissipating the excessive carriers quickly.

Using a low-injection structure for the IGBT reduces the turn-off switching time to 400 ns, which improves the switching loss. The low-injection PiN diode can also suppress the reverse recovery current and improve the turn-on loss. The loss estimation result with the improved structure is shown in Fig. 9. When compared with a high-injection structure, the switching loss is reduced to 44% and the total loss including the conduction loss at an operating frequency of 2 kHz is improved by 37%.

We compared the characteristics after the improvement with those of Si devices. In order to achieve a 13-kV withstand voltage class device the same as the SiC devices, Si devices are connected in series. Although we should not make a simple comparison, Fig. 10 suggests the probability that a single 13-kV SiC-IGBT has better forward voltage-switching loss trade-off characteristics than those of several Si devices connected in series. When SiC bipolar devices become applicable to ultra-high-withstand voltage applications, a reduction

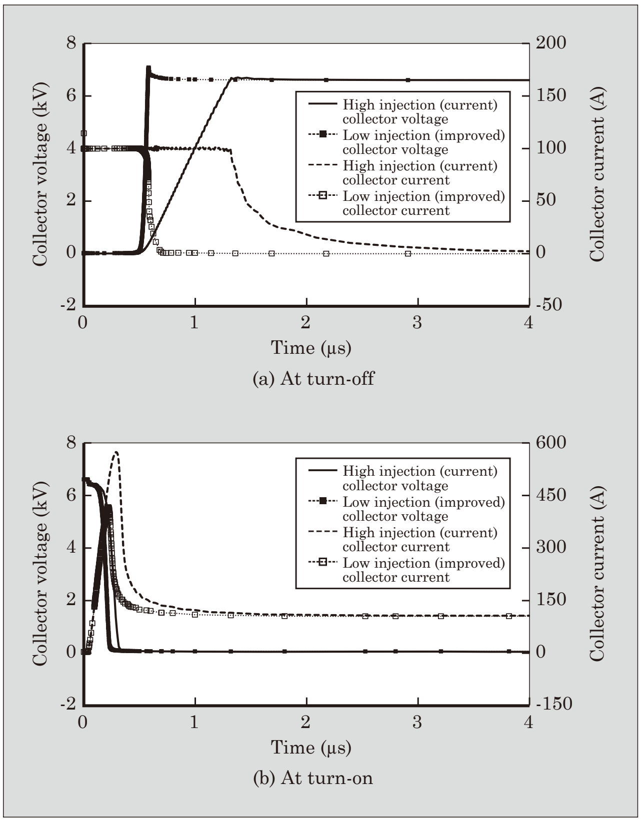

Fig.8 Expected switching waveforms of current structure and improved structure

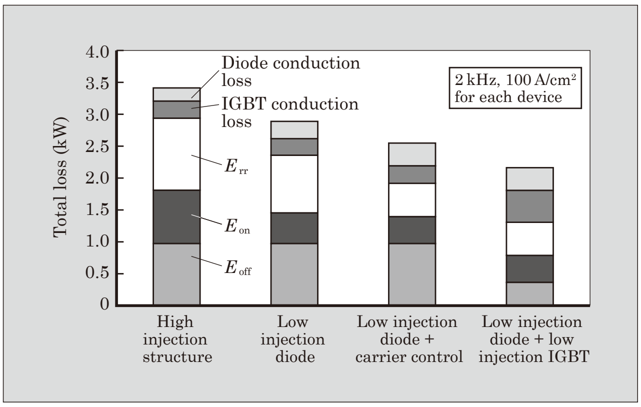

Fig.9 Loss estimation result with the improved structure

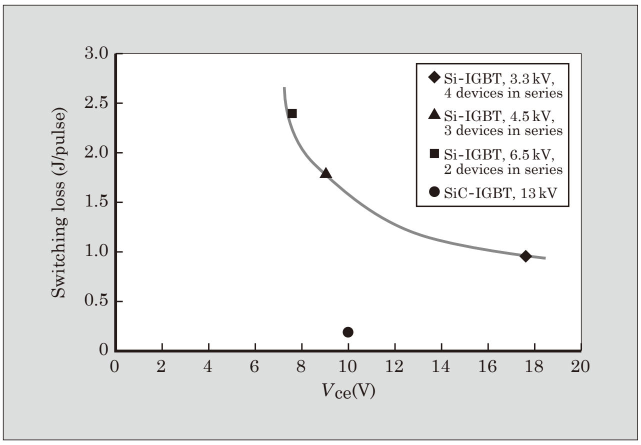

Fig.10 Forward voltage-switching loss trade-off characteristics of devices under 13-kV withstand voltage condition

in loss as well as an improvement of conversion efficiency can be expected.

For example, high-withstand-voltage SiC devices can be used in a reactive power compensator for suppressing the voltage fluctuation in a power system. This enables the current capacity to be reduced and means fewer devices are used, which leads to miniaturization and efficiency improvement of the facility.

4. Postscript

There is a limit to the accuracy of predicting characteristics of ultra-high-withstand voltage bipolar devices because their physical property parameters are lower than those of an ideal crystal. By applying measured physical property values to the simulation parameters and considering the interface charge and parasitic resistance, we could almost reproduce the actual device characteristics. With the progress of process technology, we can expect further improvements in the properties of SiC bipolar devices in the future.

Some of this study was conducted as part of the Kimoto Tsunenobu project of the Funding Program for World-Leading Innovative R&D on Science and Technology (FIRST) of the Japan Society for the Promotion of Science. We would like to express our deep appreciation to the parties involved.

References

(1) Kimoto, T; J.A.Cooper. Fundamentals of Silicon Carbide Technology, Jhon Wiley & Sons Singapore Pte Ltd. 2014.

(2) Hatakeyama, T. et al. "Impact ionization coefficients of 4H silicon carbide", Appl. Phys. Lett. 85, 2004, p.1380-1382.

Atomic Level Analysis of SiC Devices Using Numerical Simulation

HIROSE, Takayuki* MORI, Daisuke* TERAO, Yutaka*

ABSTRACT

Research and development of power semiconductor devices with SiC (silicon carbide) has been very active because of the increasing need for low-loss power electronics equipment. The electrical properties of the SiC-metal-oxide-semiconductor field-effect transistors (SiC-MOSFETs) are affected by charge trapping that is thought to be caused by the atomic level disorder at the interface between the gate oxide and SiC (SiC/SiO_2 interface). In order to analyze the origin of the disorder at the interface, we have been implementing the atomic level analysis using both the X-ray photoelectron spectroscopy and the simulation based on the first principles calculations. As a result, we were able to estimate the chemical state of Si at SiC/SiO_2 interface, as well as its terminated structure via nitrogen when the interface is nitrided.

1. Introduction

Recently, there has been an increasing need for low-loss power electronics equipment for the purpose of realizing a low-carbon society. Fuji Electric has commercialized a great number of power electronics equipment products for uninterruptible power systems (UPSs), various types of electric power application equipment, transportation infrastructures and distribution infrastructures. In order to dramatically reduce the loss of these power electronics equipment products, it is essential to improve the efficiency of inverters by having technological innovation in power semiconductor devices, circuits and control. Currently, wide band gap semiconductors such as silicon carbide (SiC) and gallium nitride (GaN) are attracting attention as the next-generation semiconductor to replace silicon (Si), which is a mainstream material of power semiconductor devices. Vigorous research and development of power semiconductor devices that use these materials is under way.

Fuji Electric has already commercialized Schottky barrier diodes (SBDs) and is currently developing SiC-metal-oxide-semiconductor field-effect transistors (SiC-MOSFETs). To reduce the loss of these SiC-MOSFETs, it is important to improve electrical characteristics such as channel mobility. One possible predominant factor of the electrical characteristics is charge trapping resulting from an atomic level disorder at the interface between the gate oxide (SiO_2) and SiC (SiC/SiO_2 interface). Accordingly, the key to improving electrical characteristics is to identify the substance of this charge trapping.

As an analysis technology for estimating the substance of charge trapping, this paper describes an atomic level analysis technology for SiC devices that employs first-principles calculation as a simulation method in addition to instrumental analysis.

* Corporate R&D Headquarters, Fuji Electric Co., Ltd.

2. SiC-MOSFET

Figure 1 shows the device structure of a SiC-MOSFET. In a MOSFET, voltage is applied to the gate electrode to form an inversion layer in the p well layer at the interface between the gate oxide and SiC substrate. Then, voltage between the source and drain is applied to let electrons to flow into the channel.

Important characteristics of a MOSFET include channel mobility, which has an effect on the on-resistance, and the threshold voltage V_{th}, at which the MOSFET is turned on. If the mobility can be increased, the on-resistance can be decreased, and this will make it possible to reduce the power consumption of equipment that uses the MOSFET.

Figure 2 shows an example of the mobility characteristics of SiC-MOSFETs. The horizontal axis represents the gate voltage V_g. It indicates that the degree of mobility and V_{th} may differ depending on the process. This difference is assumed to be due to the presence of

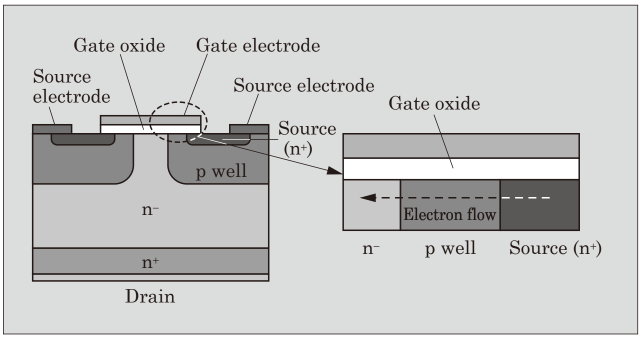

Fig.1 Outline of device structure of SiC-MOSFET

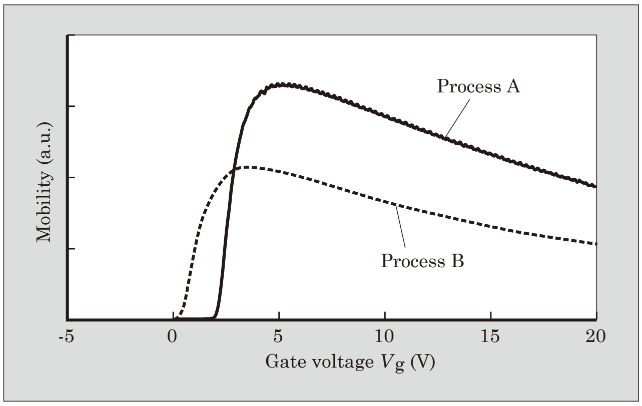

Fig.2 Example of mobility characteristics of SiC-MOSFETs

charge trapping resulting from the atomic level disorder at the SiC/SiO_2 interface. This charge trapping is considered to cause a decrease in mobility due to Coulomb scattering*1 and variation of V_{th}. Accordingly, to lower the on-resistance and to improve reliability by suppressing the variation of V_{th}, reducing the atomic level disorder is the key.

One indicator of atomic level disorder is interface state density. SiC substrates have different crystal surfaces such as the Si-face and the C-face, and they show different interface state densities. For example, Dhar et al. have reported that, when the oxide is formed by dry oxidation, the interface state density of the Si-face is lower than that of the C-face[1]. It has also been reported that the interface state density is reduced by nitriding the interface[1 to 3]. In this way, interface characteristics may depend on the crystallographic orientation of the surface and the process.

In order to reduce the interface state density, which is considered to result from the atomic level disorder, it is necessary to understand the substance (chemical states, bonding structures and geometry) of the interface state. To that end, Fuji Electric is working on atomic level analysis of the SiC/SiO_2 interface. For example, we observe the SiO_2 interface by transmission electron microscopy and X-ray photoelectron spectroscopy (XPS) using synchrotron radiation facility, to evaluate the chemical state and bonding structure of the Si atoms and others at the interface. Furthermore, for estimating the link between the bonding structure obtained by the analysis and the electrical characteristics, we conduct analysis that incorporates the first-principles calculation, which will be described later. Unlike Si, SiC is indeed difficult to grasp the substance of the interface states because of its compound nature, but analysis incorporating the first-principles calculation is considered to allow us to estimate the bonding structure and interface state.

*1: Coulomb scattering: Refer to Supplemental explanation 2 on page 62.

3. Analysis by XPS

3.1 Synchrotron radiation XPS

This section describes the analysis of the SiC/SiO_2 interface by XPS using synchrotron radiation facility.

XPS is a method of obtaining atomic information at a depth of a few nanometers from the surface of a sample and it allows quantitative analysis of the chemical state of atoms.

By using this analysis method, we analyzed the chemical state of the interface between SiC and the oxide formed in an oxygen ambient (dry oxidation) or in a nitrous ambient (N_2O oxidation). Both Si-face and C-face SiC surface were used for the measurement.

In order to obtain information about the minute amount of atoms at the interface, we etched the oxide of the samples to the thickness of about 1.5 nm and measured it at a synchrotron radiation facility (SPring-8*2 BL27SU).

Figure 3 shows a schematic diagram of the SiC/SiO_2 interface. SiO_X indicates a region where the oxidation state of Si at the interface has changed. In that region, it is considered that the chemical states of Si atoms continuously change with different numbers of the bonding oxygen. As the components of chemical states of Si, we assumed 3 types of suboxide components (Si^{1+}, Si^{2+} and Si^{3+} *3) in addition to SiC and SiO_2 components[4][5]. We modeled the data envelope to separate each component with different chemical state for

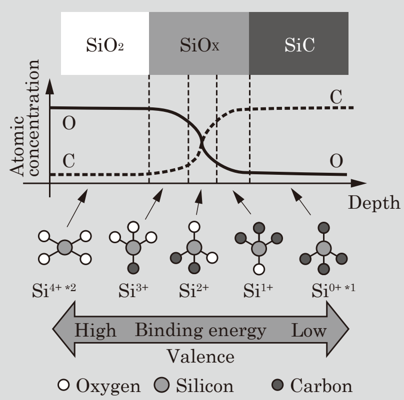

*1: Si^{0+} is a state without oxygen beside the silicon, or the chemical state of SiC.
*2: Si^{4+} is a state with oxygen taking all of the positions beside the silicon, or the chemical state of SiO_2.

Fig.3 Schematic diagram of SiC/SiO_2 interface

*2: SPring-8: Large synchrotron radiation facility capable of emitting the world's highest-performance synchrotron radiation. It is comprehensively managed by the Institute of Physical and Chemical Research (RIKEN) as the facility operator. It is expected to be applied to wide-ranging fields including material science, earth science, life science, environmental science and medical science.

spectra obtained by XPS.

3.2 Analysis of Si spectra

Figure 4 shows Si spectra at the N_2O oxidized SiC/SiO_2 interface. As a result of comparing the amounts of the respective suboxide components, we found the Si^{1+} component showed the largest amount for both the C-face and the Si-face. The amount of the Si^{3+} component for the C-face was about 4 times as large as that for the Si-face.

The tendency of suboxide components at the dry-oxidized interface showed a result similar to that of N_2O oxidation, which is not indicated in the figure.

3.3 Analysis of nitrogen spectra of N_2O oxidation

Figure 5 shows nitrogen spectra at the N_2O oxidized interface. The main components can be attributed to 3-coordinate Si_3N based on the peak position for both the C-face and Si-face[6]. In addition, a shoulder was observed on the high energy side of the nitrogen spectrum for both the C-face and the Si-face. This shoulder is attributed to distortion of Si_3N and chemical states other than Si_3N such as CN and NO_X[6].

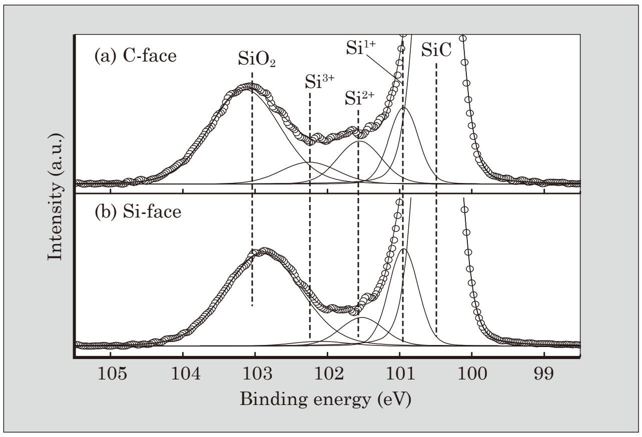

Fig.4 Spectra of Si at SiC/SiO_2 interface oxidized with N_2O

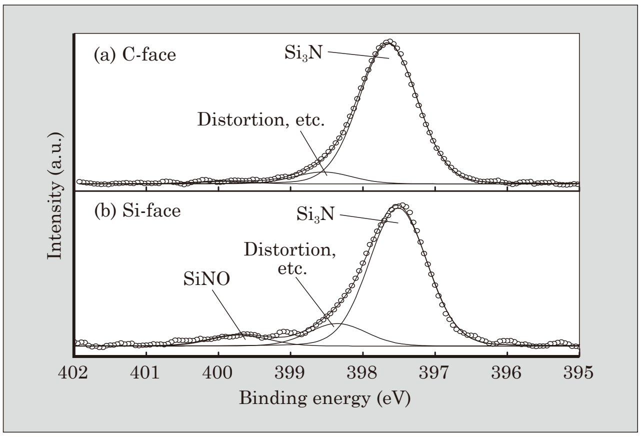

Fig.5 Spectra of nitrogen at SiC/SiO_2 interface oxidized with N_2O

4. Analysis by First-Principles Calculation

To analyze the difference between the C-face and the Si-face obtained by the XPS analysis and to estimate the bonding structure of the SiC/SiO_2 interface, we used the first-principles calculation. We assumed ideal bonding structures of the SiC/SiO_2 interface and compared them with the results of the XPS analysis, thereby analyzing the interface bonding structure.

The first-principles calculation, which means a calculation based on the most fundamental principles, is a technique of solving the state of electrons in a substance by numerical calculation at the atomic or nano-scale dimension based on quantum mechanics. The first-principles calculation makes it possible to investigate the properties of unknown substances and physical and chemical phenomena at the atomic level that cannot be measured experimentally.

$DMol^3$ *4 (7)(8) was used to perform the first-principles calculations presented in this paper.

4.1 Analysis of interface bonding structure

(1) Dry oxidation

We created a model of an ideal interface structure with an abrupt SiC/SiO_2 interface as the starting point of interface analysis for dry oxidation. We constructed a C-face and a Si-face surface model, which is shown in Fig. 6, from the crystal structure of SiC, followed by making of SiO_2 crystal surface, and bonded the surfaces together so that no C-O bond would be generated between the surfaces. To combine SiC and SiO_2, we take into consideration the suboxides obtained by the XPS analysis. Then, from the state of combination, the ideal interface structure was determined by performing a geometry optimization calculation to find the most stable atomic positions. The results are shown in Fig. 7. Figure 7 only shows some of the atoms at the interface. In the ideal interface structure obtained on the C-face shown in Fig. 7(a), Si that exists at the interface is in a chemical state Si^{3+}. With this ideal interface structure

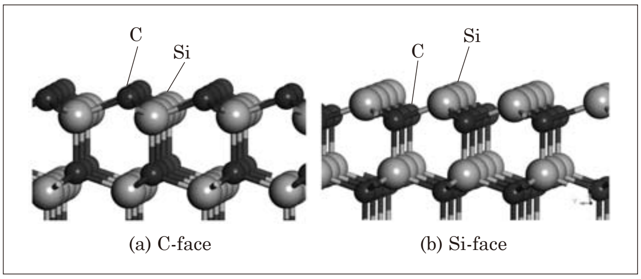

Fig.6 Models of surface structure created from SiC crystal structure

*3: These indexes shows the number of oxygen atoms existing around the Si atom.

*4: $DMol^3$: Part of the Materials Studio software environment. Materials Studio is a trademark or registered trademark of Dassault Systèmes S.A.

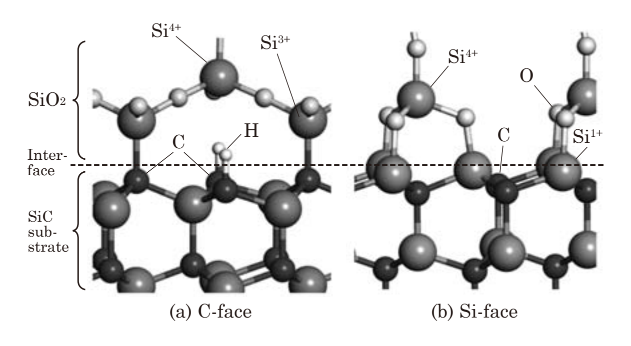

Fig.7 Estimated structural models of dry oxide interface assuming ideal interface based on structure optimization calculation

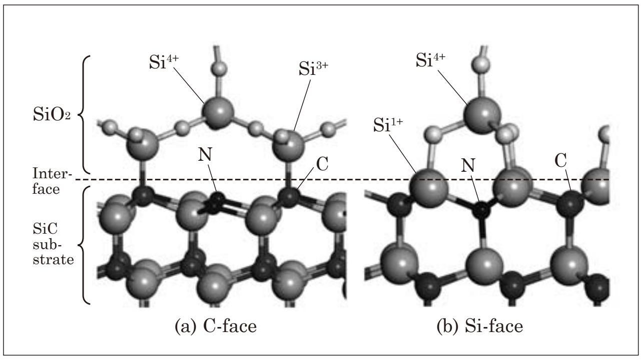

Fig.8 Models of nitrogen structure estimated at interface

considered, Si^{3+} observed in the XPS analysis of the C-face is estimated to result from an interface structure as shown in Fig. 7(a). Si^{1+} and Si^{2+} is estimated to result from interface disorder.

For the Si-face, as shown in Fig. 7(b), Si that exists at the interface is in a chemical state Si^{1+}. The Si^{1+} observed in the XPS analysis of the Si surface is estimated to result from an interface structure as shown in Fig. 7(b).

(2) N_2O oxidation

Regarding a bonding structure with nitrogen atoms introduced into the SiC/SiO_2 interface, on the Si-face, nitrogen atoms at the interface are known to enter the positions of carbon atoms of SiC to bond with Si atoms(9). Accordingly, for interface analysis for N_2O oxidation, nitrogen atoms were assumed to enter the positions of the carbon atoms on the C-face in the same way. We used an ideal interface structure that simulates dry oxidation and considered the suboxides and the bonding structure Si_3N obtained by the XPS analysis when we arrange the atoms so that the carbon atom positions would be replaced by nitrogen atoms. Then, to find the most stable atomic positions, we carried out first-principles calculation to perform geometry optimization calculations, thereby assuming the ideal interface structures.

The results obtained are shown in Fig. 8. For the C-face shown in Fig. 8(a), with the structure of Si_3N taken into account, the structure with all of the 3 bonds of nitrogen atoms bonded with Si in SiC seems appropriate. In addition, the structure with one of the bonds of nitrogen atoms oriented toward the SiO_2, which is not shown, is also regarded to be appropriate.

For the Si-face shown in Fig. 8(b), a structure with 2 of the bonds of nitrogen atoms oriented toward the SiO_2 film is thought to be appropriate. Incorporation of nitrogen atoms like these is similar to the bonding structure with nitrogen atoms, which is reported by Xu et al.(6) and Shirasawa et al.(10)

As described above, creating an interface bonding structure by the first-principles calculation has made it possible to analyze the results obtained by XPS analysis in detail.

4.2 Analysis of interface states

Examples of the SiC/SiO_2 interface model structures with dangling bonds (DBs) are shown in Fig. 9. In Fig. 9, DBs are indicated by white bars. For the C-face, we made the model interface that has 3 DBs of Si by removing one of the carbons at the interface shown in Fig. 7(a). The part of it is shown in Fig. 9(a). For the Si-face, we made the model interface with DBs by referring the paper by Okuno et al.(11), and the result is shown in Fig. 9(b). The Si atoms at the interface, as with the Si-face in Fig. 7(b), is the Si^{1+} bonding state observed in the XPS analysis.

The results of investigation of the interface state by these DBs using the first-principles calculation are shown in Fig. 10. It indicates that the interface state of a DB is formed within the band gap of SiC for both the C-face and Si-face. For the C-face, a state is also formed at the lower end of the conduction band side, which is estimated to result from the influence of the 3 DBs of Si existing adjacent to each other. The Si-face was found to be similar to the result of the paper by Okuno et al.(11)

One possible factor of reduction of the interface state density by introducing nitrogen atoms into the interface(1) to (3) is suggested to be that the nitrogen atoms bind the DBs of the Si atoms and form a terminated structure as shown in Fig. 8 to reduce the interface state.

Even in bonding states other than a DB, if inter-

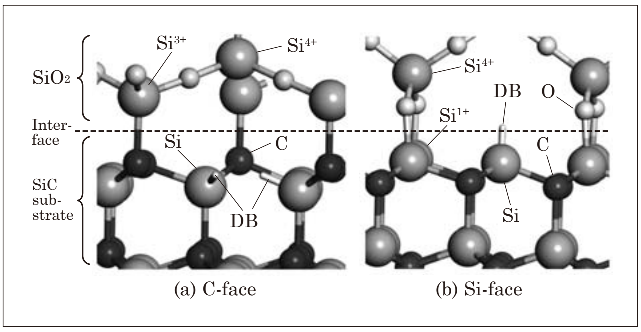

Fig.9 Ideal interface structures provided with dangling bonds (DBs)

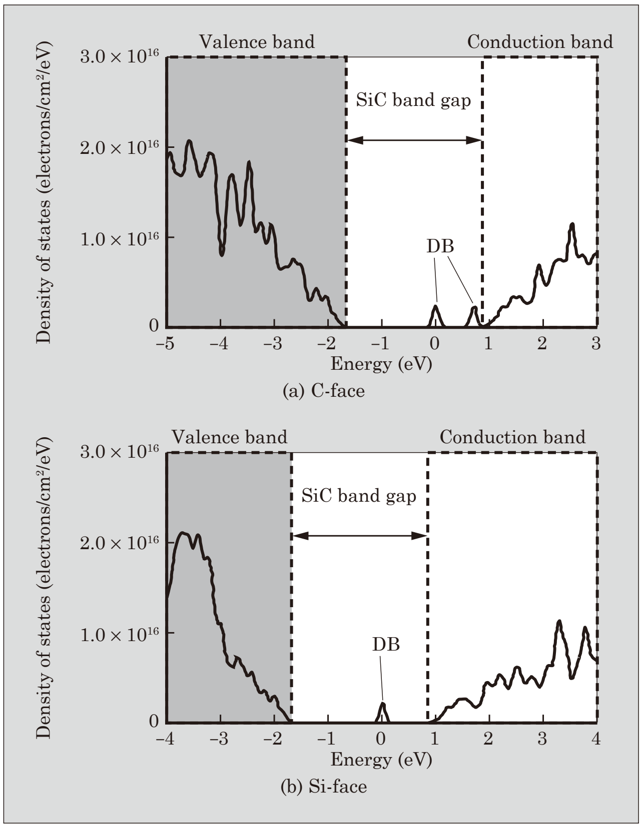

Fig.10 Density of states of interface structure with dangling bonds (DBs) of Si

face states exist within the SiC band gap, charge trapping occurs in the interface states, which may cause the mobility reduction due to Coulomb scattering and/or the variation of V_{th}.

4.3 Future issues

The first-principles calculation makes it possible not only to create a bonding structure but also to analyze the electronic state of a bonding structure for estimating whether it can be an interface state that has an effect on electrical characteristics. In addition, it makes it possible to analyze the ease of chemical reaction.

We have analyzed the change of the bonding state caused by introduction of nitrogen atoms into the interface and studied the mechanism of interface state reduction. In the future, we intend to investigate between the nitrogen introduction process and device characteristics, analysis, structural analysis by the first-principles calculation. Through these investigation, we will indicate the direction of characteristic improvement, thereby contributing to improved characteristics and processes of MOSFETs.

5. Postscript

This paper has described atomic level analysis of SiC devices using simulation.

In order to understand the characteristics of SiC-MOSFETs, it is important to analyze the bonding structure existing in the minute region of about 1 nm in the vicinity of the SiO_2 interface, which determines the characteristics, and clarify how the bonding structure affects the characteristics. In the future, we intend to continue to make use of analysis and simulation to contribute to early commercialization of high-performance SiC-MOSFETs and to the realization of a low-carbon society by achieving energy savings of power electronics equipment.

We would like to extend our sincere thanks to Professor NOHIRA, Hiroshi of Tokyo City University, who has given cooperation and advice on XPS spectrum analysis.

References

(1) Dhar, S. et al. "Interface trap passivation for SiO_2/(000-1) C-terminated 4H-SiC", J. Appl. Phys. 2005, 98, 014902.

(2) Chung, G. Y. et al. "Improved inversion channel mobility for 4H-SiC MOSFETs following high temperature anneals in nitric oxide", IEEE Electron Device Lett. 2001, 22, 176-178.

(3) Jamet, P. et al. "Effects of nitridation in gate oxides grown on 4H-SiC", J. Appl. Phys. 2001, 90, 5058.

(4) Watanabe, H. et al. "Synchrotron Radiation Photoelectron Spectroscopy Study of Thermally Grown Oxides on 4H-SiC (0001) Si-face and (000-1) C-face Substrates", Mater. Sci. Forum 2012, 717-720, 697-702.

(5) Watanabe, H. et al. "Synchrotron x-ray photoelectron spectroscopy study on thermally grown SiO_2/4H-SiC (0001) interface and its correlation with electrical properties", Appl. Phys. Lett. 2011, 99, 021907.

(6) Xu, Y. et al. "Atomic state and characterization of nitrogen at the SiC/SiO_2 interface", J. Appl. Phys. 2014, 115, 033502.

(7) Delley, B. "An all-electron numerical method for solving the local density functional for polyatomic molecules", J. Chem. Phys. 92, 508 (1990).

(8) Delley, B. "From molecules to solids with the DMol[3] approach", J. Chem. Phys. 113, 7756 (2000).

(9) Maejima, N. et al. "Site-Specific Atomic and Electronic Structure Analysis of Epitaxial Silicon Oxynitride Thin Film on SiC (0001) by Photoelectron and Auger Electron Diffractions", J. Phys. Soc. Jpn. 2014, 83, 044604.

(10) Shirasawa, T. et al. "Epitaxial Silicon Oxynitride Layer on a 6H-SiC (0001) Surface", Phys. Rev. Lett. 2007, 98, 136105.

(11) Okuno, E. et al. "First Principles Theoretical Study of 4h-SiC/SiO_2 Interfacial Electronic States on (0001), (0000-1), and (11-20)", Appl. Phys. Express 1, 2008, 061401.

Study of Adhesion of Resin Materials by Molecular Simulation

OGASAWARA, Miki* TACHIOKA, Masaaki*

ABSTRACT

Molecular simulation is a technology for evaluating the various properties of materials based on their molecular structure by using a computer. It has received attention as a method for speeding up the development of products. Semiconductor modules are being employed to an expanding range of applications such as industrial equipment and electric vehicle. In order to ensure high reliability, importance is placed on the adhesion of materials and resin. Against a backdrop of this, we implemented a study using molecular simulation for analyzing auxiliary agents for improving adhesiveness. We evaluated 2 types of adhesion assistants and elucidated molecular level mechanisms related to adhesion with aluminum.

1. Introduction

Molecular simulation is a technology for evaluating various properties of materials based on their molecular structure using a computer. It has been increasingly applied in recent years not only for the evaluation of materials that have already been launched on the market, but also as a prediction technique for enhancing the performance of or for adding new functionality to materials. As products are designed to have enhanced performance and to be more complex, predicting the properties of materials in advance can reduce the number of prototyping iterations and accelerate the development of highly reliable products. As a result, molecular simulation has been introduced not only in universities but also in companies as a technology for improving the reliability of products and shortening the development period.

Molecular simulation can also be used as a technology for complementing the molecular- or atomic-level analysis technologies such as transmission electron microscopes (TEMs) or atomic force microscopes (AFMs) to provide theoretical support for the analysis results.

This paper describes a way to effectively use molecular simulation for the adhesion analysis of resin materials of resin mold semiconductor modules such as small-capacity intelligent power modules (IPMs), All-SiC modules and automotive power modules.

2. Semiconductor Modules

2.1 Characteristics and challenges

Semiconductor modules are used in power converters and are being applied to an increasingly wide range of fields such as industrial equipment, electric vehicles and home appliances[(1)]. The semiconductor modules for these power converters must be highly reliable. Power cycle capability, which is an indicator of thermal fatigue based on the estimated temperature change in products during actual operation, is one of the items the market places importance on to prove reliability. As shown in Fig. 1[(2)], a semiconductor module consists of many components. Separation of or cracks in the components may cause a deterioration of its power cycle capability. To prevent this, it is important to improve the adhesion between the components. Because of its low resistance and high thermal conductivity, aluminum has been used for the bonding wires in semiconductor modules or as a material for insulating aluminum substrates. It has, however, a low adhesion to epoxy resin used for molding so that a certain countermeasure must be taken. In order to make practical use of modules that are more reliable than conventional products in the future, we need to select new materials with higher reliability in terms of adhesion and other properties, not only by using experience but also by taking a scientific approach.

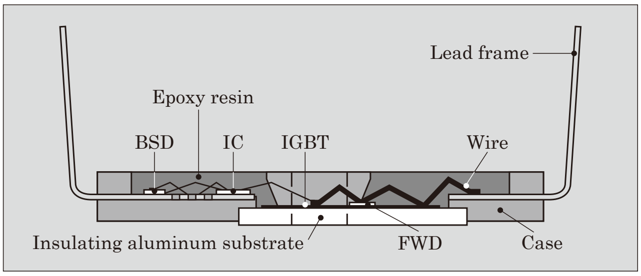

Fig.1 Structure of epoxy resin mold semiconductor module

2.2 Factors affecting adhesiveness

Although adhesiveness may be determined by many factors, particularly important ones are the an-

* Corporate R&D Headquarters, Fuji Electric Co., Ltd.

chor effect; mechanical properties including elastic modulus, linear expansion coefficient and glass transition temperature; and the chemical bonding between the module components and resin.

Among these, chemical bonding directly joins the components and resin in immediate contact and so it can have a major effect on improving adhesion. Consequently, in addition to the anchor effect and mechanical properties which have been focused on for a long time, attention is being placed on improving adhesion through chemical bonding. Since the strength of chemical bonding is determined by the molecular structures of materials, an effective way to enhance it is to carry out analysis using molecular simulation.

3. Molecular Simulation

Molecular simulation is a general term for a process that is conducted to analyze the phenomenon that results from the molecular structures of materials. In a molecular simulation, it is necessary to select an appropriate method in accordance with the phenomenon to be analyzed. For example, since the elastic modulus of macromolecules is determined by the element and bonding type of the atoms composing molecules, it is effective to use a molecular dynamics simulation by using atoms as structural units. The first-principles calculation used in this paper is a method of non-empirical calculation using electrons around atoms as structural units. It is used as a method of analyzing chemical reactions or band structures where the motion of electrons controls the material properties. It is characterized by its calculation method just specifying molecular structure based on the Schrödinger equation of quantum mechanics without using experimental data. Consequently, its greatest advantage is that calculation is possible without a real material.

The flow of the first-principles calculation consists of creating a molecular structure and performing a geometry optimization. The geometry optimization repeats the optimization of atomic coordinates and electron state alternately and finishes when a specified convergence condition is satisfied. From the calculation result, a stable molecular structure and the energy of the system in that state can be obtained. In addition, the band structure and various physical property values can be obtained by analyzing the breakdown of the energy.

4. Evaluation

4.1 Adhesion assistants

There are 2 techniques to improve the adhesion of chemical bonding: One is to change the molecular structure of the base material resin and the other is to use additives. This paper focuses on additives, which are adhesion assistants in this case, and evaluates their effect on the chemical bonding with aluminum.

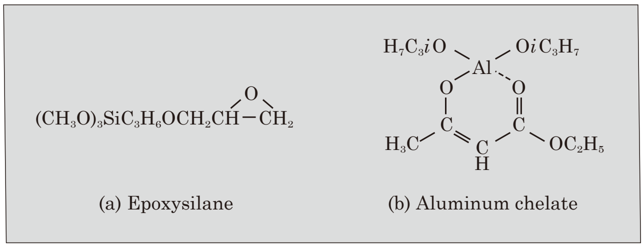

Fig.2 Molecular structures of adhesion assistants

The adhesion assistants we selected are: Epoxysilane, which is a silane coupling agent; and aluminum chelate, which is a chelate agent. We evaluated and compared their adhesiveness in a calculation and experiment. Figure 2 shows the molecular structure of the adhesion assistants.

4.2 Mechanism

Epoxysilane and other silane coupling agents are generally mixed into resin after the alkoxyl group in the molecules is hydrolyzed. The hydroxyl group that results from the hydrolyzation forms hydrogen bonds with the hydroxyl group on the surface of the aluminum. Then heat is applied to form strong covalent bonds (see Fig. 3). On the other hand, aluminum chelate and other chelate agents are mixed into resin without hydrolyzation. This causes a dealcoholization reaction between an alkoxyl group such as C_3H_7O and the hydroxyl group on the surface of the aluminum, which results in covalent bonding (see Fig. 4).

It can be presumed that both epoxysilane and aluminum chelate enhance the adhesion between the aluminum and epoxy resin by forming covalent bonds

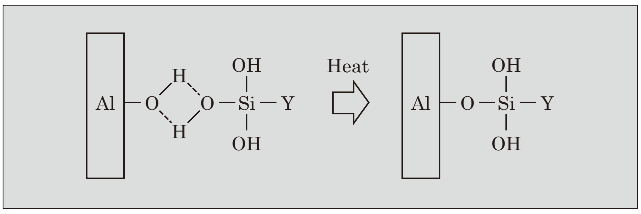

Fig.3 Reaction of a silane coupling agent

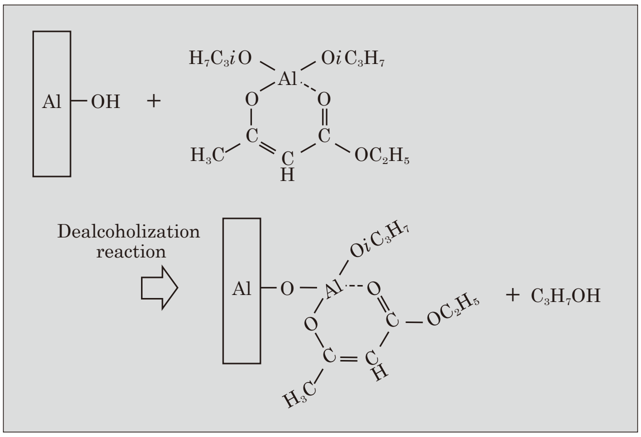

Fig.4 Reaction of aluminum chelate

with aluminum.

4.3 Calculation flow

The calculation flow is shown in Fig. 5. In order to simulate the oxide film on the surface of aluminum, we performed a geometry optimization of alumina crystal, then cut a (100) surface so that oxygen is on the surface, and terminated the oxygen on the topmost surface with hydrogen to create a hydroxyl group. To increase the calculation efficiency, we used only the molecular structure of the adhesion assistants at the section contributing to adhesion. We performed the geometry optimization for the adhesion assistants and aluminum individually and used the obtained structure to create the adhesion structures shown in Fig. 3 and Fig. 4. After performing the geometry optimization of the adhesion structures, we used the obtained structures to create structures where the adhesion assistants were dissociated from the aluminum, and then performed the geometry optimization again. We set the index of adhesiveness to be the difference between the energy of the adhesion structure and that of the dissociation structure (dissociation energy). For the calculation, we used DMol^{3} *1, which is a density-functional calculation program.

4.4 Calculation result

Figure 6 shows the molecular structures after the geometry optimization was performed for the adhesion assistants. As expected in advance, we confirmed that they form tetrahedral structures with silicon or aluminum at the center. We then used the structures in Fig. 6 to create structures after the adhesion shown in Fig. 3 and Fig. 4. Figure 7 shows the molecular structures after the geometry optimization was performed for cases where the aluminum and epoxysilane adhered and dissociated. In the adhesion structure, the silicon of epoxysilane or the aluminum of aluminum chelate bonded to the oxygen of alumina and stabilized. Furthermore, the oxygen of epoxysilane or aluminum chelate got closer to the aluminum of alumina, showing an interaction.

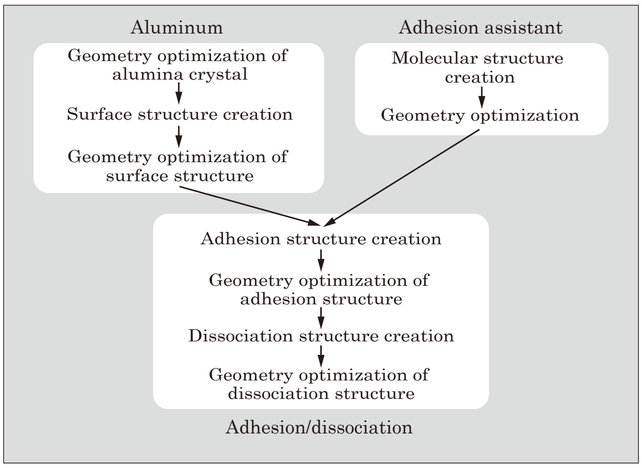

Fig.5 Calculation flow

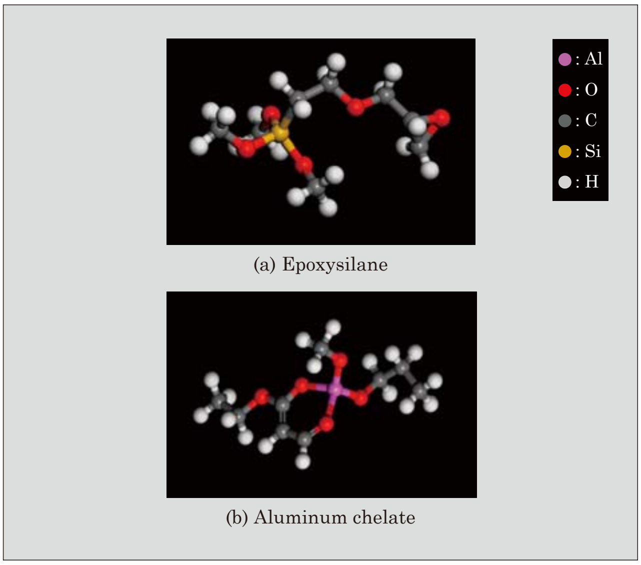

Fig.6 Molecular structures after geometry optimization

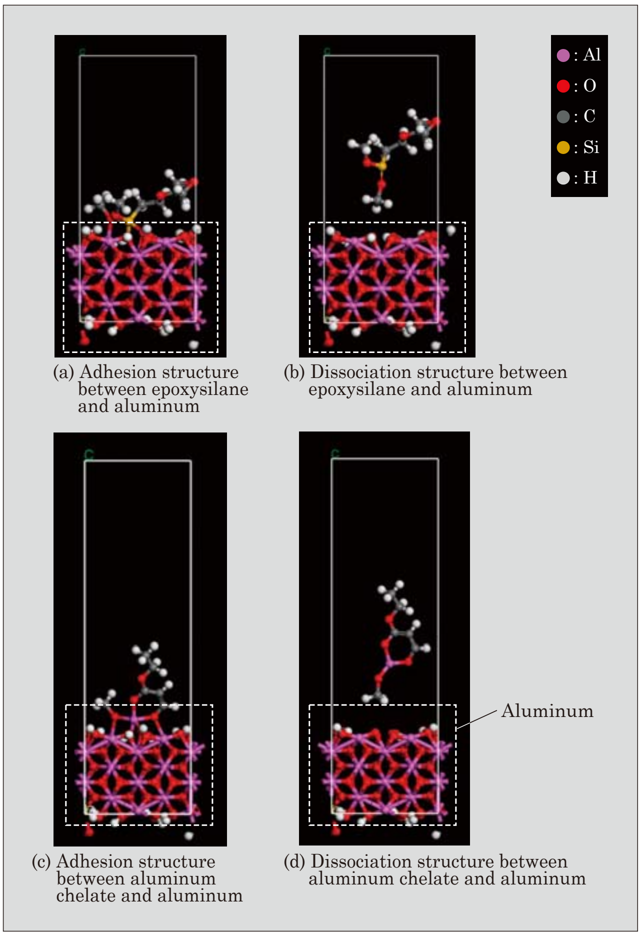

Fig.7 Molecular structures after geometry optimization of epoxysilane/aluminum chelate and aluminum

*1: DMol^{3}: Part of the Materials Studio software environment. Materials Studio is a trademark or registered trademark of Dassault Systèmes S.A.

Table 1 Dissociation energy

Item	Dissociation energy (eV)
Epoxysilane	4.81
Aluminum chelate	7.29

Table 1 shows the resulted dissociation energy values obtained from the energy difference between the adhesion structure and dissociation structure. A high dissociation energy means larger energy is needed when the object dissociates from the adhered state. From the calculation, we can expect that when epoxysilane and aluminum chelate are compared, aluminum chelate will require more dissociation energy, suggesting higher adhesiveness.

4.5 Measuring the adhesion force

(1) Measurement condition

In the experiment, we added fused silica to an acid anhydride curing agent containing bisphenol A epoxy resin, alicyclic epoxy resin and imidazole catalyst, and mixed them before adding epoxysilane or aluminum chelate.

The adhesion force was measured with the method described below. The shape of the test piece is shown in Fig. 8. A 10 mm square aluminum substrate was washed with ethanol and dried. Then a special mold was secured on the substrate surface and filled with epoxy resin. After the resin had cured under specified conditions, the mold was removed. We fixed the aluminum substrate to the obtained test piece, brought a load-applying jig into contact with the resin part, made it push the resin part in a direction parallel to the substrate surface and measured the maximum breaking load. The maximum breaking load values per unit bonding area of 5 test pieces were averaged and the result was assumed to be the adhesion force.

(2) Comparison of the measurement result with the calculation result

Figure 9 shows the dissociation energy obtained

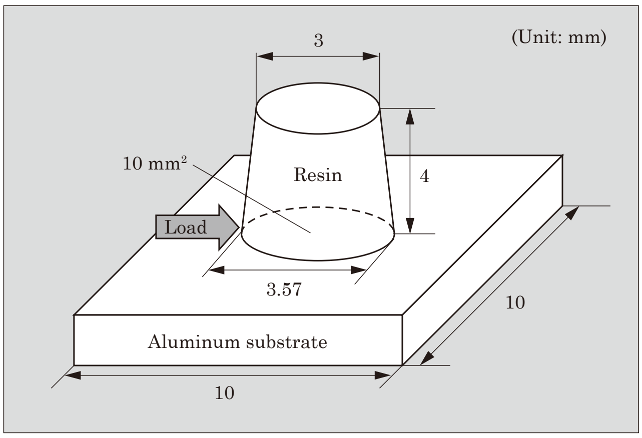

Fig.8 Test piece for adhesion force measurement

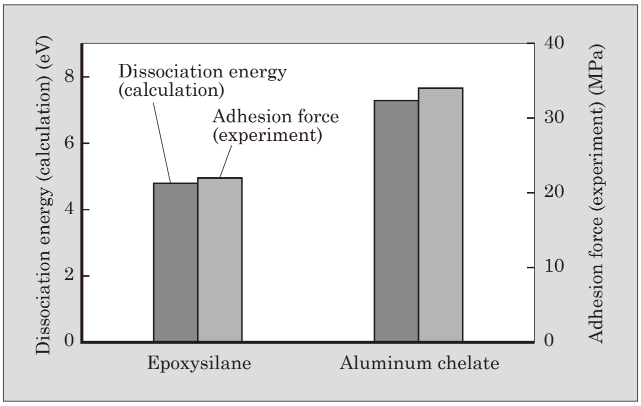

Fig.9 Comparison between calculation result and experiment result

with the calculation and the adhesion force obtained in the experiment. Not only the calculation result but also the experiment result showed that aluminum chelate had a stronger adhesion force, or was harder to dissociate, than epoxysilane. This revealed that a molecular-level mechanism was involved with the difference in adhesion forces.

5. Postscript

This paper has described the effective use of molecular simulation for the adhesion analysis of resin materials of resin mold semiconductor modules. It revealed that a molecular-level mechanism was involved with the performance of adhesion assistants that enhance the adhesion between module components and resin. We intend to identify the conditions required for auxiliary agents to give higher adhesion by analyzing the cause of different dissociation energy values between epoxysilane and aluminum chelate and their bonding density with components. We will then apply the result to guidelines for selecting auxiliary agents and contribute to enhancing the reliability of semiconductor modules.

Part of this study was carried out in cooperation with Prof. KOYAMA, Michihisa of the Frontier Energy Research Division of Inamori Frontier Research Center, Kyushu University; and Prof. MURAKAMI, Yasushi of the Faculty of Textile Science and Technology, Shinshu University. We would like to express our deep appreciation for their cooperation.

References

(1) Horio, M. et al. “New Power Module Structure with Low Thermal Impedance and High Reliability for SiC Devices”. PCIM Europe 2011, 37 (2011), p.229-234.

(2) Ikeda, Y. et al. “A study of the bonding-wire reliability on the chip surface electrode in IGBT”. 2010, Proc. of ISPSD, p.289-292.

Residual Stress Distribution and Adhesive Interface Strength Analysis of Thermosetting Resin Molding

GANBE, Tatsuya* ASAI, Tatsuhiko* OKAMOTO, Kenji*

ABSTRACT

The number of products sealed with a thermosetting resin such as semiconductor products has been increasing as the heat resistance and withstand voltage are improved and the size is miniaturized. Currently, structural design for products is being implemented using stress analysis based on CAE analysis in order to ensure reliability in products sealed with a resin. However, this type of analysis cannot predict resin cracks and interfacial peeling between the resin and component materials that cause failure. We have thus established a method for grasping curing behavior of thermosetting resin, a residual stress distribution analysis technology that can be utilized after curing has completed, and an evaluating technology for adhesive interface strength considering the adhering end distance. As a result, we can now construct structural design systems compatible with thermosetting resin sealing, thus enabling us to improve the reliability of products.

1. Introduction

The application of power electronics has been expanding in the motor control field, ranging from a conventional use in industrial equipment and electrical rolling stock to more recently adoption in hybrid vehicles and electric vehicles, as well as the power conversion field in applications for new energy sources such as photovoltaic power generation and wind power generation. As a result, the efficiency of power systems has advanced and the usage environment for these systems has diversified.

On the other hand, the increase in the world's population is expected to greatly increase power consumption from approximately 20 trillion kWh in 2013 to approximately 45 trillion kWh in 2030. In this regard, there is a great need to further reduce power usage and enhance the efficiency of energy usage. Against this background, the development and application of power modules that adopt high-efficiency SiC power semiconductors has been advancing. Power modules mounted with these SiC chips adopt thermosetting resin sealing structure to ensure reliability in various usage environments (see Fig. 1). Power module circuits are configured with various materials in complex shapes, and thermosetting resin is required to embed circuits without gaps and adhere closely to the materials.

However, since the viscosity of thermosetting resin rises as a reaction to heating, non-filling or entrainment of bubbles could occur under improper molding conditions. In addition, the occurrence of resin cracking or interfacial peeling can greatly impact reliability. Therefore, products that are going to be sealed with thermosetting resin require a careful structural design and materials design to ensure reliability.

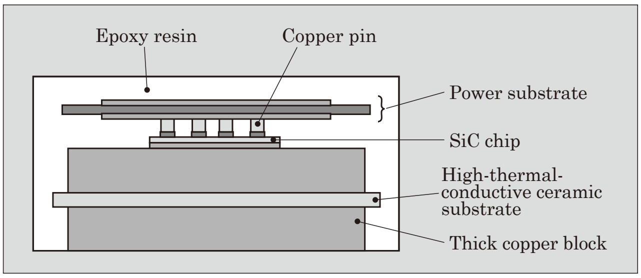

Fig.1 Cross-sectional structure of power module

In order to implement accurate structural design for products to be sealed with thermosetting resin, it is necessary to establish analysis techniques for coupling thermal stress analysis with 3D thermo-fluid analysis, which is used to reflect the curing behavior of resin. This paper describes residual stress distribution and adhesive interface strength evaluation techniques, both of which are required in establishing the coupled analysis technique.

2. Thermosetting Resin

We will describe an epoxy resin used as a sealing agent for power modules as an example of a thermosetting resin. Epoxy resin is a monomer with epoxy group properties in molecular structure. Ring opened polymerization (bridging) of the epoxy group can be done by heating with amine based or acid anhydride based curing agent. As polymerization occurs, molecular weight increases, resulting in a resin that irreversibly changes from a liquid to a gel, and then to a solid.

Many products make use of a structure that is sealed with a thermosetting resin for the following reasons.

(a) Power semiconductors: To ensure a high heat

* Corporate R&D Headquarters, Fuji Electric Co., Ltd.

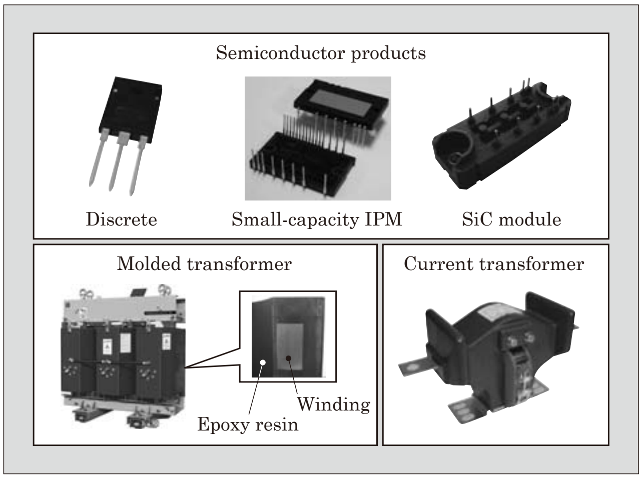

Fig.2 Products that make use of structure sealed with thermosetting resin

resistance and high withstand voltage for mounting Si chips and SiC chips

(b) Power electronics products: To facilitate miniaturization of vehicle mounted inverters and motors and to ensure vibration resistance and exothermicity

(c) Power supplies: To facilitate miniaturization and to ensure insulation compatible with the miniaturization

Figure 2 shows some standard Fuji Electric products that make use of a structure sealed with thermosetting resin.

3. Challenges Surrounding Structural Design of Products Sealed with Thermosetting Resin

Common molding methods for thermosetting resin include transfer molding, liquid injection molding utilizing a liquid resin, and cast molding. The molding process common to each of them is filling of specified mold via a flow of resin, and thereafter curing the resin through heating to create a mold of a specified shape. It is required that each of these molding processing have optimized molding conditions that correspond with the selected thermosetting resin. It is very important to grasp behavioral changes during the process of heating.

We will now give a description of an evaluation technique for the curing behavior and adhesive interface strength of thermosetting resin, both of which must be considered when carrying out the structural design of a product. As an example, we will take a look at epoxy resin, which is mainly used as a sealing agent for power semiconductors.

3.1 Curing behavior of thermosetting resin during the molding process

Figure 3 shows the time-lapse changes in the viscosity of the epoxy resin produced in a constant temperature. The epoxy resin gradually cures as heat is applied, and its viscosity rapidly increases after a certain period of time. As shown in the figure, the time extrapolated from the slope at the time of viscosity increase is referred to as gelling time, used as an indicator of curing time. Furthermore, the time up to the point when the resin reaches a viscosity limit for being able to fill the mold is the workable time at such temperature. Since temperature increase shortens the gelling time, it is necessary to optimize the resin filling process conditions in consideration of the relationship between temperature and workable time.

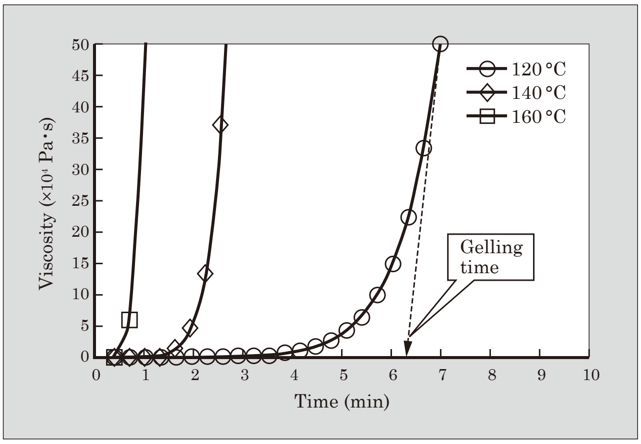

Fig.3 Time-lapse changes in viscosity of epoxy resin at constant temperature

Moreover, volume contracts due to molecular polymerization during epoxy resin curing (see Fig. 4). During curing, a heating distribution occurs for the resin depending on the structure (shape) of the molding materials and heating method. Speed differences in the curing reaction of the epoxy resin caused by the heating distribution result in volume contraction differences in the resin. As a result, it is generally recognized that a residual stress distribution occurs for the epoxy resin.

The volume contraction that occurs when the viscosity change due to heating and during the change from a liquid to a solid is a key behavior that should be considered in the thermosetting resin molding process,

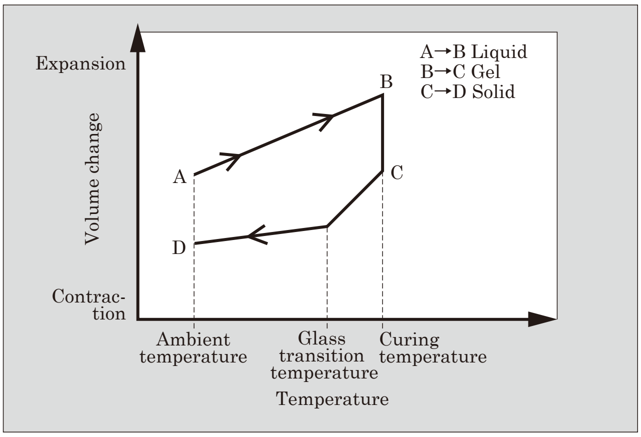

Fig.4 Behavior at time of epoxy resin curing

including that for epoxy resin.

3.2 Conventional structural design method and adhesive interface strength evaluation method

Conventional structural design for semiconductor modules use the state after resin curing as a model to perform computer aided engineering (CAE) analysis. Therefore, design has been made via a simple treatment of thermosetting resin curing behavior, such as by treating the physical properties of cured objects as elastic bodies.

Furthermore, the design of the adhesive interface strength must be done to make sure that no interfacial peeling occurs for between the structural materials and the resin of the molded product; and as such design is implemented based on the adhesive interface strength obtained from a lap-joint test piece[*1].

As a result, since it is not possible to accurately estimate adhesive interface strength without considering the behavior of the resin during molding, it is not possible to predict whether peeling will occur in the structural design process. Therefore, it is necessary to repeat testing to ensure reliability.

3.3 Structural design issues

The main defects that occur in products with regard to thermosetting resin are resin cracking and interfacial peeling between the resin and structural materials. Structural design requires selecting materials and determining the structure that prevents generation of these defects. In order to achieve this, it is necessary to be able to estimate the mechanical stress during actual operating time and assess whether it is no higher than the peeling threshold, after first accurately grasping the residual stress distribution associated with the curing behavior and curing contraction for the resin.

Therefore, some of the challenges of structural design include incorporating the analysis results of the residual stress distribution associated with resin curing, as well as establishing an evaluation technique for adhesive interface strength.

4. Residual Stress Distribution Analysis

It is difficult to directly measure or observe the residual stress distribution in the cured resin. In general, a strain gauge is mounted to measure strain, and residual stress is evaluated by converting the measurement results to stress. However, the strain gauge is only for measuring the location at which it is mounted, and it becomes necessary to secure the plane for the mounting. Therefore, in order to grasp the residual stress distribution, we implemented visualization of the residual stress distribution via CAE analysis using 3D thermo-fluid analysis software[*2] (FLOW-3D[*3]).

The 3D thermo-fluid analysis software makes use of a Macosko model by utilizing test values such as material properties of the resin including density, elastic modulus, and dependence on viscosity temperature and shear rate, to express viscosity as a function of the temperature, shear rate and curing reaction rate (see Fig. 5). Furthermore, a KAMAL model is also used to express the reaction speed by utilizing test values such as the reaction speed, reaction heat and energy associated with the curing reaction of the resin (see Fig. 6). The use of these 2 models makes it possible to express the irreversible change that occurs to the resin as it changes states from a liquid to a solid; and even for products that have a complex shape, it is possible to implement visualization by calculating the residual stress distribution from the heat distribution.

Figure 7 shows the analysis results of a stress distribution in resin by changing temperature states from the resin curing temperature to ambient temperature after sealing a thick copper plate with the resin. This is a comparison between the 3D thermo-fluid analysis and a conventional stress analysis, i.e., a 3D finite element method structural analysis that only takes into consideration the linear expansion coefficients

The most precise viscosity model for expressing viscosity as a function of temperature, shear rate and reaction rate

$$\eta = \eta' \left(\frac{\alpha_{gel}}{\alpha_{gel} - \alpha} \right)^{D+E\alpha}$$

$$\eta' = \frac{\eta_0}{\left[1 + \left(\frac{\eta_0 \gamma}{\tau^*} \right)^{1-n} \right]}$$

$$\eta_0 = F \cdot \exp\left(\frac{G}{T} \right)$$

η: Viscosity (Pa · s)
η': Temperature and shear rate dependent viscosity (Pa · s)
α_{gel}: Reaction rate at gelling time (viscosity parameter)
α: Reaction rate
τ^*, D, E, F, G: Resin inherent constants (viscosity parameters)
η_0: Viscosity at shear rate of zero (Pa · s)
γ: Shear rate (s^{-1})
n: Structural viscosity index
T: Resin temperature (K)

Viscosity parameters	α_{gel}	τ^*	D	E	F	G
Unit	–	Pa	–	–	Pa · s	K

Fig.5 Macosko model

*1: A lap-joint test piece refers to a simple laminated test piece for which an adhered laminated component is sealed with thermosetting resin.

*2: Three-dimensional thermo-fluid analysis software is a general-purpose 3D computational fluid dynamics (CFD) software for solving abnormal flow utilizing the control volume based finite difference method (FDM).

*3: FLOW-3D is a trademark or registered trademark of Flow Science, Inc. in the U.S. and other countries.

Model capable of being applied to a multi reaction patterns as a reaction speed model

$$\frac{d\alpha}{dt} = (K_1 + K_2 \cdot \alpha^M)(1-\alpha)^N$$

$$K_1 = K_a \cdot \exp\left(-\frac{E_a}{T}\right)$$

$$K_2 = K_b \cdot \exp\left(-\frac{E_b}{T}\right)$$

$$\alpha = \frac{Q}{Q_0}$$

$$\frac{dQ}{dt} = Q_0 (K_1 + K_2 \cdot \alpha^M)(1-\alpha)^N$$

$\frac{d\alpha}{dt}$: Reaction speed (s^{-1})

α: Reaction rate

t: Time (s)

K_1, K_2: Coefficients of temperature functions

M, N, K_a, E_a, K_b, E_b: Material inherent coefficients (reaction speed parameters)

T: Resin temperature (K)

Q: Calorific value until arbitrary time (J/kg)

Q_0: Total calorific value until reaction completion (reaction speed parameter)

$\frac{dQ}{dt}$: Heat-generation speed (J/kg·s)

Reaction speed parameters	M	N	K_a	E_a	K_b	E_b	Q_0
Unit	–	–	s^{-1}	K	s^{-1}	K	J/kg

Fig.6 KAMAL model

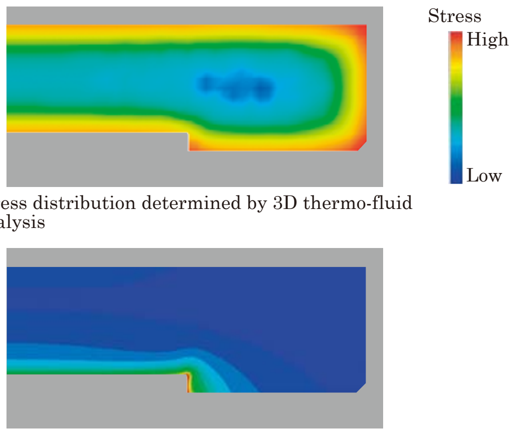

(a) Stress distribution determined by 3D thermo-fluid analysis

(b) Stress distribution determined by 3D finite element method structural analysis

Fig.7 Analysis results of the stress distribution in resin during curing

and elastic modulus of the resin. Conventional stress analysis is characterized in that some of the different components of the linear expansion coefficients (interface between resin and thick copper plate) have areas of high stress. In addition, the stress distribution of other components of the resin cannot be observed. On the other hand, when using 3D thermo-fluid analysis, the heat distribution based on the thermal conductivity showed us that there are areas of higher stress in the outside periphery of the resin than within the resin. In the residual stress distribution after resin curing, the difference with 3D finite element method structural analysis is apparent. Furthermore, aside from this, we compared the analysis and test with regard to the resin contraction distribution and amount of interfacial strain between the resin and thick copper plate, and confirmed that the results of the 3D thermo-fluid analysis were appropriate.

5. Establishing an Adhesive Interface Strength Evaluation Technique

We examined adhesive interface strength by taking measurements using the lap-joint test piece and by implementing a CAE analysis.

To begin with, we carried out a test that changed the lap length from the standard length of 10 mm to a shorter length of 2 mm in order to investigate dependence for the lap length of the adhesive interface strength (breaking load / adhesive area). The results are shown in Fig. 8. Since it is assumed that adhesive interface strength does not depend on adhesive area (lap width × lap length), breaking load should be proportional to the lap length. However, in actuality, breaking load was a constant, almost entirely independent of lap length. This result leads us to surmise that adhesive interface strength might be determined by a certain component not dependent on lap length.

Next, we used a semi-symmetric model of the lap-joint test piece to implement CAE analysis, which produced the stress distribution shown in Fig. 9 when applying a load at the time of breaking. We learned that a large amount of stress is concentrated on adhesive ends with a width of 1 mm or less, and that even long lap lengths do not contribute much to the breaking load, while only the number of low-stress central areas increases. It is thought that the stress concentration contributes to a mixed strength combining both shearing force and tensile force. Therefore, we compared the von Mises stress[*4] obtained from the CAE analysis and the adhesive interface strength obtained from the test

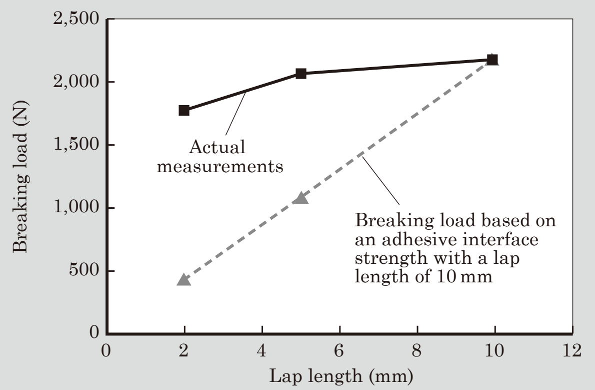

Fig.8 Dependence on breaking load lap length

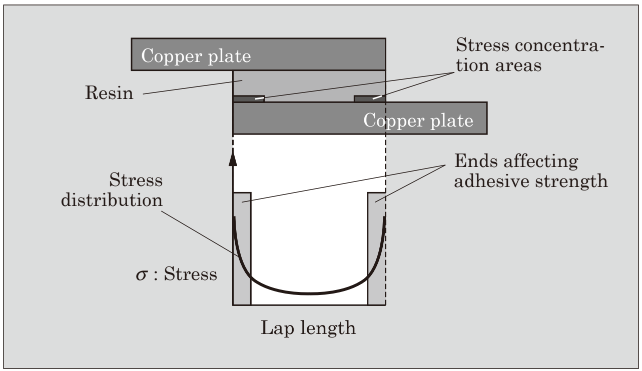

Fig.9 Stress distribution of lap-joint test piece adhesive areas

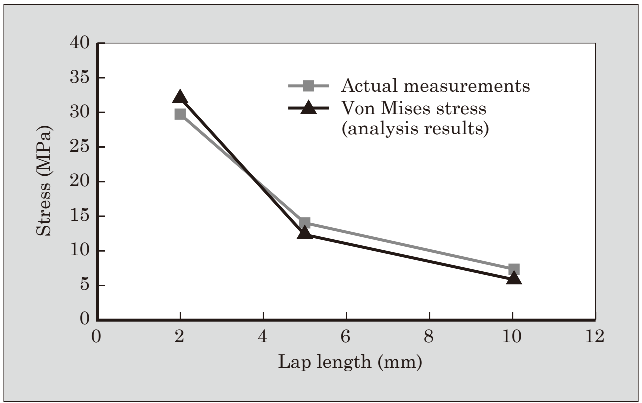

Fig.10 Evaluation results of adhesive interface strength under changed lap length

*4: Von Mises stress is the equivalent stress based on shear strain energy theory. When this stress exceeds yield stress, plastic deformation will occur. Von Mises stress was advocated by scientist Richard von Mises in the 1990s.

and learned that they matched up very well (see Fig. 10). As a result, the adhesive interface strength that causes interfacial peeling product defects can now be estimated using CAE analysis.

6. Future Tasks

Since it is important to grasp actual resin behavior when sealing with thermosetting resin, we developed a technique using 3D thermo-fluid analysis for better grasping residual stress distributions. In addition, we established an evaluation technique to investigate adhesive interface strength, which acts as a determination value for resin peeling.

In the future, we plan to continue developing thermal stress analysis tools that take into consideration residual stress, while expanding our database on the physical properties of thermosetting resin and the adhesive interface strength of thermosetting resin with various structural components.

7. Postscript

In this paper, we described the residual stress distribution and adhesive interface strength analysis of thermosetting resin molded products. As product structures become more complex with the progress of new product developments, series expansions and equipment miniaturization, an increasing number of products are requiring sealing with thermosetting resin. Through the construction of a structural design system compatible with thermosetting resin sealing, we will contribute to improving the timely supply and reliability of products such as semiconductor products.

Electromagnetic Noise Simulation Technology for Power Electronics Equipment

TAMATE, Michio* HAYASHI, Miwako* ICHINOSE, Ayako*

ABSTRACT

Power electronics have been becoming more widely used as core products for achieving energy savings and energy creation. However, power electronics equipment may cause electromagnetic noise interference, such as communication failure and malfunction and damage of electronic equipment. For preventing electromagnetic noise interference caused by conduction noise and radiation noise, Fuji Electric has been developing various simulation-based technologies, including the improvement of the analysis accuracy of electromagnetic noise generated by power electronics equipment to comply with relevant regulations, analysis models from which we can select a simplified or detailed one depending on applications, and applications for power electronics systems in addition to that for single equipment.

1. Introduction

In conserving energy to make efficient use of electric energy and in creating energy such as via photovoltaic power generation and wind power generation, power electronics are widely in use as core products. Power electronics equipment can freely convert electricity into easy-to-use forms by performing high-speed switching of power semiconductors such as insulated-gate bipolar transistors (IGBTs) and metal-oxide-semiconductor field-effect transistors (MOSFETs) and are effectively applied in various situations. Mass production of next-generation power semiconductors that use silicon carbide (SiC) and gallium nitride (GaN) started recently. With further loss reduction achieved, technologies for improving the efficiency and miniaturizing devices are being vigorously developed.

While power electronics equipment is very convenient, it emits to the surrounding environment currents and electromagnetic waves that make a noise during operation. This may cause electromagnetic noise interference and lead to the malfunction of and damage to electronic equipment. To prevent these electromagnetic noise failures, sufficient reduction of electromagnetic noise emitted to the surrounding environment is required of power electronics equipment. Increasing the switching speed in order to reduce the losses of power electronics equipment causes an increase in the energy of the electromagnetic noise emitted to the surrounding environment. This in turn requires the development of technology for protecting the surrounding environment by containing the electromagnetic noise within devices.

Fuji Electric utilizes simulation technology for preventing electromagnetic noise interference resulting from power electronics equipment.

2. Electromagnetic Noise Simulation

In recent years, many manufacturers have been working on electromagnetic noise simulation of power electronics equipment and various results are reported. Fuji Electric was among the first to undertake technological development for electromagnetic noise simulation of power electronics equipment in order to apply it to products.

2.1 Noise reduction required of power electronics equipment

Figure 1 shows a schematic diagram of electromagnetic noise generated by power electronics equipment. Because of high-speed switching (a few to a few hundred kHz) of power semiconductors, power electronics equipment generates large electromagnetic noise as

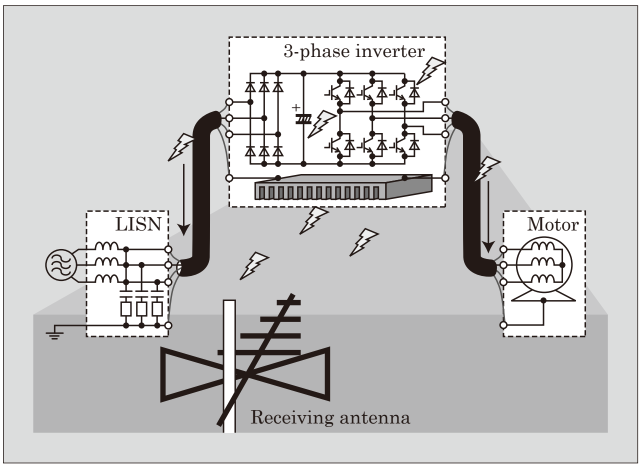

Fig.1 Schematic diagram of electromagnetic noise generated by power electronics equipment

* Corporate R&D Headquarters, Fuji Electric Co., Ltd.

conduction noise if it is radiated outside through input/output power cables, and as radiation noise if emitted as radio waves from various parts.

To prevent failures caused by these types of electromagnetic noise, electrical equipment including power electronics equipment is required to reduce the electromagnetic noise under various regulations. In particular, following the obligation to place CE marking on products, stipulated by the EMC Directive*1 in Europe (within the EU member states) in 1996, various methods of electromagnetic noise reduction have been proposed. With power electronics equipment, however, reducing the electromagnetic noise generated and improving the performance (loss reduction) are in a trade-off relationship. This requires repetition of trial and error every time a product is developed to take electromagnetic noise countermeasures, which consumes large amounts of time and labor.

To conform to the EMC Directive without going through trial and error, Fuji Electric started developing technology to simulate the electromagnetic noise of power electronics equipment.

2.2 Simulation of conduction noise

In order to conform to the EMC Directive, the intensity (level) of conduction noise radiated outside through cables must be measured and evaluated over a range from 150 kHz to 300 MHz as noise voltage (noise terminal voltage) at a line impedance stabilization network (LISN) that simulates a power system. The noise voltages for all of the phases must be reduced the regulation value or less.

The conduction noise simulation for deriving the noise terminal voltage of the power electronics equipment subject to the regulation is illustrated in Fig. 2. As shown in Fig. 2(a), conduction noise simulation can be roughly divided into 3 phases: (1) detailed modeling of a device to reproduce the impedance of the device, (2) circuit analysis that simulates circuit operation and (3) data processing of the results of circuit analysis. For modeling a device, an equivalent circuit model is built: For circuit components that allow measurement of impedance, LCR circuit elements are combined based on the results of measurement and, for printed boards and structural components that do not readily allow measurement, electromagnetic field analysis is used. For input/output power cables, the effects of the length and layout at the time of measurement are also factored into the circuit analysis. In addition, to ensure an agreement between the results obtained by circuit analysis and those measured as noise terminal voltages, data processing is done to reproduce the bandwidth of the spectrum analyzer, etc. when temporal waveforms are converted into frequency spectra.

*1: EMC Directive: Refers to one of the technical requirements to be met for acquisition of a CE Mark that relates to electromagnetic compatibility (EMC).

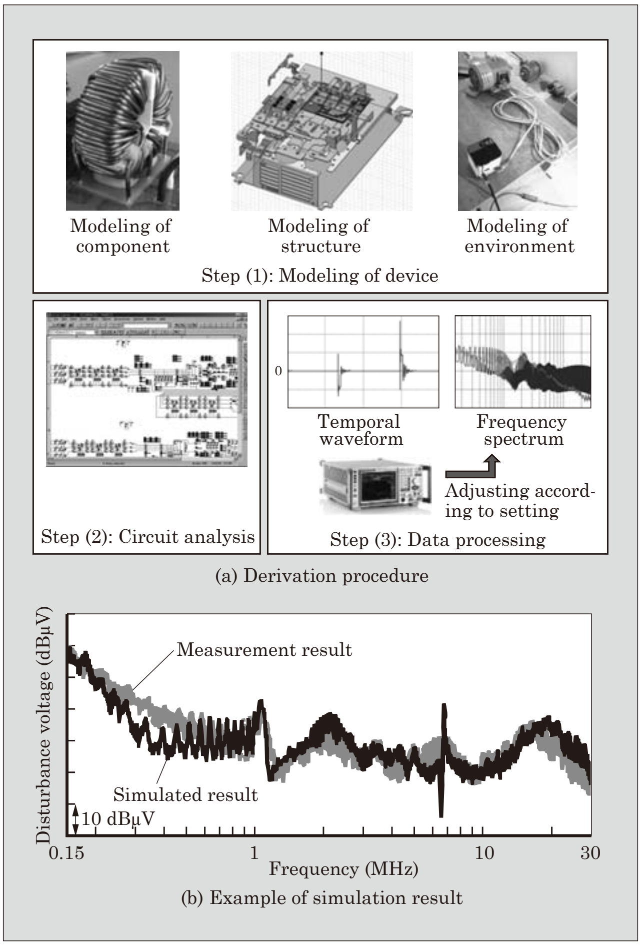

Fig.2 Conduction noise simulation

The accuracy of estimating the noise terminal voltage improves as the device is modeled in more detail. With the conditions used for building the most complicated model, simulation results are almost agree with measurement results over the entire range from 150 kHz to 30 MHz subject to the regulation for noise terminal voltage as shown in Fig. 2(b).

2.3 Simulation of radiation noise

The intensity (level) of radiation noise is measured as the radiation field intensity by using a receiving antenna located 10 m away from the power electronics equipment. In this case, the power electronics equipment must be rotated by 360 degrees. Then, the maximum value obtained as the height and angle (horizontal and vertical) of the receiving antenna is varied must be reduced to no higher than the regulation value.

Simulating radiation noise is much more difficult than conduction noise. This is because that, as shown in Fig. 1, while conduction noise is evaluated only by the voltage that has reached the LISN, radiation noise is emitted into space from numerous sources of radiation unintentionally formed in the device. Figure 3 shows an example of measuring and simulating radiation noise, which is an area that Fuji Electric is work-

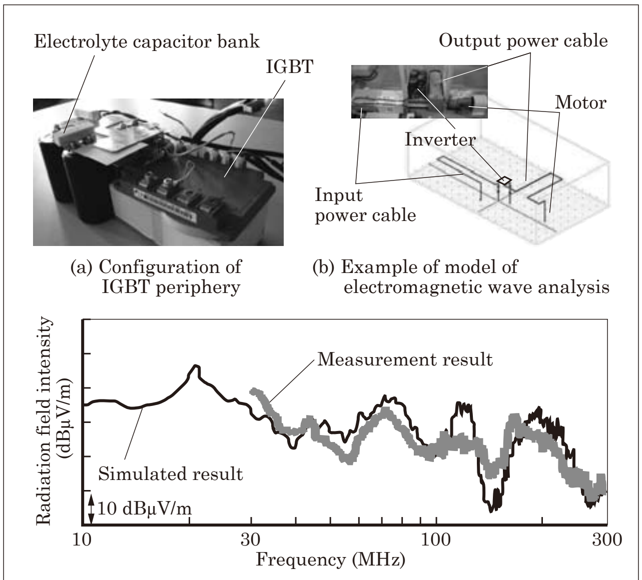

(a) Configuration of IGBT periphery (b) Example of model of electromagnetic wave analysis

(c) Example of simulated result

Fig.3 Radiation noise simulation

ing on. The description here is mainly about the difference from conduction noise simulation.

As compared with the switching frequency of power electronics equipment, the evaluation frequency for radiation noise is high at 30 to 300 MHz. This makes it difficult to obtain switching waveforms that include this frequency component accurately by circuit analysis. Accordingly, for electromagnetic noise simulation at 10 MHz or higher, switching waveforms measured by simulating IGBT peripheral circuitry as shown in Fig. 3(a) are factored into circuit analysis.

What is required next is electromagnetic wave analysis. For simple circuit operation, circuit analysis and electromagnetic wave analysis can be obtained at the same time. But it is difficult to link analyses on the complicated circuit operation of power electronics equipment with electromagnetic wave analysis. Radiation noise simulation can be roughly divided into modeling, circuit analysis and electromagnetic wave analysis and a different analysis software application is used for each of them. For this reason, handing over data to link these processes with each other is the key. First, for impedance modeling, a distributed constant circuit, rather than a lumped constant circuit combining LCR circuit elements, must be simulated. In particular, print pattern and component arrangement have a major effect, and electromagnetic field analysis is used to model them into a distributed constant circuit, which is factored into circuit analysis. In circuit analysis, the current that flows to the antenna formed in each location is determined. Antennas are formed unexpectedly here and there in the device but the dominant antenna is identified, and this is then factored into the electromagnetic wave analysis. For electromagnetic wave analysis, only the shapes of major antennas are modeled to derive the radiation field 10 m away based on the current that flows.

Figure 3(b) shows an example of a model for analyzing radiation noise from an inverter. The inverter is simulated by using a loop antenna for the IGBT peripheral structure and dipole antennas for the input/output power cables. The effective area of the loop antenna and the effective length of the dipole antennas greatly contribute to the analysis accuracy, so the antenna shapes must accurately simulate these. The interference between the antennas caused by phase difference is determined by data processing based on the results of the electromagnetic wave analysis for the respective antennas.

Figure 3(c) shows an example of the result of radiation field intensity simulation obtained by these processes. It can be confirmed that the general trends agree in the range from 30 to 300 MHz, in which significant electromagnetic noise is generated in power electronics equipment. Note, however, that it still has various issues such as finding a method to identify in advance the antenna that provides the dominant source of radiation, in addition to improving the accuracy.

3. Examples of Application of Electromagnetic Noise Simulation Technology

3.1 Application to product development

As shown in Section 2, electromagnetic noise simulation of power electronics equipment achieves high accuracy by reproducing the devices and measurement environment with high accuracy. However, it is difficult to apply such simulation to product development due to its long analysis time in addition to the cumbersome procedure. To deal with the issue, we use simple and detailed analysis models appropriately according to the product development process.

To obtain results, radiation noise simulation requires more labor and time than conduction noise simulation, so we consider applying it only to those targets for which it is more effective. This subsection presents a case in which it is applied to the design of housing of power electronics equipment.

Figure 4 shows an example of housing analysis. As shown in Fig. 4(a), the housing of an inverter may be configured by combining cooling fins and sheet metal or made by aluminum die casting, and the former tends to generate larger radiation noise. The housing is grounded and the potential at any point is ideally equal to 0 V. However, with the large area, minute potential variations may occur. It has been found that this minute potential variation may cause large radiation noise. Hence we use a simulation to design housing that mitigates the minute potential variations. Figure 4(b) shows an analysis model that extracts the cooling fins, sheet metal and electrolyte capacitors at the ground potential. Based on the results of simulation that uses a partial model like this, the housing is designed to achieve a configuration that reduces the

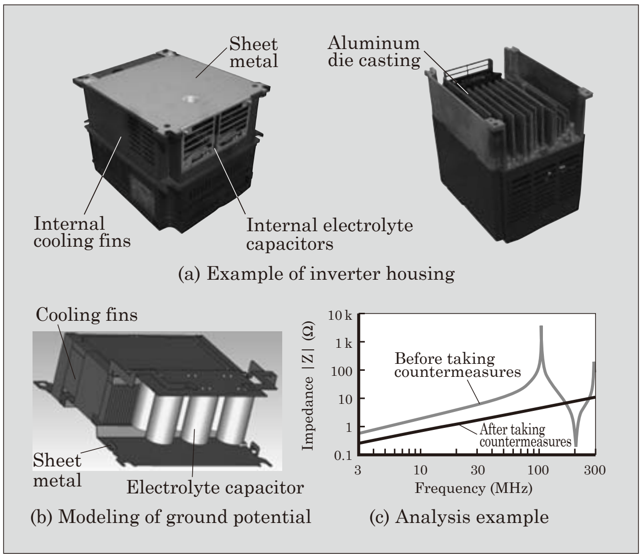

Fig.4 Housing analysis example

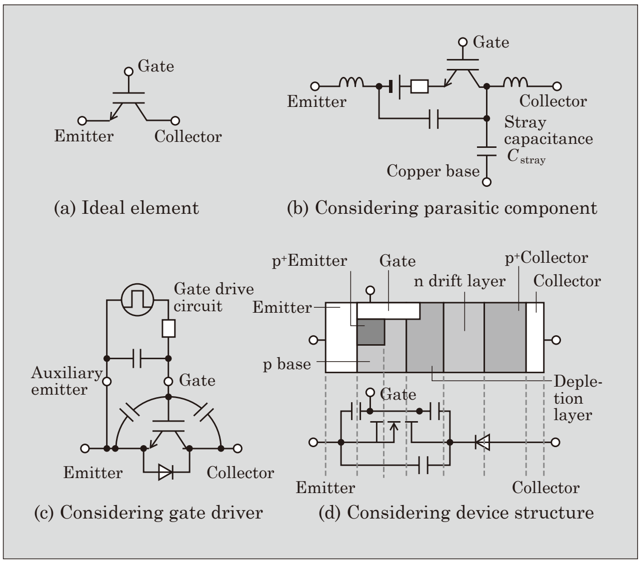

Fig.5 Transition of IGBT device model

impedance between the connection points, for which the minute potential variation should be mitigated, and prevents the formation of an unwanted resonant peak as shown in Fig. 4(c). This is effective in reducing radiation noise.

Such simulation with part of the device extracted, which features simple modeling and short analysis time, allows exploration of a better configuration by repeated analysis.

3.2 Study of accuracy improvement

Sometimes, electromagnetic noise arises from a product-specific circuit and/or structure, where the generation mechanism is unclear and is difficult to deal with. In those cases, we build a more detailed model to further improve the analysis accuracy, thereby gaining an understanding of the generation mechanism to formulate countermeasures to take.

(1) Mode conversion

Conduction noise is subject to a phenomenon called mode conversion. The common mode component conducted through the ground wire and the differential mode component conducted through the power supply line may have their paths changed during conduction through various locations, and this is referred to as mode conversion. The noise caused by this mode conversion is generally difficult to reduce. With actual measurement, grasping the generation of mode conversion itself is difficult. However, use of simulation allows the paths and mechanism of mode conversion to be grasped relatively easily. In addition, to reduce the noise caused by mode conversion, countermeasures can be formulated such as those that eliminate the paths of mode conversion and shift the resonance frequency, which are difficult to identify by measurement alone.

(2) Modeling of switching characteristics

To improve the accuracy of electromagnetic noise simulation, we are developing technology to accurately model the switching characteristics of power semiconductors, which is the source of the noise. In the development of power semiconductors, device simulators capable of accurately reproducing a single switching characteristic have been utilized. But they are difficult to combine with circuit operation of power electronics equipment, which is characterized by repeated switching. For this reason, applying device models of power semiconductors to circuit analysis of electromagnetic noise simulation had many problems.

Figure 5 shows transition of an IGBT device model. With the ideal element in Fig. 5(a) as the basis, the initial noise analysis had surrounding parasitic components (inductance and capacitance) added to the model as shown in Fig. 5(b). Adding the stray capacitance C_{stray} has made it possible to simulate paths of noise without omission. In Fig. 5(c), the gate driver characteristics are also added to model the switching characteristics in more detail. However, switching characteristics are reproduced by fitting to measurement data. This lead to the problem of larger errors caused by significant changes in the peripheral circuitry and/or device temperature. Recently, as shown in Fig. 5(d), a model based on the device internal structure has been built to allow for more accurate simulation of switching characteristics[1]. By applying this model, high estimation accuracy has been realized in electromagnetic noise simulations without the need for measurement data.

3.3 Application to power electronics systems

To prevent electromagnetic noise interference on site while conforming to standards, we are moving ahead with a study on simulations intended for power electronics systems composed of power electronics equipment, control devices, detectors, etc.

Figure 6 shows an example of the configuration of a motor drive system. A motor drive system has a large

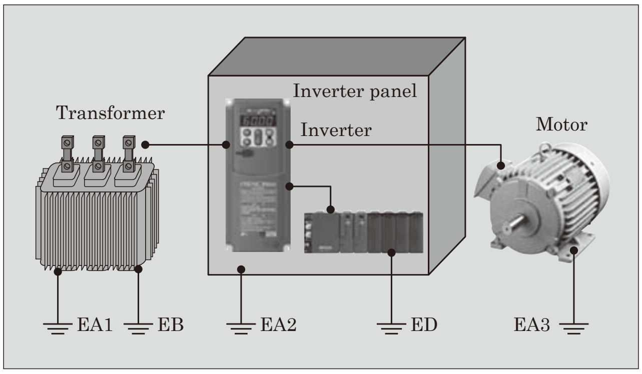

Fig.6 Example of motor drive system configuration

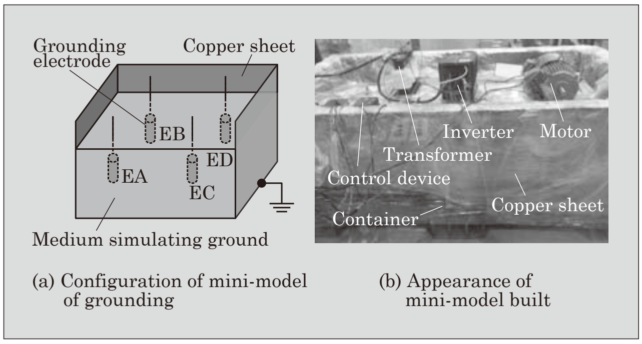

Fig.7 Configuration of mini-model for evaluating effect of grounding portion

transformer, inverter panel, motor, etc. laid out in a vast area that can be as large as a few tens of meters square. In a power electronics system like this, electromagnetic noise emitted to the surrounding environment and the conduction noise flowing into control devices and detectors located in the inverter panel may greatly vary depending on how devices are grounded.

Traditionally, the respective devices in a motor drive system are connected to grounding electrodes of Classes A to D with the grounding resistance values specified according to the voltage and purpose of the respective devices. However, the choices of grounding methods have increased as the use of equipotential bonding for grounding, which is specified in the International Electrotechnical Commission (IEC) standards, has been permitted along with the revision of the "Interpretation of Technical Standards for Electrical Equipment" in FY2011. If the merits and demerits of various grounding conditions can be grasped by verification in advance, it will be effective for mitigating electromagnetic noise.

Accordingly, in order to grasp the effect of the grounding portion on electromagnetic noise, we built a mini-model for evaluating the effect of the grounding portion (see Fig. 7). In this mini-model, a medium simulating the ground is filled in a container and electrodes simulating grounding electrodes are implanted, as shown in Fig. 7(a). Then, as shown in Fig. 7(b), the transformer, inverter, motor and control device connected to the respective grounding electrodes are combined to build a mini-model of the power electronics system in an area of about 2 m × 1 m. We have made use of the results of verification obtained with this model and built an equivalent circuit that simulates the behavior of the grounding portion. By combining with the conduction noise simulation described earlier, it is now possible to grasp the behavior of electromagnetic noise through grounding of the power electronics system. This has made it possible to identify in advance the best combination of the grounding methods of various types of devices that can be performed on site.

4. Postscript

This paper has described Fuji Electric's electromagnetic noise simulation technology for power electronics equipment. The study started with theoretically reproducing electromagnetic noise generated by power electronics equipment. And it is now widely utilized to include applications to product development by streamlining and applications to power electronics systems, not to mention improvement of analysis accuracy.

In the future, we intend to continue expanding the scope of application of electromagnetic noise simulation and work on establishing the technology to prevent electromagnetic noise interference.

References

(1) Matsumoto, H. et al. Simulation Technology for Power Electronics Equipment. FUJI ELECTRIC REVIEW. 2015, vol.61, no.1, p.63-67.

Aerodynamic Noise Simulation Technology for Developing Low Noise Products

KANEKO, Kimihisa*　MATSUMOTO, Satoshi*　YAMAMOTO, Tsutomu*

ABSTRACT

The size reduction trend of electric power equipment causes increased heat generation density along with an accompanying need for increased airflow for cooling. In this situation, aerodynamic noise can be the dominant noise source for air-cooled electric equipment. Grasping the noise generation mechanism and the noise reduction by measurements are often difficult, getting physical information through simulation can be an effective approach. In order to achieve noise reduction of equipment, we elucidated the aerodynamic noise generating mechanism by focusing the fan, the main source of noise in air cooling equipment, and estimated noise change caused by cooling structure differences. Simulated sound pressure level and peak frequencies are in good agreement with the measurement. This technology can be applied to understand the noise generation mechanism, and can also be used to structure design.

1. Introduction

The trend toward smaller electric equipment products is causing them to have a higher heat generation density. To help this heat dissipate, a common measure taken for air cooling systems is to increase the airflow. However, the aerodynamic noise generated from the cooling air may become an issue as the air volume increases. Aerodynamic noise is caused by pressure variations generated due to flow disturbance. In order to clarify and take measures for this phenomenon, techniques that mainly use measurements have been traditionally applied. However, taking measurements is often difficult if the object to be measured rotates or moves or the space to be measured is large, for example. To address this issue, it is effective to run a simulation that allows a large quantity of physical information to be obtained in the target space. Note, however, that an aerodynamic noise simulation requires that turbulence phenomena are accurately reproduced and tremendous amounts of computation time are necessary.

In response, in addition to improving computer processing speeds, parallel computing using more than one CPU has been applied for reducing the computation time. Taking floating point operation per second (flops) as an example, the “Earth Simulator” achieved 35 trillion operations (35 Tflops) in 2002 and the “K computer” 10 quadrillion operations (10 Pflops) in 2011. This means that a computational speed increase of 100 times was achieved in about 10 years. Following this development, faster computers for science and technology purposes owned by private companies and an improved and diffused cloud environment available for public use have made it possible to perform massively parallel computing. In addition, execution speeds of computations performed for research and development have been improving dramatically.

This paper describes aerodynamic noise simulation technology intended for power electronics equipment with an air cooling structure.

2. Products and Noise

2.1 Types of noise and related products

Figure 1 shows major types of noise sources and related products of Fuji Electric. Noise sources can be roughly classified into mechanical vibrations, electromagnetic vibrations and aerodynamic pressure variations. Noise caused by mechanical vibrations is mainly generated in products with mechanical structures that involve rotation and/or movement such as rotating machines. Noise resulting from electromagnetic vibrations is mainly generated in products in which electromagnetic force works, such as transformers. Noise caused by aerodynamic pressure variations is mainly generated in products such as air-cooled devices and power electronics equipment. Many products have their heat-generating components cooled by using fans and establishment of the technology is expected to produce a ripple effect among products.

2.2 Issues with analysis of aerodynamic noise

In order to reduce the noise resulting from flow, any unsteady turbulence phenomenon that provides an acoustic source should be identified so that appropriate measures can be taken. Flow analysis here allows the user to capture a wider range of flow phenomena as compared with measurement and is becoming an effective tool.

The Reynolds-averaged Navier-Stokes (RANS) model is generally used for flow analysis of turbulence

* Corporate R&D Headquarters, Fuji Electric Co., Ltd.

UPS

PCS for photovoltaic power generation

Motor

Data center

Fuel cell

Vending machine

Field	Related product	Major noise source		
		Mechanical vibration	Electromagnetic vibration	Pressure variation of fluid
Power electronics equipment	UPS, PCS, power supply, inverter, etc.	–	Core (reactor)	Cooling fan
	Motor	Resonance, bearing	Core/coil	Cooling fan, rotor
Industry	Clean room, data center	–	–	Fan filter unit
	Electric distribution facility	–	Core (reactor)	Cooling fan
Power generation/society	Turbine/peripheral equipment	Resonance, bearing	–	Labyrinth seal
	Generator	Resonance, bearing	Core/coil	Cooling fan, rotor
	Fuel cell	–	–	Cooling fan
Power reception and distribution/control equipment	Magnetic contactor	Contact collision	–	–
Food distribution	Vending machine	Compressor vibration	–	Cooling unit fan

Fig.1 Types of noise sources and related products

phenomena. It is based on the flow statistically time-averaged for specific flow conditions and cannot be said to adequately reproduce the phenomenon as a fluid analysis method. Meanwhile, large eddy simulation (LES) can be used to directly solve the behavior of eddies that cause a time variation of flow. However, LES requires more than 100 times as much computation time as RANS, and hence one issue was to reduce the computation time. Still, massively parallel computing that uses a few hundred to a few thousand CPUs, in addition to the improved computation time of recent CPUs, has led to a stage where LES computation is practicable[(1) to (4)].

3. Application of Aerodynamic Noise Analysis Technology

3.1 Principle of generation of aerodynamic noise

A mechanism of generation of aerodynamic noise that takes a cylinder as an example is shown in Fig. 2. Aerodynamic noise can propagate to an observation point from 2 types of acoustic source. One is an acoustic source caused by pressure variations on a solid surface generated by eddies and the other is generated by variations of momentum due to turbulent eddies (Kármán vortices) in a space. The level of noise of the former is proportional to the 6th power and of the latter to the 8th power of the flow speed. In a low-Mach-number region with a low flow speed, the former is dominant[(5)]. The flow speed from an air cooing fan considered in this paper is a low-Mach-number flow of about 20 to 30 m/s and the noise arising from pressure

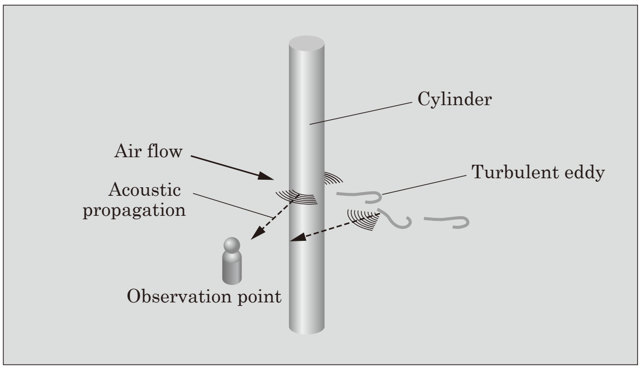

Fig.2 Mechanism of generation of aerodynamic noise with cylinder taken as example

variations on a solid surface is dominant.

3.2 Analysis methods

Aerodynamic noise analysis methods can be roughly classified into direct noise simulation method and integral methods on acoustic analogy. Major characteristics of the 2 types of methods are listed in Table 1. There are differences in the computation time and type of information that can be obtained and the method should be selected according to the purpose.

The direct method determines the flow and acoustic propagation at the same time. By considering fluid compressibility, which is variation of the fluid density according to the pressure, the acoustic pressure variation can be analyzed at the same time. With this method, meshes for analyzing the wavelength of sound to the observation point are required in addition to

Table 1 Major characteristics of aerodynamic noise analysis methods

Item	Direct method	Integral method
Calculation method	○ Compressible flow + unsteady ○ Direct calculation of sound pressure	○ Incompressible flow + unsteady ○ Acoustic calculation from wall surface pressure
Fluid analysis	Unsteady compressible flow LES analysis	Unsteady incompressible flow LES turbulence analysis
Noise analysis		FW-H, Curle's equations*, etc.
Advantage of method	○ Precise method featuring high accuracy ○ Interference between object and sound field also reproducible	○ Allows relatively easy handling. Highly accurate as well ○ Computation time nearly adequate to be practical (a few days with existing machines)
Issue	Requires high spatial resolution and leads to ultra-large-scale computation	Coupling with sound field analysis necessary for considering reflection and sound absorption

*FW-H, Curle's equations: representative calculation methods for noise estimation with the distance from pressure variations on a solid surface to the observation point taken into consideration

meshes for reproducing turbulent eddies in a flow field in the vicinity of the acoustic source. For this reason, the direct method tend to require a larger number of meshes, and hence a longer computation time.

With the integral method, flow and sound are computed independently. After obtaining pressure variations on a solid wall surface by flow analysis, the sound at the observation point is estimated(5) to (7). It is not necessary to consider compressibility of the fluid and it is sufficient to simply focus on meshes capable of reproducing the turbulent eddies that provide the acoustic source. This makes it possible to reduce the computation time as compared with the direct method.

In flow analysis, it is important to reproduce turbulent eddies that change over time. Currently, using LES for this reproduction is the most effective method. For the present target of verification, it is not practical to perform a few hundred to a few thousand parallel computations using the in-house computer facilities for completing LES computation in a few days. Accordingly, we have used the "K computer" for the computation. We have studied noise from the cooling fan unit and noise from the cooling fan and an obstacle in the case of using a cooling structure.

With the cooling fan unit, the pressure variations of the fluid that work on the blades and casing surface may provide an acoustic source to directly reach the observation point. For this reason, we used the integral method, which is relatively easy to handle. Meanwhile, in a structure with a cooling fan and obstacle, noises from the cooling fan and the obstacle and their interference are a possibility. Therefore, we used the direct method for studying the noise.

3.3 Analysis results

As shown in Fig. 3, we studied the noise generated in 2 types of configuration: a cooling fan unit and a cooling fan integrated into a cooling unit.

Using a wind tunnel conforming to the JIS B 8330, we measured the noise from the fan unit and obtained the fan characteristics (flow rate and pressure difference as well as flow rate and noise) at the same time. We used a model structure similar to the actual equipment, structure of which has flow resistance, i.e. a block installed in the flow channel that simulates electronic components and a heat sink.

(1) Fan unit

We used the integral method and performed calculation with the same layout and conditions as those used for measuring the noise. Figure 4 shows the flow speed distribution by LES at the maximum efficiency point. It has allowed us to reproduce the details of vortex variations in the fan wake flow, which was not possible with analysis by the conventional RANS.

The results of analysis and experiment on a sound pressure spectrum at the observation point are shown in Fig. 5. The horizontal axis represents the frequency and the vertical axis the sound pressure level. It indicates that the spectra observed consist of peak sounds and wideband sounds. With the blade rotation frequency represented by N, the peak sounds consist of 4N resulting from the casing shape, 5N or the blade

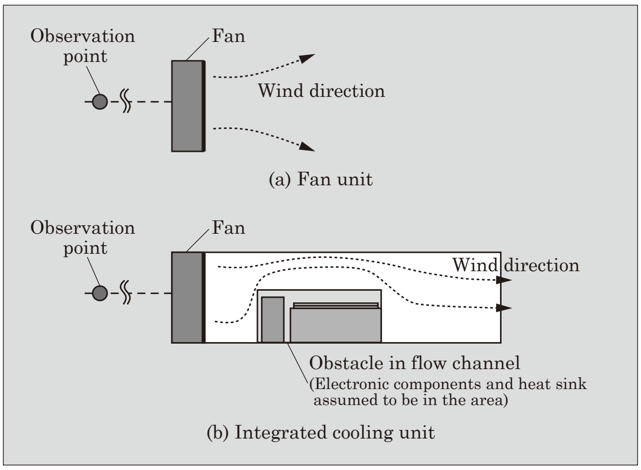

Fig.3 Structure studied

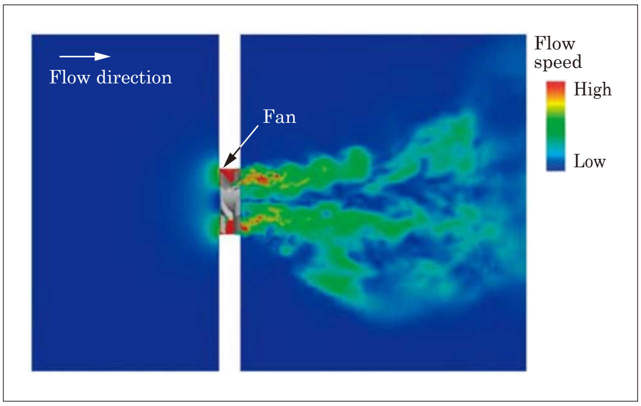

Fig.4 Flow speed distribution by LES at maximum efficiency point (instantaneous value)

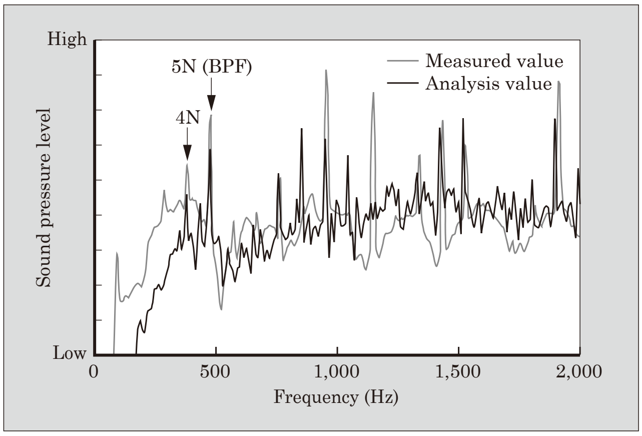

Fig.5 Sound pressure spectra for fan unit

passing frequency (BPF) resulting from the number of blades (5 blades) and their harmonic components. The portions that are not the peak sounds result from turbulence and are referred to as wideband sounds. In the analysis, of the peak frequencies, the peak sounds of 4N and BPF and wideband sounds, which provide the fundamental wave, are reproduced. In addition, the difference of the overall value (overall value of the sound pressure arrived at by adding up the sound pressure levels of the respective frequencies) between the results of analysis and measurement was not more than 5 dB. The reason why the measured values are at higher levels in the low-frequency region (approximately 300 Hz or lower) is assumed to be the acoustic effect of the measurement wind tunnel. Further, reproduction is estimated to become more accurate by including the wind tunnel structure in the target of analysis.

(2) Integrated cooling unit

We assumed a case of using actual power electronics equipment and studied the noise. The obstacle in the flow channel was modeled as a block to analyze the noise by using the direct method.

With the direct method, non-stationary variation of the sound level can be solved at the same time as the flow. Figure 6 shows the pressure distribution determined by LES at the maximum efficiency. It shows that the pressure propagates to the space upwind from the fan, i.e. the acoustic source. Because of the pressure change in the direction of rotation due to the blades, the pressure isosurface has a 3D structure. At this time, pressure variations at the observation point translate to sound. Figure 7 shows sound pressure spectra obtained in analysis and actual measurement. The analysis is generally successful in reproducing characteristics including the BPF and other peak frequencies, wideband noise distributed over wideband frequencies due to turbulence and resonance noise with peaks over a few hundred Hz. The results show that the analysis values are partly over-evaluated under 200 Hz. One factor in this is assumed to be that the effect of sound attenuation on wall surfaces of the

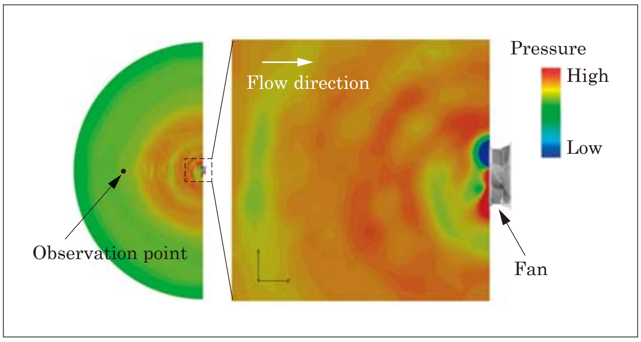

Fig.6 Pressure distribution at maximum efficiency point (instantaneous value)

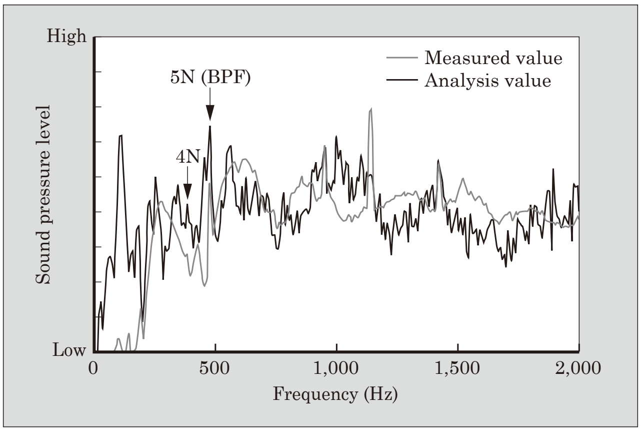

Fig.7 Sound pressure spectra with integrated cooling unit

structure is not taken into account.

When studying the cooling structure of a product, the distance between the fan and the obstacle as shown in Fig. 3(b) is one of the important design factors that should be considered for noise reduction. Accordingly, we used this method to verify the variation of the sound pressure level as this distance was varied (see Fig. 8). It shows that, as the distance increases, the sound pressure level decreases. This is considered to be a result of a decrease in the pressure variation generated by the flow from the fan outlet hit-

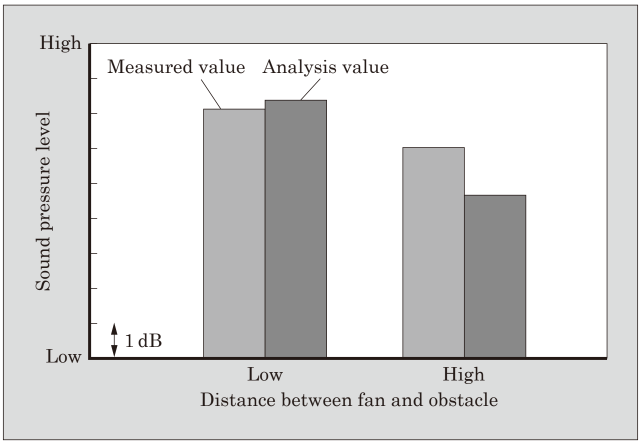

Fig.8 Distance between fan and obstacle and sound pressure level

ting the obstacle.

(3) Application of analysis results

We have obtained knowledge by studying noise with the fan unit and the cooling unit. And based on it, we are gradually working to apply aerodynamic noise analysis to the structural design of power conversion equipment such as uninterruptible power systems and power conditioning sub-systems.

4. Postscript

This paper has described aerodynamic noise simulation technology for developing low noise products.

Aerodynamic noise simulation has made it possible to visualize the variations of flow and pressure that provide noise sources. It can be used to grasp mechanisms and apply them to structural designs in order to reduce noise. In the future, we intend to contribute to eco-friendly product development while helping to enhance product performance, which are areas we have worked on up to now.

Some of the results mentioned in this paper have been obtained in cooperation with the organizations listed below. We would like to extend our sincere gratitude to the parties involved.

Computations were performed as industrial use (project number: hp140072, hp150143) of the “K computer” of the Institute of Physical and Chemical Research (RIKEN).

Some of the analysis of a fan unit was conducted under “Turbomachinery HPC Project: Prediction of Fan Performance and Noise WG3” of the Turbomachinery Society of Japan.

WG3 is participated in by the following organizations: the University of Tokyo, Waseda University, Hitachi, Ltd., DMW Corporation, Ebara Corporation, Mizuho Information & Research Institute, Inc., Advanced Simulation Technology of Mechanics R&D, Co. Ltd.

References

(1) Kato, C. et al. “An overset finite-element large-eddy simulation method with application to turbomachinery and aeroacoustics”, Trans. ASME, Journal of Applied Mechanics, 70 (2003), p. 32-43.

(2) Takayama, T.; Kato, C. “Numerical Prediction of Aerodynamic Noise Radiated from Propeller Fan”, Institute of Industrial Science The University of Tokyo. 2011, vol.63, no.1, p.61-64.

(3) Iwase, T. et al. “Prediction of aerodynamic noise for centrifugal fan of air-conditioner”, FAN 2015, Lyon (France), 15-17 April 2015.

(4) Kaneko, K. et al. The 13th Asian International Conference on Fluid Machinery (AICFM13), 2015, AICFM13-097.

(5) Curle, N. “The influence of solid boundaries upon aerodynamic sound”, Proceedings of the Royal Society, Series A, 231 (1955), 504.

(6) Powell, A. “The Theory of Vortex Sound”, J. of Acoust. Soc. Am., 33, (1964).

(7) Howe, M. S. “The Generation of Sound by Aerodynamic Sources in an Inhomogeneous Steady Flow”, J. Fluid Mech., 67-3 (1975), p.597-610.

Analysis of Pressure Rise During Internal Arc Faults in Switchgear

ASANUMA, Gaku * ONCHI, Toshiyuki * TOYAMA, Kentaro *

ABSTRACT

Switchgear include devices that play an important role in operations such as electric circuit switching and power measuring and monitoring, and IEC standards stipulate safety performance criteria regarding arc discharge (internal arc faults) in switchgear. Fuji Electric has developed an analysis technology for predicting pressure rise and pressure discharge performance during internal arc faults in order to design safe switchgear. By incorporating a pressure loss model in the vicinity of devices that discharge pressure and an arc model derived from the results of actual device testing, we have been able to implement highly accurate analysis. We have developed IEC standard compliant switchgear based on this analysis technology.

1. Introduction

In power reception and distribution facilities that connect power systems and power equipment, switchgear contains important devices responsible for electric circuit switching and power measuring and monitoring. To switchgear for overseas markets, an IEC standard (IEC 62271-200) applies. This standard contains enhanced approaches to safe structures such as classification relating to protection of people in the surrounding areas during failure and maintenance. It provides, among others, for safety performance against arc discharges (internal arc faults) in switchgear. If an internal arc fault occurs, energy supply from the arc heats up the atmospheric gas in the switchgear, and this causes the internal pressure to rise along with the increase in gas temperature. If the housing of the switchgear cannot withstand the pressure rise, the hot gas that has leaked out may make contact with people in the vicinity, developing into a critical accident. Accordingly, together with interlock technology that prevents internal arc faults in switchgear, it is important to have technology for venting hot gas in switchgear to the outside in the unlikely event of internal arc faults.

This paper describes analysis technology for predicting the pressure rise and pressure relief performance during internal arc faults as technology for designing safe switchgear.

2. Analysis Method

If an internal arc fault occurs, the following operations take place to prevent damage to the housing of the switchgear.

(a) Internal pressure rise due to arc energy (heating energy)
(b) Activation of the pressure relief device at the specified pressure
(c) Venting of hot gas via the pressure relief device
(d) Decrease of the pressure in the switchgear

Accordingly, the pressure rise value during internal arc faults must be predicted for designing the housing and pressure relief device. Specifically, it is necessary to predict the correlation between the arc energy generated and the internal pressure rise, and predict the operating performance of the pressure relief device.

To predict the arc energy, circuit analysis should be conducted that considers the relationships between the system voltage and impedance and between the short circuit current and arc voltage generated. An arc voltage is a potential difference generated between the 2 ends of an arc, and it causes a pressure rise in the switchgear. At the same time, it limits the current that flows through the system in the event of failure because it provides a back electromotive force against the system voltage. This arc voltage constantly changes according to the arc length, electrode material and current flowing into the arc, which makes it important to estimate it with accuracy.

Meanwhile, to predict the pressure relief performance in the switchgear, the mass flow rate of the hot gas that blows out must be determined by solving thermo-fluid equations. However, an internal arc fault may heat the gas around the arc to a high temperature of a few hundred to a few thousand K and ionization and dissociation may occur in the process, and this can cause the gas density and specific heat to vary in a nonlinear manner. The gas pressure, in particular, greatly depends on the gas density. For that reason, the nonlinear behavior of the property values of the gas must be taken into consideration. As shown in Fig.

* Corporate R&D Headquarters, Fuji Electric Co., Ltd.

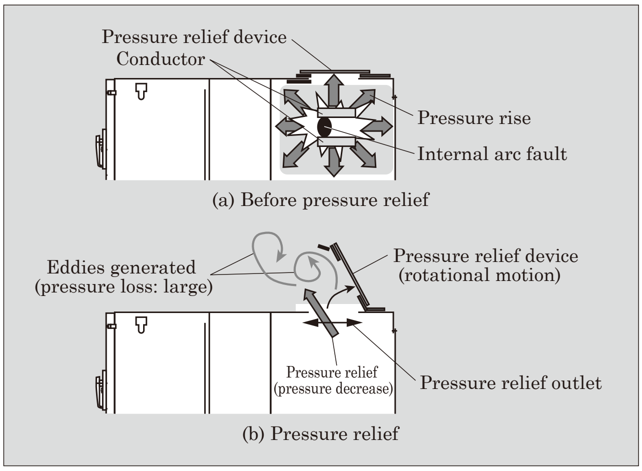

Fig.1 Operation of pressure relief device

1, the pressure relief device involves rotational motion at the time of pressure relief and the hot gas flows to the periphery and generates unsteady eddies. These may contribute to pressure loss. This makes it difficult to predict the pressure loss in the periphery of the pressure relief device.

We have built an analysis method that offers high accuracy for the pressure rise during internal arc faults by incorporating into numerical analysis the arc model and model of the pressure loss in the vicinity of the pressure relief device derived from the results of actual device testing.

2.1 Construction of arc model

An arc voltage can be represented as the sum of the positive column voltage shown in the first term and the electrode drop voltage shown in the second term in Equation (1). A positive column is the region between the electrodes where a strong light emission is observed.

$$V_{arc} = E_{arc}L_{arc} + V_{con} \quad \text{(1)}$$

$$E_{arc} = f\,(I_{arc}) \quad \text{(2)}$$

V_{arc}: Arc voltage (V)
E_{arc}: Arc electric field (V/m)
L_{arc}: Arc length (m)
V_{con}: Electrode drop voltage (V)
I_{arc}: Current flowing into the arc (A)

The electrode drop voltage, which is a voltage in the vicinity of the electrode generated when electrons and ions collide with the electrode, is a value specific to an electrode material. For copper used for power lines and bus bars of switchgear, the electrode drop voltage is 16.5 V[1]. Meanwhile, the arc electric field that constitutes the positive column voltage depends on the current that flows into the arc (flowing current), as shown by Equation (2). Accordingly, Equations (1) and (2) can be used to determine the arc electric field experimentally by defining the arc length (distance between electrodes), flowing current and arc voltage.

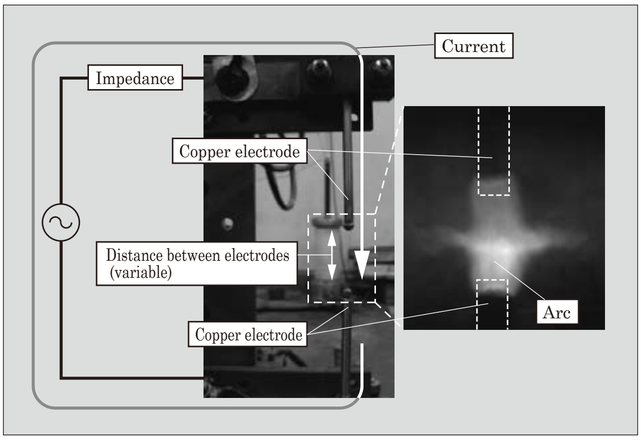

Fig.2 Basic test for arc electric field evaluation

Then, as shown in Fig. 2, we evaluated and obtained the current dependence of the arc electric field by basic testing for arc electric field evaluation. The following 2 test parameters were used.

○ Distance between electrodes L_{arc}: 2 to 20 mm
○ Flowing current I_{arc}: 1 to 10 kA

Figure 3 shows the results of measuring the arc voltage against the flowing current for different distances between electrodes. It indicates that, in the

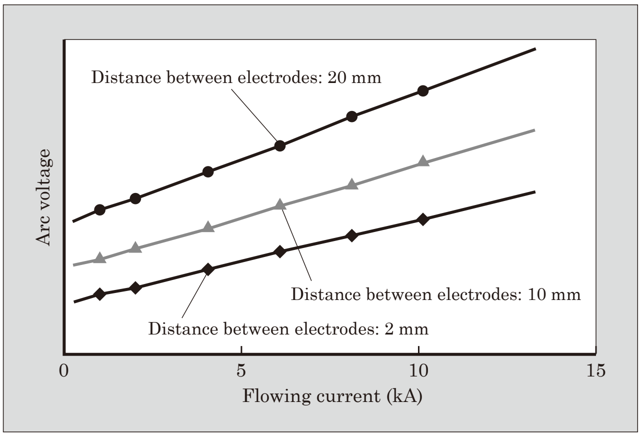

Fig.3 Relationship between flowing current and arc voltage

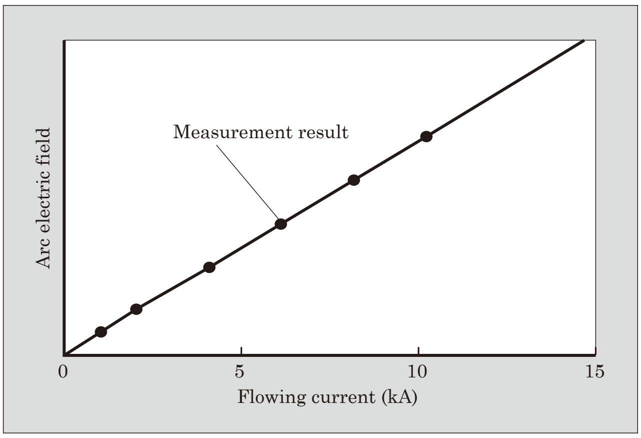

Fig.4 Relationship between flowing current and arc's electric field

current range that has been obtained, the arc voltage and flowing current are in a linear relationship. The relationship of the arc electric field with the flowing current calculated by using Equations (1) and (2) is shown in Fig. 4. It shows that the arc electric field and the flowing voltage are also in a linear relationship. Based on this finding, we used linear approximation to formulate the arc electric field against the flowing current and incorporated it into the arc model built for circuit analysis.

2.2 Simplified thermo-fluid analysis method

For thermo-fluid analysis, the finite volume method is generally used. The atmospheric gas in the switchgear is air (compressible viscous fluid) and, at the time as pressure relief operation, eddies are generated in the vicinity of the pressure relief device due to the viscosity and a pressure loss is generated by the change (rapid reduction and rapid expansion) in the flow channel's cross-sectional area of the opening. In addition, the pressure relief device is subject to a change in angle over time due to the rotational motion. For that reason, the pressure loss is unsteady. In order to predict this change in the pressure loss, it is necessary to solve fluid equations that allow for the shape of the pressure relief device changing over time. Unsteady coupled analysis of fluid in a structure involving a shape change requires a large amount of computation time and was difficult to apply to actual design of components of switchgear, which are individually designed.

The simplified thermo-fluid analysis method that has been developed is aimed to realize both reduced computation time and ensured analytical precision and built as a finite volume heat dissipation fluid analysis method specialized in prediction of pressure rises during internal arc faults by measuring the behavior during pressure relief operation, which involves high computational load, and reflecting the results to analysis. This method has 3 characteristics:

(1) Element breakdown with rectangular parallelepiped meshes

In order to simulate a general 3D shape of switchgear composed of rectangles, rectangular parallelepiped meshes have been used to break down the elements.

(2) Accommodation of nonlinearity of property values

When an internal arc fault occurs, property values related to pressure and temperature (density, specific heat and thermal conductivity) become nonlinear due to ionization and dissociation of the gas. The constructed method accommodates this nonlinearity and rapid change in the pressure, etc. due to ionization and dissociation can be solved with high accuracy.

(3) Analysis of pressure relief portion with ensured accuracy

In order to allow for pressure losses due to viscosity in the vicinity of the pressure relief device, we measured the relationships that the opening area, rotation angle and pressure loss of the pressure relief device have with the flow speed of the gas that passes through the pressure relief outlet in the basic test. We then incorporated the results into the analysis. This has made it possible to analyze the pressure relief portion with ensured accuracy and reduced the computational load.

2.3 Obtaining pressure-loss characteristics in the vicinity of pressure relief device

To obtain the pressure-loss characteristics in the vicinity of the pressure relief device, we used a pressure vessel equipped with a pressure relief device to conduct a basic test (see Fig. 5). For the test, the pressure vessel was filled with pressurized air from a high-pressure cylinder and the pressure was relieved by pulling out the movable lever. We used a pressure sensor to measure the pressure loss in the vicinity of the pressure relief device during pressure relief and the estimated outlet speed of the gas vented to the outside of the vessel from the pressure change. We also determined the change in rotation angle of the pressure relief device by using a high-speed camera.

As the test parameters, the opening area of the pressure relief outlet, maximum rotation angle of the pressure relief device and the filling pressure for the pressure vessel were used and their relationships with the pressure loss were evaluated.

An example of pressure-loss characteristics obtained from the test results is shown in Fig. 6. The flow speed of the gas that flows out of the pressure relief outlet increases along with the rotation of the pressure relief device and reaches its peak at the maximum rotation angle (60° in Fig. 6). Subsequently, the flow speed decreases as the pressure in the vessel decreases. The process of decrease of the gas flow speed is nonlinear. However, it has been incorporated into analysis by simulating with an approximate curve derived from the pressure loss in the vicinity of the pressure relief outlet, maximum rotation angle of the

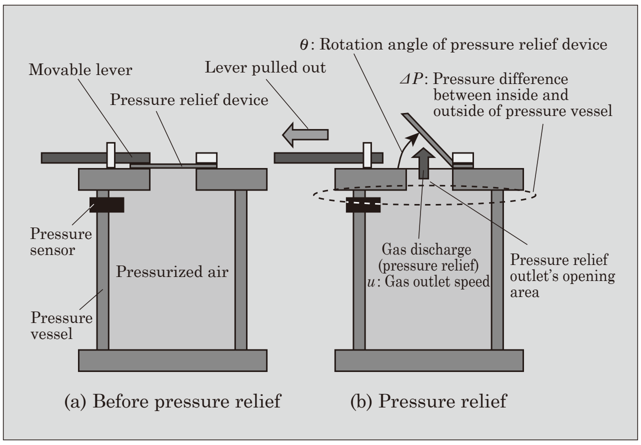

Fig.5 Outline of basic test for obtaining pressure loss characteristics in vicinity of pressure relief device

issue: Simulation Technologies for Product Development

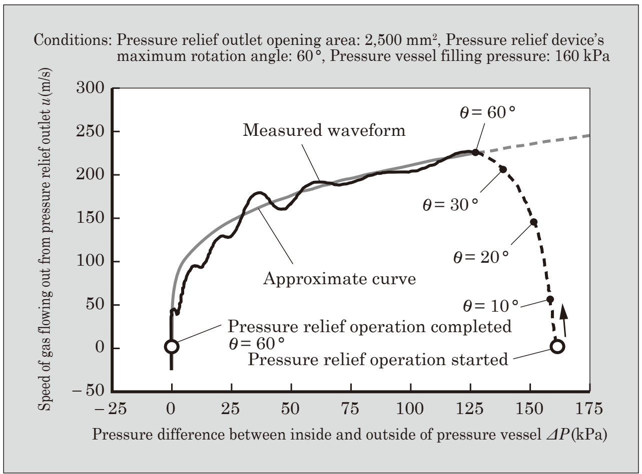

Fig.6 Example of pressure-loss characteristics in vicinity of pressure relief device

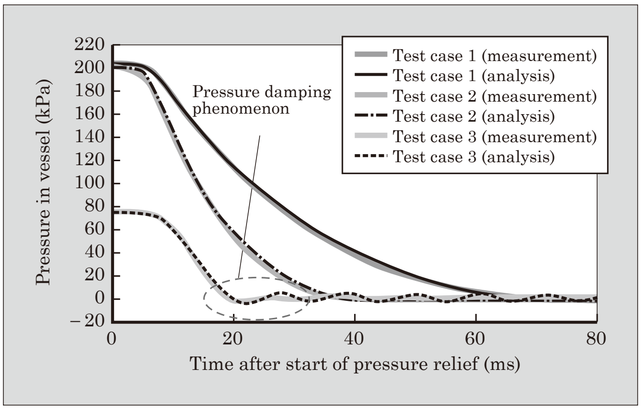

Fig.7 Comparison between results of measurement in pressure-decreasing process during pressure relief and of analysis

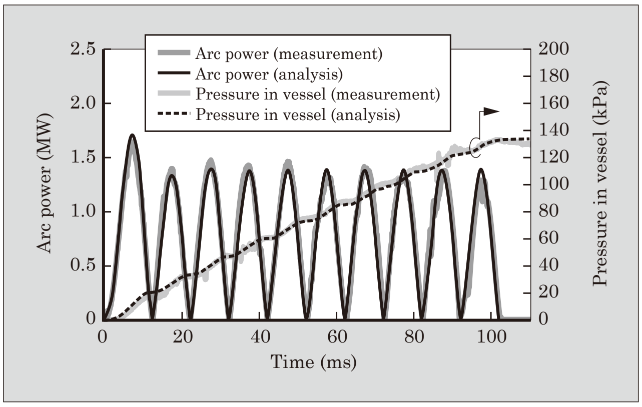

Fig.8 Comparison between results of measurement and analysis in pressure rising process during arcing

pressure relief device and opening area of the pressure relief outlet.

3. Analysis Results

To evaluate the validity of the analysis method developed, we conducted 2 tests for comparison with the analysis.

(1) Pressure decreasing process in pressure relief

For verifying the validity of the analytical precision in the pressure decreasing process that takes place during pressure relief, we made a comparison with the pressure relief test using the pressure vessel described above. Table 1 lists the test conditions. This test does not include heating of the gas (pressure rise) by arcing and is sufficient only for evaluating the validity of the model of the pressure loss in the vicinity of the pressure relief device incorporated into the analysis. Figure 7 shows a comparison between the results of measurement in the pressure-decreasing process during pressure relief and of the analysis. The pressure waveforms from the results of measurement and analysis show good correspondence with each other, which indicates that the analysis is capable of simulating the phenomenon that occurs during pressure relief. The volume of gas that passes through the pressure relief outlet is large when the opening area of the pressure relief outlet and the maximum rotation angle of the pressure relief device are large and the inertial force of the gas flow causes a damping phenomenon around 0 kPa. It has been verified that the analysis simulates this phenomenon.

Table 1 Test conditions for pressure relief test using pressure vessel

Condition No.	Size of pressure relief outlet	Filling pressure of pressure vessel	Maximum rotation angle of pressure relief device
Test case 1	50 × 50 (mm)	200 kPa	30°
Test case 2	70 × 70 (mm)	200 kPa	60°
Test case 3	100 × 100 (mm)	75 kPa	90°

(2) Pressure-rising process during arcing

We wished to verify the validity of the analytical precision in the pressure-rising process that takes place when an arc is formed. Therefore, we sealed the pressure vessel and had an arc form in the pressure vessel to measure the actual pressure rise. The results were then compared with the analysis results. We calculated the results of the circuit analysis on the arc power and of the simplified thermo-fluid analysis using the calculated arc power as the input and compared them with the results of measurement for them respectively, which is shown in Fig. 8. Both the arc power and pressure waveforms show good correspondence with the measured values, which indicates that this analysis method is capable of simulating the phenomenon during a pressure rise.

4. Application to Switchgear Conforming to IEC Standard

By using the method of analyzing pressure rise during internal arc faults that has been developed, we studied switchgear conforming to the IEC Standard. The analysis conditions used are the same as the test conditions for internal arc testing conforming to an international standard IEC 62271-200, as shown in Table 2. Figure. 9 shows interphase arc power waveforms derived by circuit analysis. As a result of analysis, arc power has been found to peak immediately after the occurrence of an internal arc fault and decrease thereafter.

We next present the results of pressure analysis that uses as the input the arc power waveforms obtained by the circuit analysis. Figure 10 shows the shape of the switchgear analyzed and the result of analysis of pressure distribution immediately after arcing. As the figure indicates, pressure waves have been found to propagate through the switchgear from the arc at the center.

Furthermore, we compared the results of analysis with the results of measurement for validity evaluation. Figure 11 shows the results of measurement by using pressure sensors located in the vicinity of the pressure relief device and arc respectively and results of analysis of pressure in the respective sensor locations.

The pressure during an internal arc fault is shown to continue to increase even after activation of the pressure relief device. This is because it takes a few ms before the pressure relief device reaches the maximum opened state after starting rotational motion. As shown in Fig. 11, the results of measurement and analysis show good correspondence and validity of the analysis method has been verified. In addition, this method has the analysis time reduced from the general-purpose thermo-fluid analysis method, which allows it to be applied to actual design.

In the development of switchgear shown in Fig. 12, we conducted structural analysis with the aforementioned analysis results used as the input data, thereby estimating the locations to be reinforced, which was fed back to the structural design. In this way, we have

Table 2 Internal arc test conditions for switchgear conforming to IEC Standard

Item	Condition
System voltage (RMS value)	11 kV
Short circuit current	18 kA
System frequency	50 Hz
Short circuit mode	3-phase short circuit

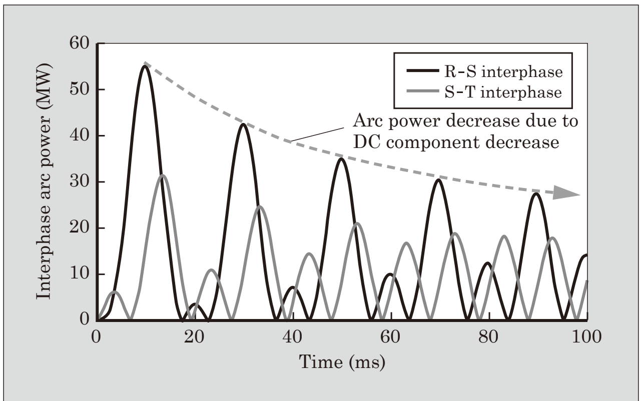

Fig.9 Results of analysis of interphase arc power generated

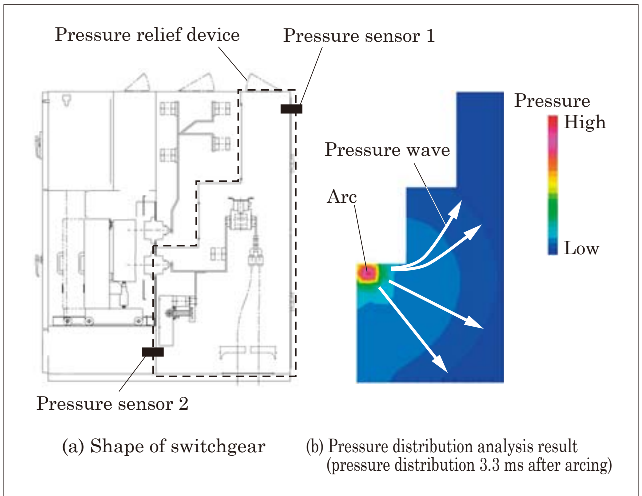

Fig.10 Shape of switchgear and result of pressure distribution analysis

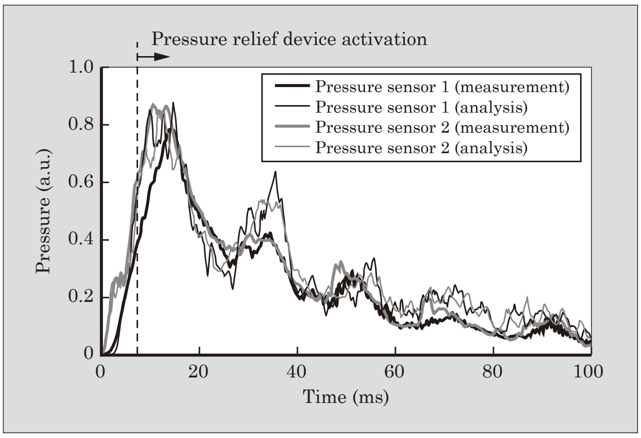

Fig.11 Comparison between pressure waveforms between different pressure sensor mounting locations

Fig.12 7.2-kV switchgear conforming to IEC Standards completed the development of a product conforming to the IEC Standard.

5. Future Development

We have successfully predicted pressure rise during internal arc faults of switchgear by applying the analysis method described in this paper. This method also allows prediction of the flow speed, density and temperature of the hot gas flowing out of the pressure relief device and, in the future, we plan to study diffusion outside the switchgear of the hot gas after passing through the pressure relief device.

6. Postscript

This paper has presented analysis of pressure rise during internal arc faults in switchgear. Power demand is expected to continue to increase overseas, especially in Asia, which involves addition and equipment replacement of switchgear estimated. Analysis technology (prediction technology) is required for designing safe power reception and distribution facilities and, schemes to satisfy computational speed requirements adequate for actual design are necessary. In the future, we intend to continue to work on the building of analysis technology in view of actual design of devices.

References

(1) Yokomizu, Y. et al. Total voltage drops in electrode fall regions of SF_6, argon and air arcs in current range from 10 to 20000 A, Journal of Physics D: Applied Physics. 1996, vol.29, no.5, p.1260-1267.

Thermo-Fluid Simulation Technique for Achieving Energy Saving in Open Showcases

NAKAJIMA, Masato* ASADA, Tadashi*

ABSTRACT

More than half of the electric power load in open showcases used in stores such as supermarkets and convenience stores is heat invasion that comes from the front opening of the displays. In order to save energy on the showcases, it is necessary to improve the performance of air curtains that suppress this heat invasion. Air curtain performance changes over time based on the impact of frost formation on the evaporator. Fuji Electric has developed a thermal-fluid simulation technique for elucidating this phenomenon, and based on this technique, we have developed a new air curtain system. Demonstration results achieved improved energy saving of more than 30% compared with conventional systems.

1. Introduction

Stores such as supermarkets and convenience stores are required to save energy due to the amendment to the Act on the Rational Use. of Energy (Energy Saving Act) and its enforcement. Fuji Electric offers smart stores that make efficient use of energy to save on the energy consumed by an entire store. The equipment that consumes the most electric power in a store is refrigeration equipment such as an open showcase. With an open showcase, about 80% of the heat load is accounted for by heat invading through the air curtain and improving the performance of the air curtain is the key. The performance of air curtains varies with time due to the attachment of frost (frost formation) to the evaporator. Fuji Electric has developed a thermo-fluid simulation technique for clarifying this change in air curtains over time. We have also made use of this technique to develop a new air curtain system for saving energy.

2. Open Showcase Configuration

Figure 1 shows the structure of an open showcase. Open showcases do not have a door and the warm air entering through the front opening is blocked by using air curtains so that products are kept cool. The evaporator installed in the duct generates cold air, which is blown out of the air curtain outlet and the back outlets in the back panel by using a fan and drawn into the air inlet, forming an air curtain. The evaporator that generates cold air develops frost over time as shown in Fig. 2 because warm air containing moisture enters through the air curtain. The frost attached causes resistance in the air trunk and decreases the circulating air volume, which causes more air to enter through the front opening. Accordingly, in the development of open showcases, it is important to control the air flow of air curtains in view of changes in frost attachment over time.

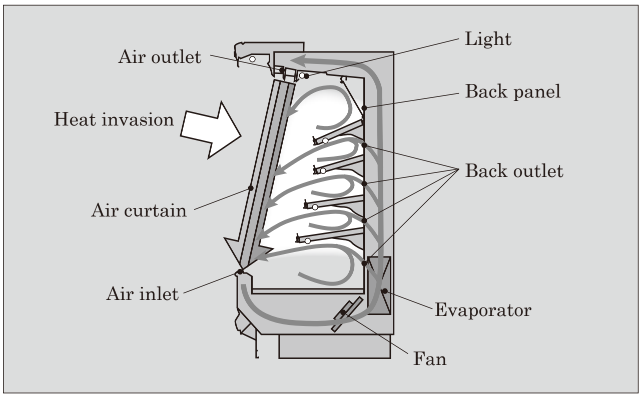

Fig.1 Open showcase structure

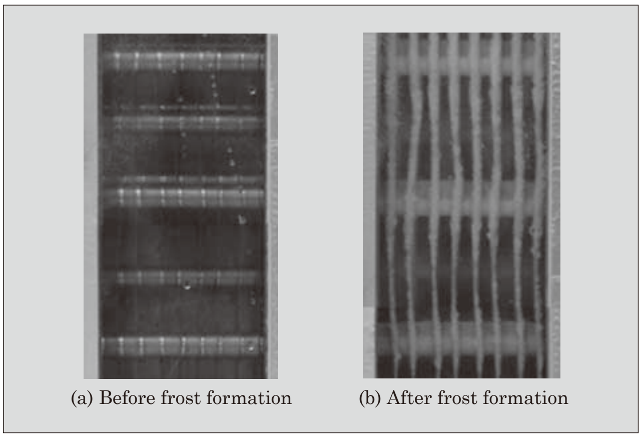

Fig.2 Frost formation phenomenon of evaporator

* Corporate R&D Headquarters, Fuji Electric Co., Ltd.

3. Simulation Technique

3.1 Incorporation of effect of frost formation

The flow of the developed simulation is shown in Fig. 3. With thermo-fluid simulation alone, as is the conventional way, the effect of changes in frost attachment over time cannot be taken into consideration. Hence, we independently developed and introduced a frost formation simulator that predicts the growth of frost. First, thermo-fluid simulation was conducted in the initial conditions with no frost formed to determine the temperature, humidity and velocity of the air drawn into the evaporator. Based on the temperature, humidity and velocity, the wind velocity according to the frost thickness, surface temperature of the frost and humidity of the air blown out of the evaporator were calculated in the frost formation simulator. The results were then reset to thermo-fluid simulation as the boundary conditions. We repeated this operation and proceeded to the calculation for the next period when the temperature and humidity changes of the air drawn into the evaporator were conversed. We completed the calculation when the specified period elapsed.

The frost calculation model in the frost formation simulator is shown in Fig. 4. Growth of frost is mainly influenced by the temperature of the cooling surface and the temperature, humidity and velocity of the air flowing through the evaporator, and these have been used as parameters to build a frost calculation model. When frost is formed, the frost's surface temperature is used instead of the temperature of the cooling surface. The frost formed is distributed in the direction of flow of the evaporator. A large amount of frost is attached especially on the inlet side, where the temperature and humidity of air are the highest. For this reason, to more accurately predict frost formation it is necessary to run a simulation of frost distribution in the direction of flow of the evaporator. Accordingly, we used a model of an evaporator divided into several sections in the direction of flow and predicted the frost thickness and thermal conductivity in the respective sections based on the temperature and humidity of the air drawn in. The frost thickness was used as the basis to calculate the pressure loss of the evaporator and the humidity after dehumidification. Then, the air temperature and humidity calculated were passed on to the following section. In this way, calculation is performed in all sections in this model.

Changes in the average temperature inside showcase over time were calculated by simulation with frost formation taken into consideration. The results were then compared with the result of measurement (see Fig. 5). There is no change in the temperature without frost formation taken into consideration. By considering frost formation, however, the temperature was found to rise over time, which agreed with the actual trend. The temperature rise is due to frost formation that not only decreases the heat exchange amount between the evaporator and the circulating air but also lowers the wind velocity of the air curtain, which causes more air to enter through the front opening.

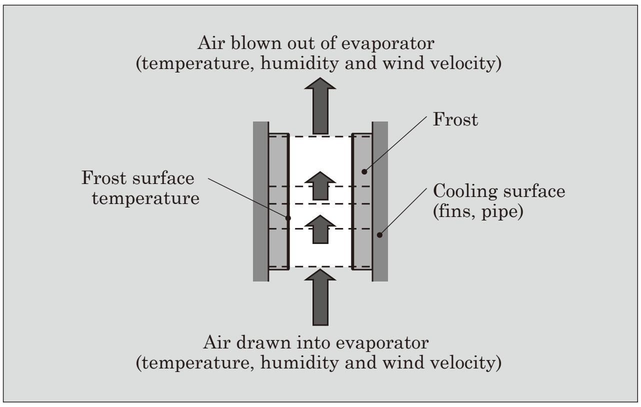

Fig.4 Frost calculation model

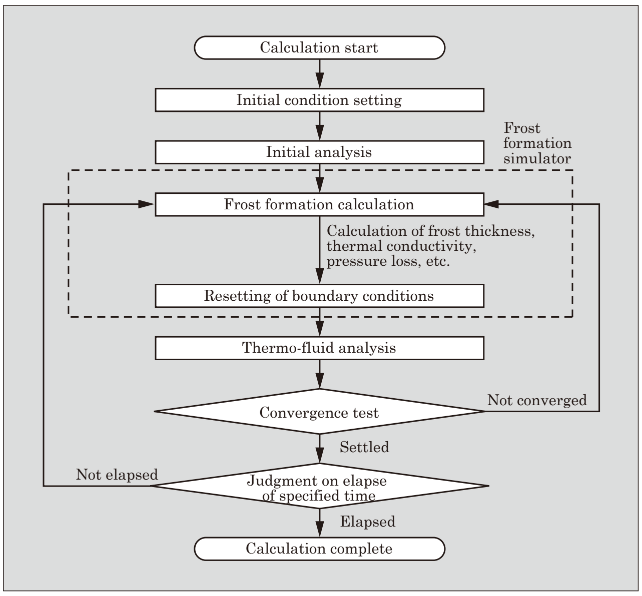

Fig.3 Flow of simulation

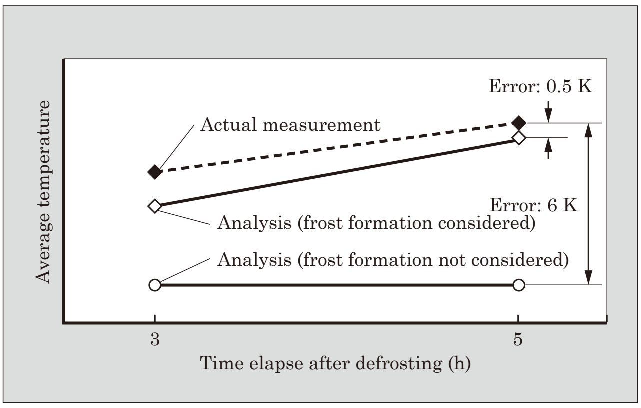

Fig.5 Example of change in average temperature inside showcase over time

3.2 Optimization design technique

As shown in Fig. 6, there are many factors involved in controlling the air curtain of open showcases and we have developed an optimization design technique for balancing them. Figure 7 shows the flow of a design that uses the technique. Open showcases may come in many different models and the number of factors may vary depending on the model. An ability to accommodate multiple factors is also required. Accordingly, we determined the parameters for the calculation samples based on Latin hypercube design (LHD), which allows the number of factors to be freely specified. Next, based on the calculation samples arranged, the analysis model is created by using the showcase design tool that applies the thermo-fluid simulation technology described in 3.1 (see Fig. 8) to perform analysis. Then, the results of analysis (characteristic values) were used to approximate the response surface using a radial basis function (RBF) network and the optimal solution was found by particle swarm optimization (PSO). For example, for the design of the open showcase shown in Fig. 6 with 12 factors, we calculated samples with 66 different conditions to obtain the optimal solution.

The showcase design tool developed for the purpose of creating many sample models and reducing the analysis time can create meshes, execute analysis and display the results simply by using general-purpose software (Excel[*1]) to input parameters of each sample, as shown in Fig. 8.

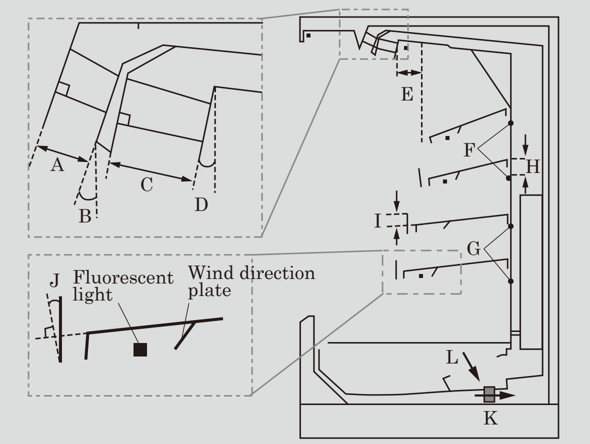

A	B	C	D	E	F
Outer width	Outer angle	Inner width	Inner angle	Inner position	Back width 1
G	H	I	J	K	L
Back width 2	Back position	Fence height	Fence angle	Outer wind velocity	Wind velocity

Fig.6 Factors involved in air curtain control of open showcases

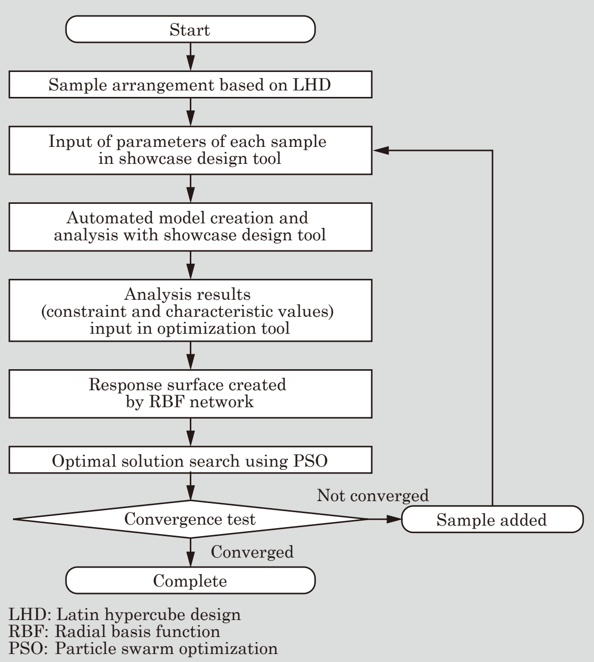

Fig.7 Design flow by optimization design technique

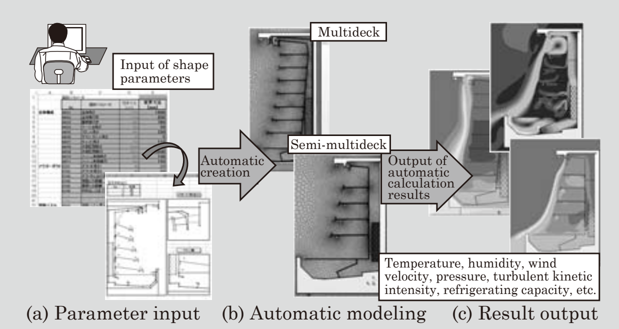

Fig.8 Showcase design tool

4. Effect of Application of Simulation Technique

For the new air curtain system developed by using the optimization design technique and the conventional system, we simulated the wind velocity and turbulent kinetic energy distributions (see Fig. 9 and 10). The conventional system is characterized by a high wind velocity that is used to maintain the external air blocking performance from the air outlet to the inlet of the air curtain. This causes the turbulent kinetic energy to rise, increasing the amount of warm air dragged in at the front opening. Meanwhile, in the new air curtain system, the cold air from the back outlets is gradually mixed with the air curtain, which reduces the supply air flow velocity of the air curtain, decreasing the turbulent kinetic energy and hence the amount of warm air dragged in.

We built a demonstration model based on this simulation result and performed evaluation. The re-

*1: Excel is a trademark or registered trademark of Microsoft Corporation of the U.S.

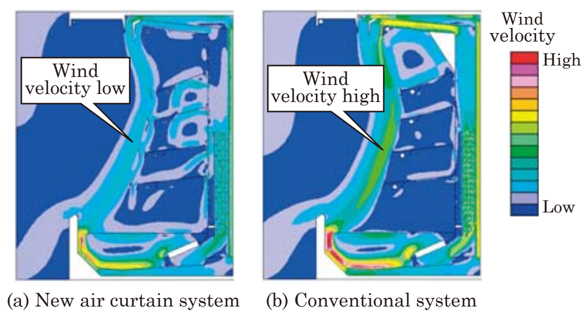

Fig.9 Results of simulation of wind velocity distribution

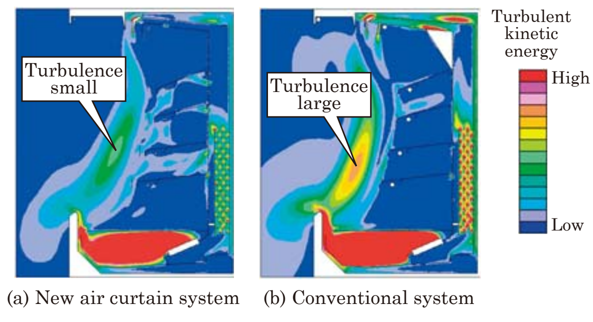

Fig.10 Results of simulation of turbulent kinetic energy distribution

sults showed we had successfully saved energy by over 30% as compared with the conventional system. In addition, the decrease of the air entering through the front opening has allowed the refrigerant evaporation temperature to increase by approximately 4K. This reduces the amount of frost developed, which is also considered to have contributed to energy saving.

5. Future Development of Simulation Technique

Fuji Electric is studying open showcases to work

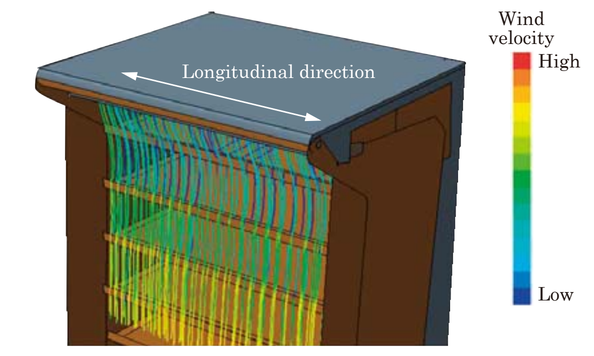

Fig.11 Example of air flow analysis by 3D simulation

on a 3D thermo-fluid simulation technique for achieving further energy saving and enhancing the design of a showcase that cannot be simulated by 2D cross sections. Figure 11 shows an example of air flow analysis by 3D thermo-fluid simulation. We have made use of 3D simulation to develop a structure that provides a uniform wind velocity distribution in the longitudinal direction of air curtains. In this way, we intend to establish technology for verifying the air flows in the 3D directions of air curtains and in ducts in the future. The aim is to further improve the energy efficiency of open showcases.

6. Postscript

We have developed a thermo-fluid simulation technique for open showcases that takes frost formation into consideration and realized energy savings by using a new air curtain system that applies an optimization design technique. In the future, we intend to further the application of this simulation technique to development and design so that we can offer even more ecological and energy-saving open showcases.

Simulation Technologies Supporting Quality Improvement in Injection Molding

YAJIMA, Asuka* SUGATA, Yoshinobu* YOKOMORI, Noriharu*

ABSTRACT

Plastic has excellent electrical insulation properties and is often utilized in various products due to its mechanical properties and characteristics. In order to improve the quality of plastic parts, Fuji Electric has utilized resin flow analysis to elucidate the quality and productivity issues that exist during the early stages of development. Furthermore, we have been reflecting our findings into the design of our products and molds. We have verified ease of assembly in consideration of warping by using the analysis results and a 3D printer, and as a result, we developed parts suitable for automated assembly in a short time. We have also utilized unsteady heat transfer analysis to optimize the temperature control circuit for molds and have significantly reduced the molding cycle. Furthermore, we have been working to estimate the fiber length of fiber-reinforced plastic, and are now able to determine the distribution trends of the fiber length that affects the strength of parts.

1. Introduction

Plastic has excellent electrical insulating properties and many types of plastic have mechanical properties, sliding properties and thinner resistance that makes them applicable to industrial parts. Fuji Electric uses plastic in many of its products including power electronics equipment, food distribution facilities and electronic devices.

In recent years, as the globalization of production bases accelerates, needs have arisen for products that have the same quality all over the world. In order to meet such requirement in plastic parts molding, it is important to establish quality by making every problem that results from product/mold design apparent. This must be done during the early stages of development in which product shapes or mold structures can be designed more freely and modified at lower cost.

Resin flow analysis and other simulation technologies are effective tools not only for predicting improper dimensions or poor external appearance but also for designing products and molds. This should be done in consideration of productivity at stages including verification of the ease of assembly or the optimization of the mold temperature control circuit.

This paper describes our approaches for increasing the quality of injection molded parts by taking advantage of simulation technologies.

2. Simulation Technologies in Injection Molding

In injection molding, plastic material is fed into a mold in the injection process, sent to the dwelling and cooling processes and then removed from the mold. During these processes, the resin, which is the major component of plastic material, changes from a flowing state to a solid as heat is exchanged with the mold, and shrinks after it is released from the mold until the temperature equilibrates. Moreover, the reinforcement fiber in fiber-reinforced plastic material is oriented along the flow of the resin in the mold, which produces anisotropy in shrinkage or strength. Resin flow analysis is a technology for simulating the behavior and state of the resin over this period.

Figure 1 shows the relationship between injection molding processes and resin flow analysis. Resin flow analysis can be used to determine whether molding is possible or not based on filling pressure or the occurrence of unfilled area. It can also be used for predicting various factors of molding quality, such as warp-

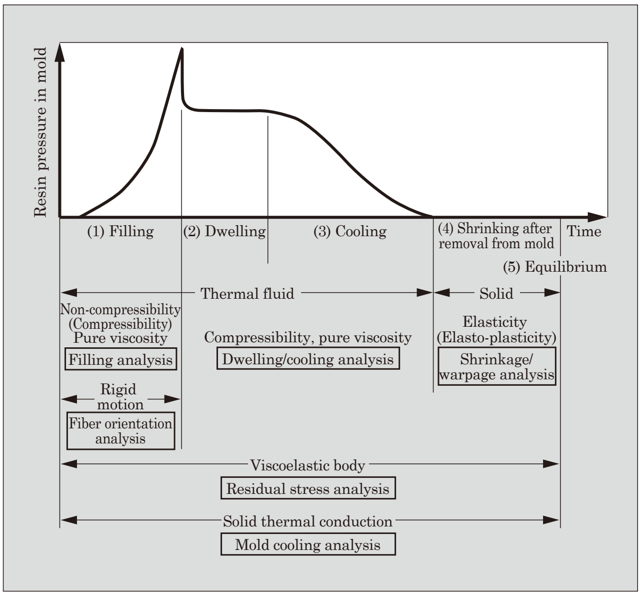

Fig.1 Relationship between injection molding processes and resin flow analysis

* Production & Procurement Group, Fuji Electric Co., Ltd.

age, the deformation of insert parts, or the position of weld[*1]. It is also possible to predict fiber orientation which determines the strength of fiber-reinforced plastic.

Filling pressure can be used not only for calculating a mold clamping force of the injection molding machinery (the force applied to the mold to prevent it from opening), but also together with structural analysis for predicting mechanical stress or deformation of the mold. By checking the strength of mold parts and studying optimum shapes with minimum waste before creating molds, we can ensure more refined mold design and provide more reliable products.

The fiber orientation, position of weld and warpage predicted in resin flow analysis can be incorporated into an analysis model for structural analysis to predict the strength of molded products. In recent years, it has become possible to analyze not only fiber orientation but also fiber damage in the flowing resin including those in the molding machinery cylinder. This is then used to predict the fiber length distribution in molded products. Consequently, it has become possible to predict the strength with higher accuracy and reflect it in the design of products and molds.

Mold temperature is a factor that greatly affects productivity as well as the ease and quality of molding. Conventional mold cooling analysis was steady analysis assuming that the average value was constant while the temperature fluctuated in the molding cycle. By using unsteady mold cooling analysis, we can now see the chronological change in the temperature of various sections of the mold from the start of molding to when the mold temperature stabilizes, and check for hot spots after the temperature stabilizes.

3. Resin Flow Analysis

3.1 Warpage analysis utilization

Warpage in molded products caused by resin shrinkage not only reduces the functionality of parts but also affects the fit with other parts and the feasibility of automated assembly.

We have already utilized the result of warpage analysis for studying fitting state (see Fig. 2). The ease of assembly has been checked with prototypes created by cutting or with a 3D printer based on the drawing dimensions; however, the influence of warpage was mainly verified with products molded with prototyped molds. In recent years, we have been using a 3D printer to print out a deformed shape obtained in the warpage analysis and using it to check the ease of assembly (see Fig. 3). Such an approach makes it possible to optimize parts shapes or mold structures to determine dimensions applicable to automated assembly in the design stage. This results in less mold modifications and a shorter development period.

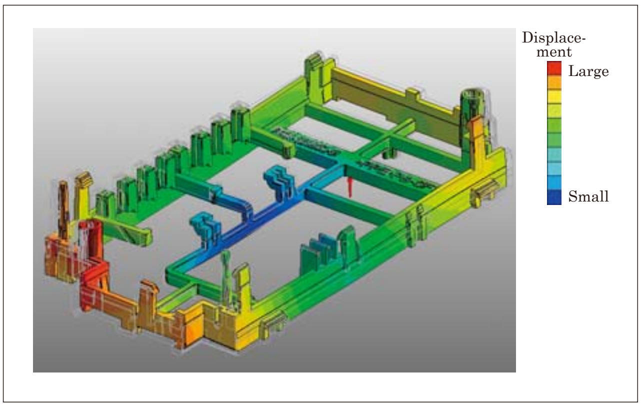

Fig.2 Example of warpage analysis of power electronics equipment part

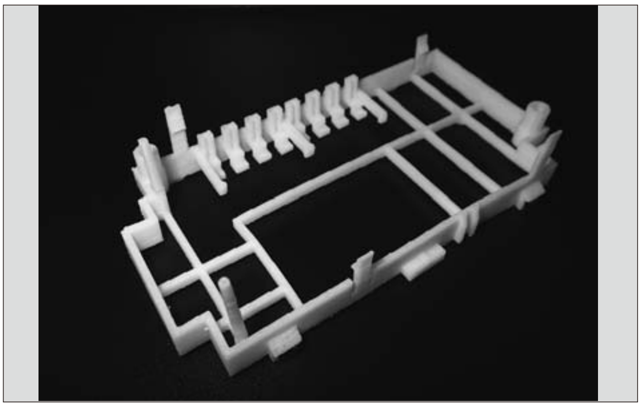

Fig.3 Example of 3D printer printout of power electronics equipment part

3.2 Weld avoidance

Not only does a weld have a poor external appearance, but also it is known that weld regions have extremely low strength that might cause fractures especially in the case of fiber-reinforced plastics.

Many of the plastic parts that Fuji Electric handles are product housings and mechanical parts that require good mechanical properties. Due to their

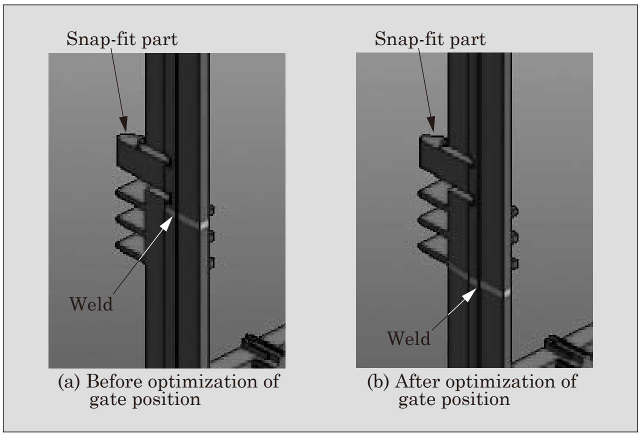

Fig.4 Example of prediction of weld positions

*1: Weld refers to a thin line-shaped molding failure generated at the section where the flows of molten resin meet.

complex shapes and openings, weld is inevitable. We therefore use filling analysis to predict the positions where welds will be generated. We then avoid placing welds in high-stress sections by optimizing gate positions and product shapes in consideration of molding possibility (filling pressure, occurrence of unfilled area), fiber orientation and the amount of warpage.

Figure 4 shows an example of predicting weld positions. In the power electronics equipment part shown above, optimizing the gate position allows us to avoid placing welds at the base of the snap-fit part to which high stress is applied.

3.3 Mold corrosion prevention

In injection molding, the air in the mold before plastic material is fed in and the decomposition gas generated from the plastic material flowing into the mold may cause various molding failures such as short shots (incomplete filling) or burn marks (scorch on the product surface). Fire-resistant plastic materials, in particular, generate corrosive gases which must be discharged efficiently from the mold. This is because they may be heated to a high temperature by adiabatic compression at the final filling area in the mold and cause mold corrosion that degrades productivity and quality.

Filling analysis enables us to predict the position of final filling or trapped air (gas trapped by resin), and we use it for optimizing gate and the gas vent (opening for discharging the gas from the mold) position and product shapes.

Figure 5 shows an example of filling analysis for the housing of a low-voltage circuit breaker. This is an example of optimizing a product shape to prevent mold corrosion. The images show that, before the optimization, resin filling was completed faster on the gas vent side and inhibited the discharge of the gas. After the optimization, the resin is filled more slowly on the gas vent side so that the gas can be discharged more easily.

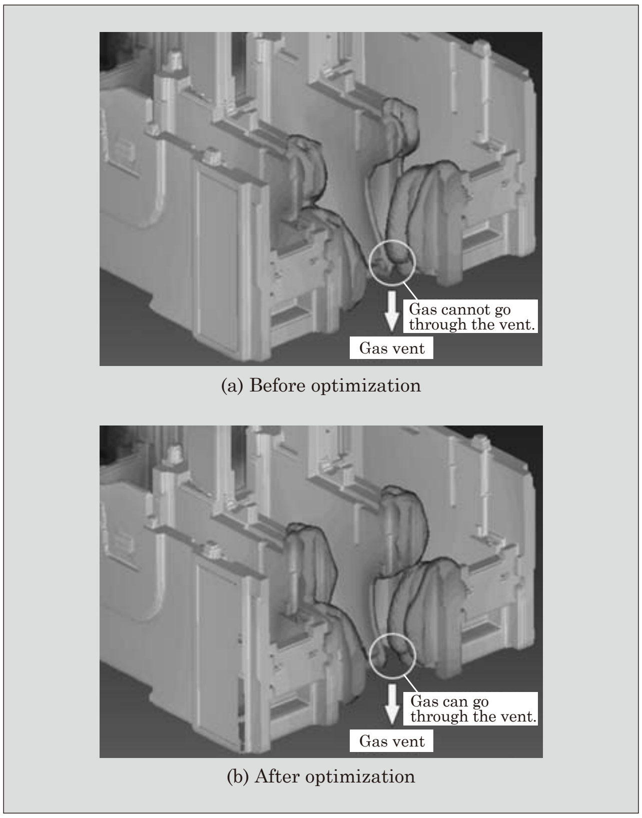

Fig.5 Example of filling analysis for housing of low-voltage circuit breaker (filling ratio: 90%)

4. New Approaches for Increasing Quality

4.1 Optimization of the temperature control circuit of the mold for high-speed molding

In injection molding, the cooling time takes up most of the molding cycle. The larger the size of molded products, the higher the ratio tends to be. Consequently, one possible measure for improving productivity is to lower the mold temperature and shorten the time for cooling injection molded parts. It must be noted that lowering the mold temperature may cause insufficient filling or transfer failure.

To solve this problem, Fuji Electric has established a high-speed molding technology that proactively controls mold temperature during a molding cycle. By this technology, greatly shortens the molding cycle time while ensuring high quality. Figure 6 shows the mold temperature profile obtained with the high-speed molding technology. Specifically, a heater is placed near the contact surface between the mold and plastic material. It heats the mold quickly after the molded product of the previous shot is removed and until the next injection starts. After the filling is complete, the temperature is controlled to help the material be cooled with cooling water.

This technology cannot be achieved without a temperature control circuit that can heat and cool the mold quickly and uniformly. We use resin flow analysis to predict the resin temperature distribution, determine the sections that should be heated or cooled proactively, and reflect the result in the design of the mold for high-speed molding. Since we need to proactively cool the mold parts which heat up easily, we achieved a

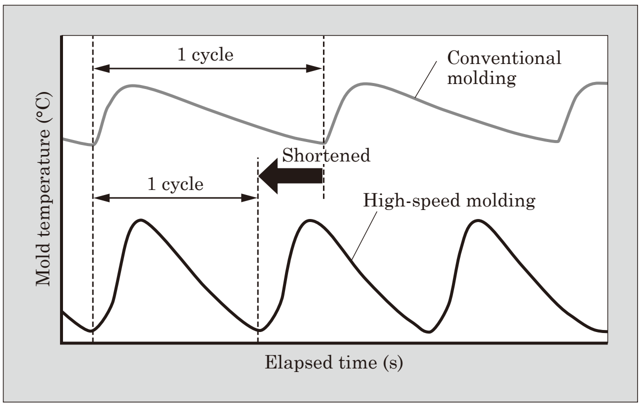

Fig.6 Mold temperature profile

cooling effect and uniform temperature of the mold by using a 3D printer to form a 3D cooling water channel inside, which is shown in Fig. 7.

We optimized the layout of the heater by checking the temperature rise rate and temperature distribution of the heated surface through unsteady heat transfer analysis. We considered a heater installation method to increase thermal efficiency and installed heaters onto moving parts with small and complex structures. Figure 8 shows a comparison between the analysis value and measured value of the temperature distribution of the mold. Figure 9 shows a comparison between the analysis value and measured value of the heater current dependence of the mold temperature rise rate. The measured values of the temperature distribution and temperature rise rate of the mold well match with the analysis result.

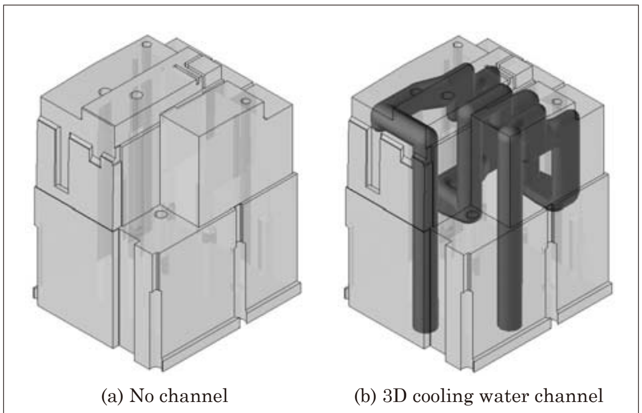

Fig.7 3D cooling water channel in mold part

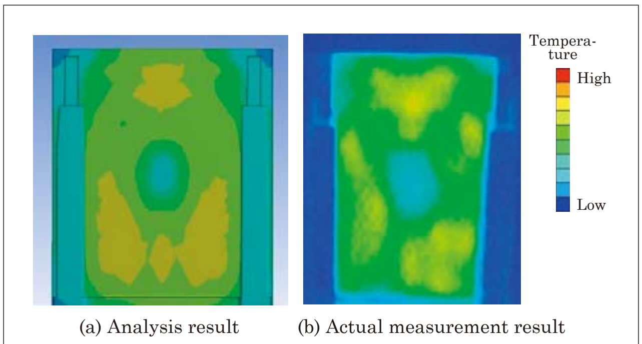

Fig.8 Comparison of temperature distribution in mold

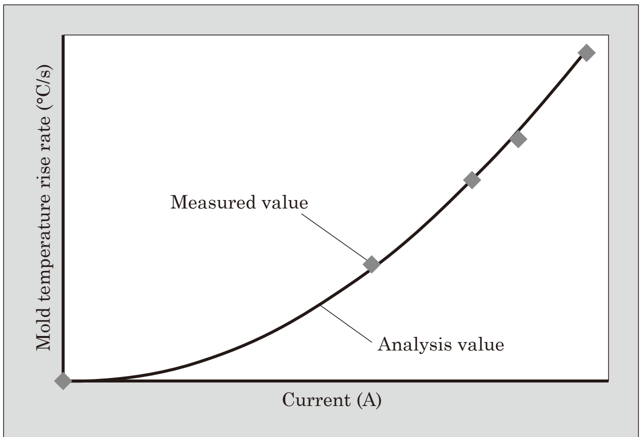

Fig.9 Comparison between analysis value and measured value of mold temperature rise rate

4.2 Prediction of glass fiber length

The strength of fiber-reinforced plastic depends on the length and orientation of the reinforcement fiber contained in the molded products. The fiber is damaged while flowing and this makes it shorter and causes it to have a lower strength. A longer reinforcement fiber is damaged more easily. Consequently, in the application of long fiber glass-reinforced plastic offering a strength equivalent to metal, it is important to establish technology to predict the glass fiber length contained in the molded products and reflect the result in the design of products and molds.

We have revealed so far that the area of modeling and consideration of the damage inside the molding machinery cylinder (incorporation of the injection screw shape into analysis conditions) will affect the result of analysis of glass fiber length. Furthermore, we have been studying analysis parameters including the possibility of glass fiber damage or the degree to which a compression force that results from resin flow contributes to fiber damage.

Figure 10 is a result of analyzing glass fiber length in a shape simulating a mechanical part for which high strength is required. Figure 11 is a comparison of the changes in the glass fiber length of the same part during a molding process with an actually molded part. The glass fiber becomes shorter as the molding progresses. The glass fiber length matches well with the measured value from when the resin was inside the cylinder until the point immediately after it passed through the gate.

We will improve the accuracy of the analysis after the resin passes through the gate by optimizing the element breakdown, glass fiber physical properties and fiber length distribution parameters. We will then apply the result to the design of long fiber glass-rein-

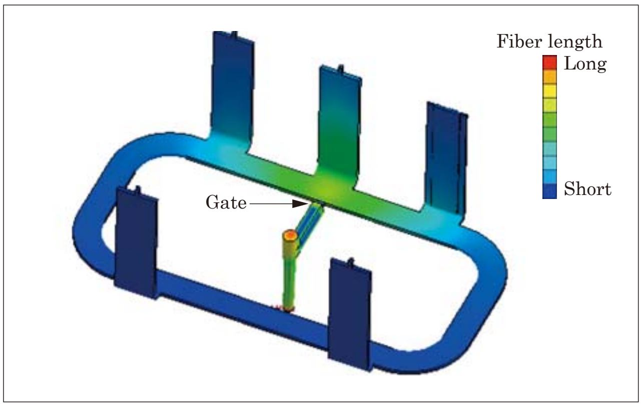

Fig.10 Analysis result of glass fiber length

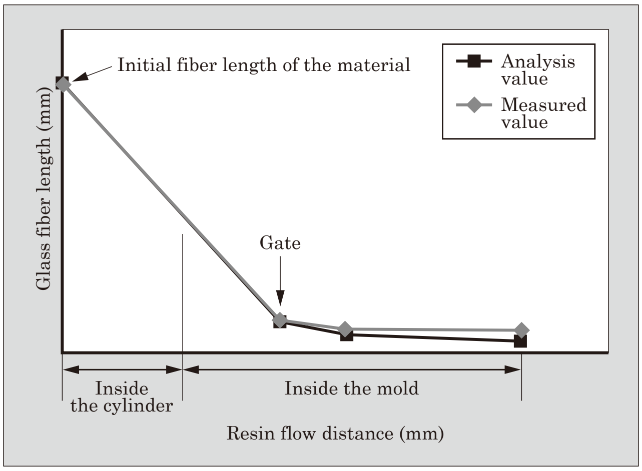

Fig.11 Change in glass fiber length during molding process

forced plastic molded products and their molds.

5. Postscript

This paper has described our approaches for increasing the quality of injection molded parts by taking advantage of simulation technologies.

We will continue working to achieve further sophistication and higher accuracy of analysis technologies so that we can provide products of higher quality to our customers.

Supplemental Explanation

Supplemental explanation 1 SiC Crystal Types and Crystal Surface p.4, 13

SiC crystals can be configured by one of several layered structures, such as crystal polymorphism (poly type) as shown in Fig. 1. The material properties are different for each poly type. 4H-SiC and 6H-SiC wafers for power device applications are both being sold on the market. 4H-SiC is currently the mainstream wafer with its wide band gap. In addition, SiC is characterized by a carbon-terminated C-face (carbon face) and silicon-terminated Si-face (silicon face) even for crystal surface with the same {0001} face, and it also exhibits different electrical conductivity when forming a MOSFET gate. Furthermore, we have also been studying the m-face $(1\bar{1}00)$, a-face $(11\bar{2}0)$ and $(0\bar{3}3\bar{8})$ face for device applications, where each has its own properties suitable for specific applications (see Fig. 2).

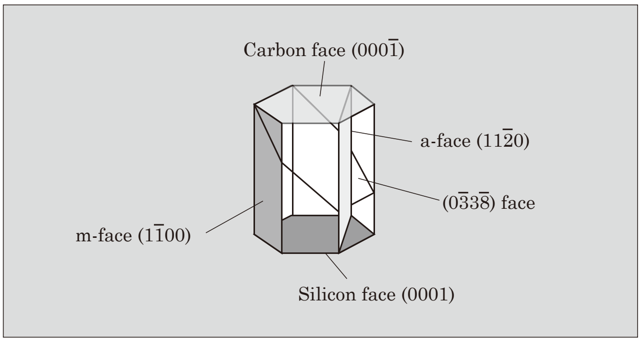

Fig.2 Main 4H-SiC crystal surfaces and their face directions for use in devices

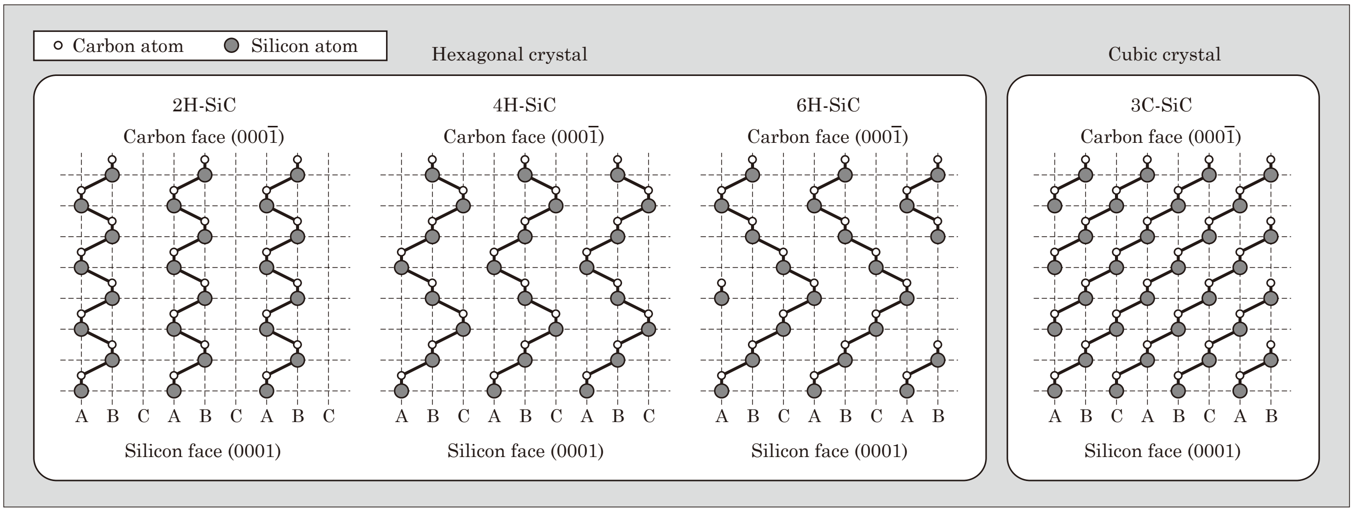

Fig.1 SiC crystal types

Supplemental explanation 2 MOSFET Carrier Scattering p.5, 13, 24

Applying high voltage to the gate electrode in MOSFET can dent the potential on the semiconductor surface, creating a path (channel) for the moving charge (carrier, e.g., electrons). Since the channel is an extremely thin layer, various factors prevent carriers from moving straight path (scattering). The main types of scattering includes Coulomb scattering, phonon scattering and surface roughness scattering.

(1) Coulomb scattering

Since carriers have a charge, they move while being affected by a fixed charge or ion located inside the channel or its vicinity. A Coulomb force affects the movement of a carrier because it creates repulsion for homopolarity and attraction for heteropolarity. This type of scattering mainly occurs at low temperatures.

(2) Phonon scattering

Carriers move while being affected by a potential in a state (lattice) in which atoms are arranged in order. In particular, the intense vibration of atoms at high temperatures can impact the movement of the carriers due to lattice vibration. This type of scattering mainly occurs at high temperatures.

(3) Surface roughness scattering

Carriers move in a channel created near the interface of the semiconductor and insulator. The existence of order irregularities in the atomic layer near the interface can impact the movement of the carrier. This type of scattering mainly occurs in a high electric field.

Silent Magnetic Contactor “SL Series”

DAIJIMA, Hideki*

Magnetic contactors are increasingly being used in overseas markets, especially in China and Southeast Asia, as a result of industrialization in various fields that accompanies economic development.

For China’s elevator market, Fuji Electric has launched the “SL Series” of silent magnetic contactors which feature quieter operation than our standard products.

1. Features

(a) Operating noise

10 to 15 dB less noise compared to Fuji Electric’s standard products (Measured 1 m from the mounting surface of the electromagnetic contactor)

(b) Control coil voltage

Can be used at the same voltage for both AC and DC

(c) Coil surge absorption function

Suppresses the occurrence surges from the control coil

(d) Auxiliary contacts

Adoption of twin contact structure that provides high contact reliability

(e) Standards

IEC standard-compliant and GB standard-compliant (CCC certification)

2. Specifications

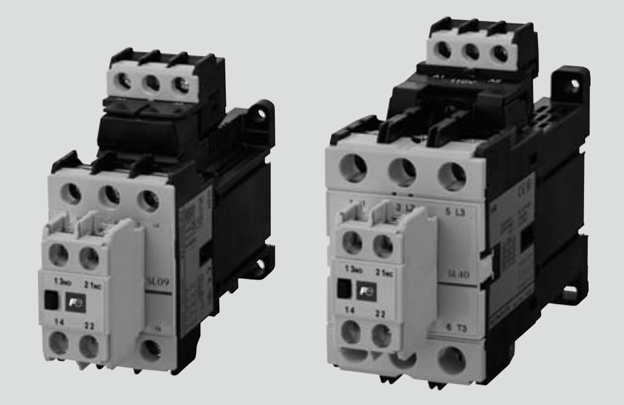

(a) “SL09” (b) “SL40”

Fig.1 “SL Series”

Table 1 “SL Series” formats and ratings

Type	Rated insulation voltage (V)	3-phase squirrel-cage type motor (AC-3)								Rated thermal current (A)
		Rated capacity (kW)				Rated operational current (A)				
		240 V	440 V	550 V	690 V	240 V	440 V	550 V	690 V	
SL09	690	2.2	4	4	4	9	9	7	5	20
SL25		5.5	11	11	7.5	25	25	17	9	32
SL40	1,000	11	18.5	18.5	15	40	40	29	19	60

Table 2 “SL Series” performance

Type	Rated operational voltage (V)	Rated operational current (A)	Operating frequency (Times/hr.)	Durability (million times or more)		Making/breaking current (A)	
				Mechanically switched	Electrically switched (AC-3, 400 V)	Making current	Breaking current
SL09	240	9	1,800	10	2	90	72
	440						
SL25	240	25	1,200	10	1.5	250	200
	440						
SL40	240	40	1,200	10	1.5	400	320
	440						

Figure 1 shows the external appearance, Table 1 lists the types and ratings, and Table 2 lists the performance of the SL Series.

3. Background Technology

In general, there are two types of magnetic contactors, AC-operated magnetic contactors that are driven by AC power supplies and DC-operated magnetic contactors that are driven by DC power supplies.

The AC electromagnet in an AC-operated magnetic contactor has a wide core gap, and when the contact is made, a large drive current will flow due to the large magnetic resistance. Since its operation is quick and the mechanical impact at the time of switching is large, the impact noise is also loud. The impact noise during operation is generated by collisions of the fixed core and moveable core when the contact is made, and by collisions with the moveable core and body frame when released. In the elevator industry, machine-roomless configurations have become popular in recent years, and since the control panel is mounted in the vicinity of the car, quieter operation of the devices used is sought. The AC-operated magnetic contactors widely used in devices for industries such as elevators have a disadvantage of large impact noise, however.

On the other hand, the DC electromagnet in a DC-

* Development Group, Fuji Electric FA Components & Systems Co., Ltd.

operated magnetic contactor has a narrow core gap, and current flows according to the time constant of the coil resistance, without regard for the core gap or the current flowing in the coil. In this case, the operation is slower than with an AC electromagnet, and the ability to reduce the operating noise is an advantage. For the Chinese market, however, power is supplied from an AC source, and the AC power has to be converted to a DC power supply.

3.1 Noise reduction

Figure 2 shows the structure of the SL Series The SL Series is configured from a rectifying unit that converts AC to DC, and a low-noise DC-operated magnetic contactor. Even during AC operation, the rectifying circuit converts the operating voltage to DC so that the DC electromagnet can operate to improve the noise performance.

3.2 Use of current delay effect of rectifier diodes

The rectifying unit contains a full-wave diode bridge circuit in which four rectifying diodes, D1 to D4, are connected in a bridge configuration as shown in Fig. 3.

As described above, with a DC-operated magnetic contactor, the coil current increases gradually when the power supply is turned ON. When the power supply is OFF, if there were no diodes, the energy stored in the coil would be released instantaneously; however, it will be self-consumed by the regeneration through the diodes and attenuated (current delay effect). Due to this effect, the opening speed decreases and the generation of impact noise is suppressed. In contrast to the approximately 80 dB (Fig. 4) impact noise level of an AC operation type magnetic contactor having the same conduction specifications, the noise level of this contactor could be reduced to about 70 dB (Fig. 5), and the noise performance improved.

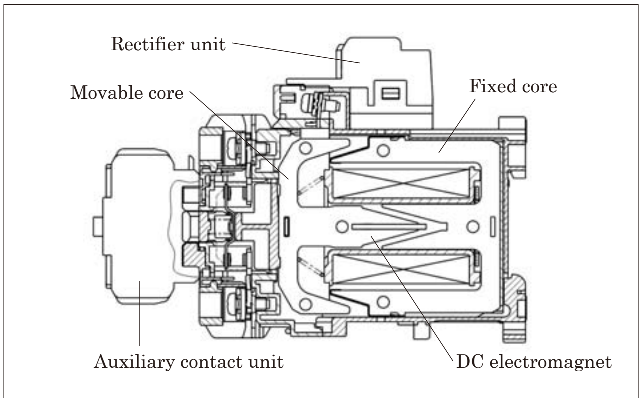

Fig.2 “SL Series” structure

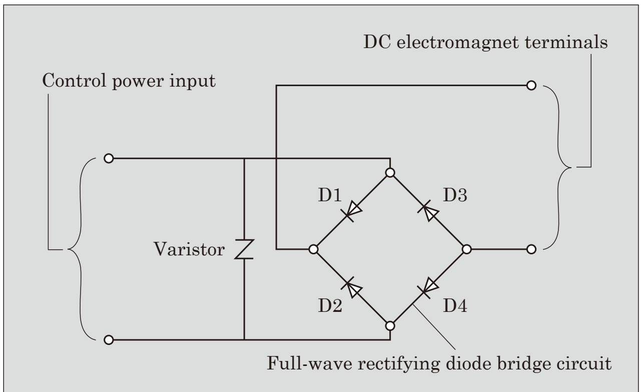

Fig.3 Rectifier unit circuit diagram

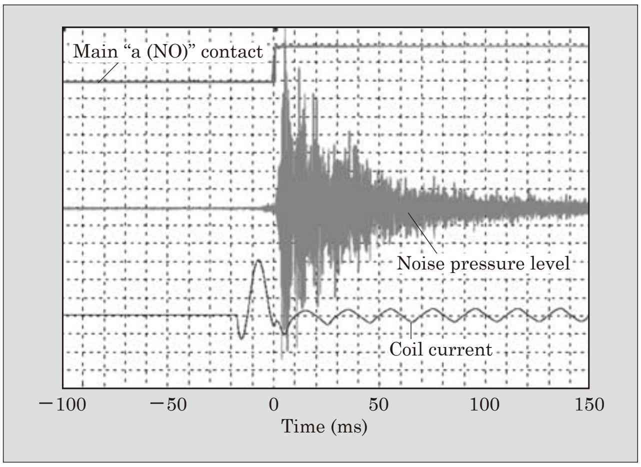

Fig.4 Operating noise of AC-operated magnetic contactor (during closed circuit operation)

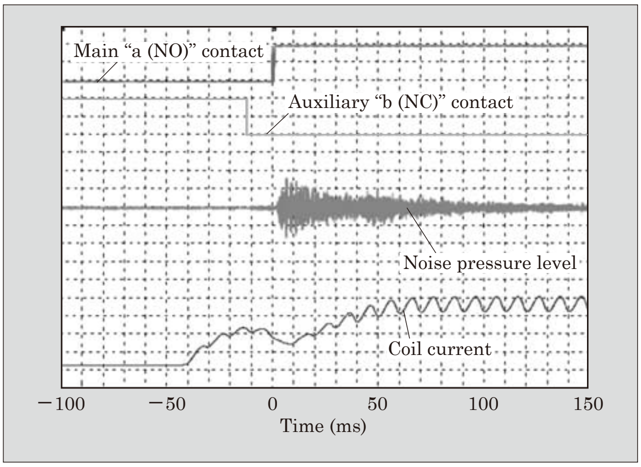

Fig. 5 Operating noise of silent magnetic contactor (during closed circuit operation)

Launch time

July 2015

Product Inquiries

Switching Products Section, Product Management Department Business Planning Group., Fuji Electric FA Components & Systems Co., Ltd.
Tel: +81 (3) 5847-8060

Air Conditioning Inverter for Asian Market "FRENIC-eHVAC Series"

KONO, Hiroyuki*

With the increasing global demand for energy, there is growing interest in energy-saving measures, and energy-saving products are being introduced at a rapid pace. In office buildings, for example, approximately 40% of the total energy consumption is used for heat sources and heat transport, and as a result, greater energy efficiency of air conditioning equipment has increasingly been demanded. On the other hand, a major challenge facing Asia, which has undergone significant economic development and where future growth is also expected, is how to continue economic development while conserving energy.

To meet this challenge, Fuji Electric is deploying its inverters for air conditioning use throughout the world. This paper describes Fuji Electric's "FRENIC-eHVAC Series" that has been commercialized in response to specification and price requirements of the Asian market in particular (see Fig. 1).

1. Functions Required for Air Conditioning Applications

1.1 PID control

As a standard feature, the inverters are equipped with two PID modules for PID control. One is used for the output frequency control of the inverter, and the other can be used with external systems. As a result, since modules are provided as a standard feature, the addition of an external PID module is no longer necessary for applications that require PID control.

Fig.1 "FRENIC-eHVAC Series"

* Power Electronics Business Group, Fuji Electric Co., Ltd.

1.2 Cascade operation

By using the FRENIC-eHVAC Series, cascade operation can be implemented to operate a water supply system consisting of multiple pumps connected via header tubes with optimal power.

For this cascade operation, the following five usage methods are available so that various systems can be supported flexibly.

- ○ Inverter drive motor fixed system
- ○ Inverter drive motor floating system
- ○ Inverter drive motor floating + commercial power-driven motor system
- ○ Communications-linked inverter drive motor floating system
- ○ Communications-linked all motors simultaneous PID control system

1.3 Fire mode

A fire mode is provided as a standard feature for forcibly continuing operation at a specified speed during an emergency or the like. During the fire mode, operation will continue even under conditions such as when an inverter alarm has been triggered. Moreover, even if instantaneous overcurrent protection is triggered, a retry function will enable operation to continue. This function allows for trip-free operation that prevents stoppages due to the detection of abnormalities.

1.4 Other functions

The FRENIC-eHVAC Series also comes equipped with the following standard functions.

(1) EMC filter

A built-in EMC (electromagnetic compatibility) filter (C2/C3) is provided as a standard feature, and is compatible with any installation environment.

(2) PM (Permanent Magnet) motor drive

A PM sensorless vector control function is provided to meet the needs for additional energy savings.

(3) Password setting

Two levels of passwords can be set to securely protect the configuration data.

2. Customizable Logic

Program editing, which as previously been limited to 14 steps, has been expanded to 200 steps. Customizable logic, enhanced with this expanded functionality, is provided as a standard feature, so that the dedicated functions requested by end users can be supported flexibly. Following in the footsteps of the “FRENIC-Ace Series”, by using more than 50 types of logic symbols such as for logic operations, counters, timers, etc., control devices such as external relays and timers can be newly incorporated into the inverter, which can operate as a simple PLC.

When programming with customizable logic, editing can be performed easily using the “FRENIC Visual Customizer,” a programming tool provided for free.

This customizable logic can be used to implement various forms of energy saving control, including temperature difference constant control and estimated end pressure control, when used in combination with a resistance temperature detector (RTD) option card.

3. Communication Function

As communication protocols*1 for air conditioning equipment, the frequently used BACnet protocol is supported as a standard feature, and METASYS N2 and MODBUS RTU protocols are also supported.

As communication system options*2, DeviceNet, CC-Link, PROFIBUS-DP and LonWorks are supported. As control system options, an analog I/O card, relay output card, and RTD card are available to facilitate system support.

4. Multilingual Support

The ability for users to review and verify function codes and other inverter information in their native language is important not only because of improved readability, but because it leads to fewer incidents associated with configuration errors or misunderstandings. Accordingly, a multi-function keypad panel that supports 19 languages is available as an option so that the FRENIC-eHVAC series can be used in many countries.

The 19 supported languages are Japanese, English, German, French, Spanish, Italian, Chinese, Russian, Greek, Turkish, Polish, Czech, Swedish, Portuguese, Dutch, Malay, Vietnamese, Thai, and Indonesian.

In addition to these 19 languages, many other languages require unique characters. Moreover, even among English-speaking countries, the terminology used may differ by country, and in some cases, expressions normally used by Fuji Electric may be difficult for users to comprehend. Therefore, in order to create special characters, the character editing screen shown in Fig. 2 is provided is a standard feature. Data that has been created may be saved as text data, and characters shown on a display can be changed as desired. Moreover, Fuji Electric has developed a user-customized language (UCL) creation tool so as to be able to support all characters and text. By using this tool, nuanced language expressions (phrases) can be set and modified from the data creation screen shown in Fig. 3.

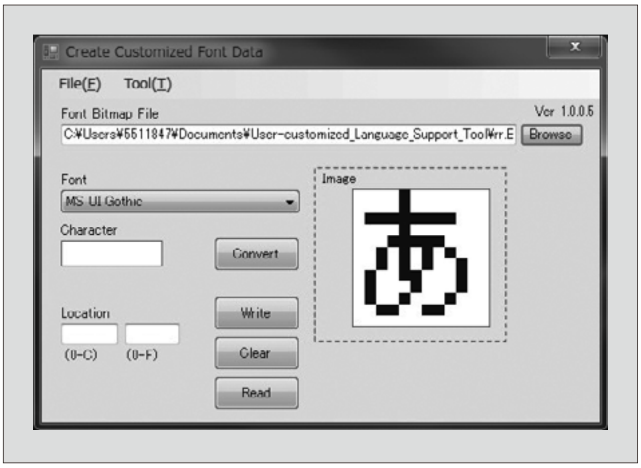

Fig.2 Character editing screen

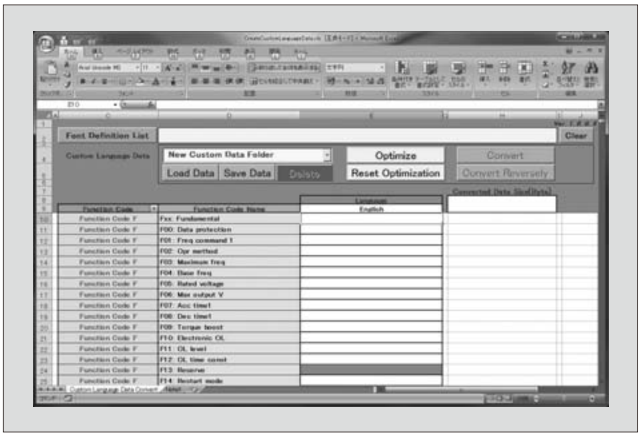

Fig.3 Data creation screen

*1: Communication protocols:
BACnet is a trademark or registered trademark of the American Society of Heating, Refrigeration and Air-Conditioning Engineers (ASHRAE).
METASYS is a trademark or registered trademark of Johnson Controls.
MODBUS is a trademark or registered trademark of Schneider Automation, Inc. of France.

*2: Communication system options:
DeviceNet is a trademark or registered trademark of the ODVA (Open DeviceNet Vendor Association, Inc.).
CC-Link is a trademark or registered trademark of CC-Link Partner Association.
PROFIBUS-DP is a trademark or registered trademark of the PROFIBUS User Organization.
LonWorks is a trademark or registered trademark of the Echelon Corporation of the United States.

Launch time:

June 2015

Product Inquiries:

Business Planning Department, Drive Division, Power Electronics Business Group, Fuji Electric Co., Ltd.
Tel: +81 (3) 5435-7190

Innovating Energy Technology

Through our pursuit of innovation in electric and
thermal energy technology,
we develop products that maximize energy efficiency and
lead to a responsible and sustainable society.

Fuji Electric

Overseas Subsidiaries

* Non-consolidated subsidiaries

America

Fuji Electric Corp. of America
Sales of electrical machinery and equipment, semiconductor devices, drive control equipment, and devices
Tel +1-732-560-9410
URL http://www.americas.fujielectric.com/

Fuji Electric Brazil-Equipamentos de Energia Ltda *
Sales of inverters, semiconductors, and power distribution
Tel +55-11-2283-5991
URL http://www.americas.fujielectric.com/portugues

Reliable Turbine Services LLC
Repair and maintenance of steam turbines, generators, and peripheral equipment
Tel +1-573-468-4045

Fuji SEMEC Inc.*
Manufacture and sales of door opening and closing systems
Tel +1-450-641-4811

Asia

Fuji Electric Asia Pacific Pte. Ltd.
Sales of electrical distribution and control equipment, drive control equipment, and semiconductor devices
Tel +65-6533-0014
URL http://www.sg.fujielectric.com/

Fuji SMBE Pte. Ltd. *
Manufacture, sales, and services relating to low-voltage power distribution board(switchgear, control equipment)
Tel +65-6756-0988
URL http://smbe.fujielectric.com/

Fuji Electric (Thailand) Co., Ltd. *
Sales and engineering of electric substation equipment, control panels, and other electric equipment
Tel +66-2-210-0615

Fuji Electric Manufacturing (Thailand) Co., Ltd.
Manufacture and sales of inverters (LV/MV), power systems (UPS, PCS, switching power supply systems), electric substation equipment (GIS) and vending machines
Tel +66-2-5292178

Fuji Tusco Co., Ltd. *
Manufacture and sales of and provision of maintenance services for transformers
Tel +66-2324-0100
URL http://www.ftu.fujielectric.com/

Fuji Electric Vietnam Co.,Ltd. *
Sales of electrical distribution and control equipment and drive control equipment
Tel +84-4-3935-1593

Fuji Furukawa E&C (Vietnam) Co., Ltd. *
Engineering and construction of mechanics and electrical works
Tel +84-4-3755-5067

PT. Fuji Electric Indonesia *
Sales of inverters, servos, UPS, tools, and other component products
Tel +62 21 398-43211
URL http://www.id.fujielectric.com/

Fuji Electric India Pvt. Ltd. *
Sales of drive control equipment and semiconductor devices
Tel +91-22-4010 4870
URL http://www.fujielectric.co.in

Fuji Electric Philippines, Inc.
Manufacture of semiconductor devices
Tel +63-2-844-6183

Fuji Electric (Malaysia) Sdn. Bhd.
Manufacture of magnetic disk and aluminum substrate for magnetic disk
Tel +60-4-403-1111
URL http://www.fujielectric.com.my/

Fuji Furukawa E&C (Malaysia) Sdn. Bhd. *
Engineering and construction of mechanics and electrical works
Tel +60-3-4297-5322

Fuji Electric Taiwan Co., Ltd.
Sales of semiconductor devices, electrical distribution and control equipment, and drive control equipment
Tel +886-2-2511-1820

Fuji Electric Korea Co., Ltd.
Sales of power distribution and control equipment, drive control equipment, rotators, high-voltage inverters, electronic control panels, medium- and large-sized UPS, and measurement equipment
Tel +82-2-780-5011
URL http://www.fujielectric.co.kr/

Fuji Electric Co.,Ltd. (Middle East Branch Office)
Promotion of electrical products for the electrical utilities and the industrial plants
Tel +973-17 564 569

Fuji Electric Co., Ltd. (Myanmar Branch Office)
Providing research, feasibility studies, Liaison services
Tel +95-1-382714

Representative office of Fujielectric Co., Ltd. (Cambodia)
Providing research, feasibility studies, Liaison services
Tel +855-(0)23-964-070

Europe

Fuji Electric Europe GmbH
Sales of electrical/electronic machinery and components
Tel +49-69-6690290
URL http://www.fujielectric-europe.com/

Fuji Electric France S.A.S
Manufacture and sales of measurement and control devices
Tel +33-4-73-98-26-98
URL http://www.fujielectric.fr/

Fuji N2telligence GmbH *
Sales and engineering of fuel cells and peripheral equipment
Tel +49 (0) 3841 758 4500

China

Fuji Electric (China) Co., Ltd.
Sales of locally manufactured or imported products in China, and export of locally manufactured products
Tel +86-21-5496-1177
URL http://www.fujielectric.com.cn/

Shanghai Fuji Electric Switchgear Co., Ltd.
Manufacture and sales of switching equipment, monitoring control appliances, and related facilities and products
Tel +86-21-5718-1234
URL http://www.fujielectric.com.cn/sfswgr/

Shanghai Fuji Electric Transformer Co., Ltd.
Manufacture and sales of molded case transformers
Tel +86-21-5718-7705
URL http://www.fujielectric.com.cn/sfswgr/

Wuxi Fuji Electric FA Co., Ltd.
Manufacture and sales of low/high-voltage inverters, temperature controllers, gas analyzers, and UPS
Tel +86-510-8815-2088

Fuji Electric (Changshu) Co., Ltd.
Manufacture and sales of electromagnetic contactors and thermal relays
Tel +86-512-5284-5642
URL http://www.fujielectric.com.cn/csfe/

Fuji Electric (Zhuhai) Co., Ltd.
Manufacture and sales of industrial electric heating devices
Tel +86-756-7267-861
http://www.fujielectric.com.cn/fez/

Fuji Electric (Shenzhen) Co., Ltd.
Manufacture and sales of photoconductors, semiconductor devices and currency handling equipment
Tel +86-755-2734-2910
URL http://www.szfujielectric.com.cn/

Fuji Electric Dalian Co., Ltd.
Manufacture of low-voltage circuit breakers
Tel +86-411-8762-2000

Fuji Electric Motor (Dalian) Co., Ltd.
Manufacture of industrial motors
Tel +86-411-8763-6555

Dailan Fuji Bingshan Vending Machine Co.,Ltd.
Development, manufacture, sales, servicing, overhauling, and installation of vending machines, and related consulting
Tel +86-411-8754-5798

Fuji Electric (Hangzhou) Software Co., Ltd.
Development of vending machine-related control software and development of management software
Tel +86-571-8821-1661
URL http://www.fujielectric.com.cn/fhs/cn/

Fuji Electric FA (Asia) Co., Ltd.
Sales of electrical distribution and control equipments
Tel +852-2311-8282
URL http://www.fea.hk/

Fuji Electric Hong Kong Co., Ltd.
Sales of semiconductor devices and photoconductors
Tel +852-2664-8699

Hoei Hong Kong Co., Ltd.
Sales of electrical/electronic components
Tel +852-2369-8186
URL http://www.hoei.com.hk/

Printed on recycled paper